MEL 海洋生物地球化学全国重点实验室（厦门大学）
State Key Laboratory of Marine Environmental Science

厦門大學 Optical Oceanography Laboratory

Inherent Optical Properties (IOPs)

Lecture 2: Inversion & Application

Contents:

I. Inversion algorithms for IOPs

II. Applications of inverted IOPs

I. Inversion algorithms for IOPs

Remote-sensing reflectance (sr^{-1}):

$$R_{rs}(\lambda) = \frac{L_w(\lambda, 0^+)}{E_d(\lambda, 0^+)}$$

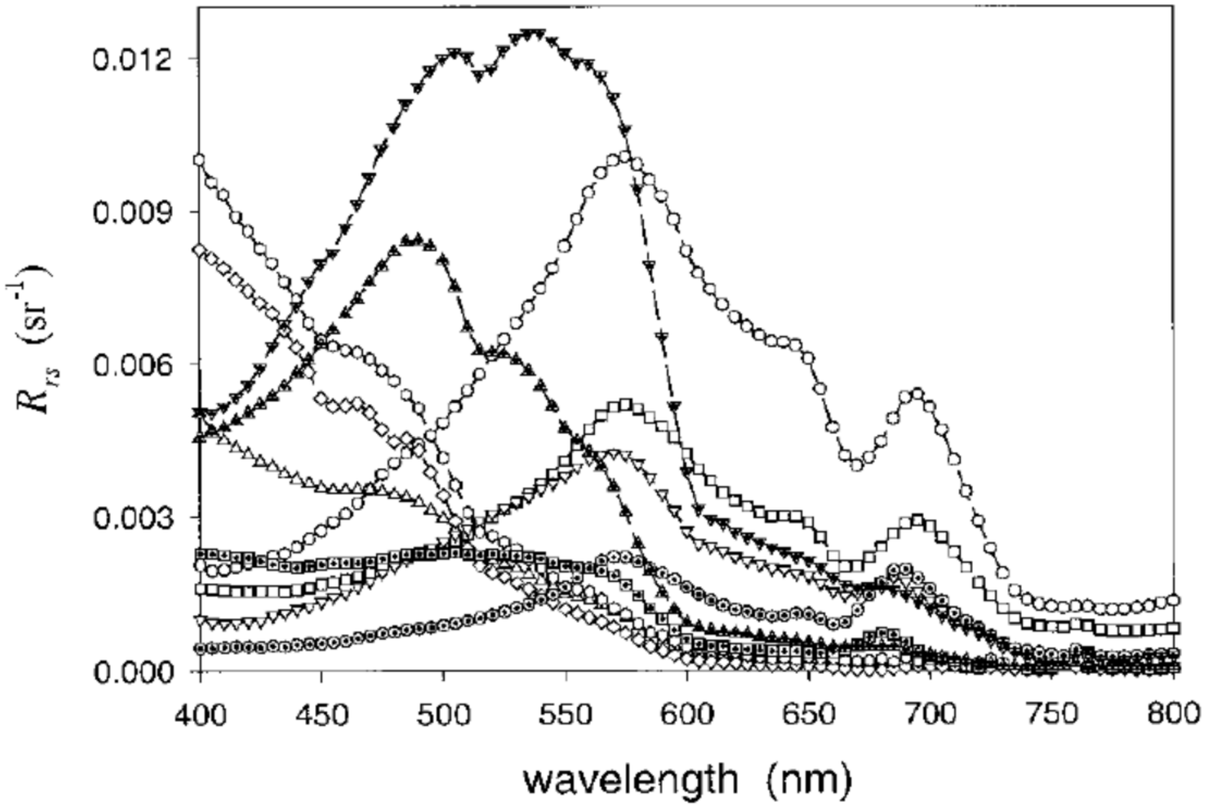

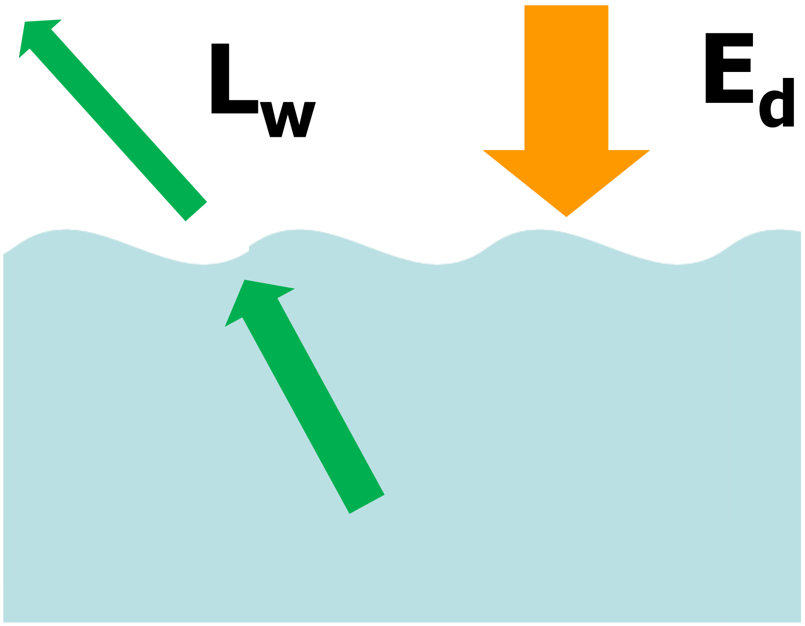

The ultimate objective of RS: Retrieval useful/important environmental information

How?

algorithm!

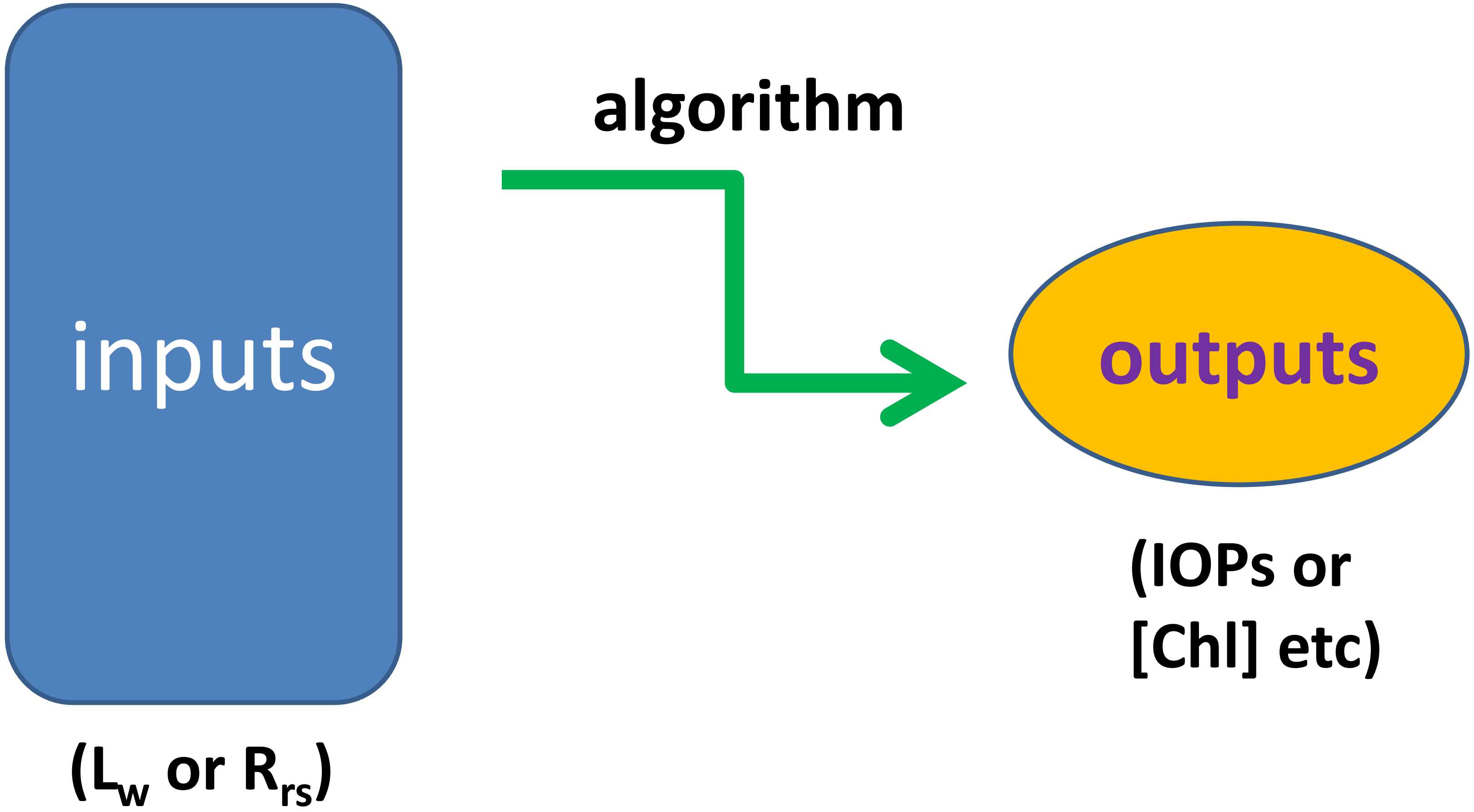
inputs
algorithm
outputs
(IOPs or
[Chl] etc)
(L_w or R_{rs})

Empirical
(explicit or implicit)

Bio-optical models： **No need**

Semi-analytical
(algebraic, LUT, optimization)

Bio-optical models： **Yes**

- **Bottom Up Strategy (BUS)**
- **Top Down Strategy (TDS)**

band-ratio algorithms for Chl

Algorithm	Type	Result Equation(s)	Band Ratio (R), Coefficients (a)
Global processing (GPs)	power	$C_{13} = 10^{(a0+a1*R1)}$ $C_{23} = 10^{(a2+a3*R2)}$ $[C + P] = C_{13}$; if C_{13} and $C_{23} > 1.5\ \mu g\ L^{-1}$ then $[C + P] = C_{23}$	$R1$ = log(Lwn443/Lwn550) $R2$ = log(Lwn520/Lwn550) a = [0.053, 1.705, 0.522, 2.440]
Clark three-band (C3b)	power	$[C + P] = 10^{(a0+a1*R)}$	R = log((Lwn443 + Lwn520)/Lwn550) a = [0.745, −2.252]
Aiken-C	hyperbolic + power	$C_{21} = \exp(a0 + a1*\ln(R))$ $C_{23} = (R + a2)/(a3 + a4*R)$ $C = C_{21}$; if $C < 2.0\ \mu g\ L^{-1}$ then $C = C_{23}$	R = Lwn490/Lwn555 a = [0.464, −1.989, −5.29, 0.719, −4.23]
Aiken-P	hyperbolic + power	$C_{22} = \exp(a0 + a1*\ln(R))$ $C_{24} = (R + a2)/(a3 + a4*R)$ $[C + P] = C_{22}$; if $[C + P] < 2.0\ \mu g\ L^{-1}$ then $[C + P] = C_{24}$	R = Lwn490/Lwn555 a = [0.696, −2.085, −5.29, 0.592, −3.48]
OCTS-C	power	$C = 10^{(a0+a1*R)}$	R = log((Lwn520 + Lwn565)/Lwn490) a = [0.55006, 3.497]
OCTS-P	multiple regression	$[C + P] = 10^{(a0+a1*R1+a2*R2)}$	$R1$ = log(Lwn443/Lwn520) $R2$ = log(Lwn490/Lwn520) a = [0.19535, −2.079, −3.497]
POLDER	cubic	$C = 10^{(a0+a1*R+a2*R^2+a3*R^3)}$	R = log(Rrs443/Rrs565) a = [0.438, −2.114, 0.916, −0.851]
CalCOFI two-band linear	power	$C = 10^{(a0+a1*R)}$	R = log(Rrs490/Rrs555) a = [0.444, −2.431]
CalCOFI two-band cubic	cubic	$C = 10^{(a0+a1*R+a2*R^2+a3*R^3)}$	R = log(Rrs490/Rrs555) a = [0.450, −2.860, 0.996, −0.3674]
CalCOFI three-band	multiple regression	$C = \exp(a0 + a1*R1 + a2*R2)$	$R1$ = ln(Rrs490/Rrs555) $R2$ = ln(Rrs510/Rrs555) a = [1.025, −1.622, −1.238]
CalCOFI four-band	multiple regression	$C = \exp(a0 + a1*R1 + a2*R2)$	$R1$ = ln(Rrs443/Rrs555) $R2$ = ln(Rrs412/Rrs510) a = [0.753, −2.583, 1.389]
Morel-1	power	$C = 10^{(a0+a1*R)}$	R = log(Rrs443/Rrs555) a = [0.2492, −1.768]
Morel-2	power	$C = \exp(a0 + a1*R)$	R = ln(Rrs490/Rrs555) a = [1.077835, −2.542605]
Morel-3	cubic	$C = 10^{(a0+a1*R+a2*R^2+a3*R^3)}$	R = log(Rrs443/Rrs555) a = [0.20766, −1.82878, 0.75885, −0.73979]
Morel-4	cubic	$C = 10^{(a0+a1*R+a2*R^2+a3*R^3)}$	R = log(Rrs490/Rrs555) a = [1.03117, −2.40134, 0.3219897, −0.291066]

(O'Reilly et al. 1998)

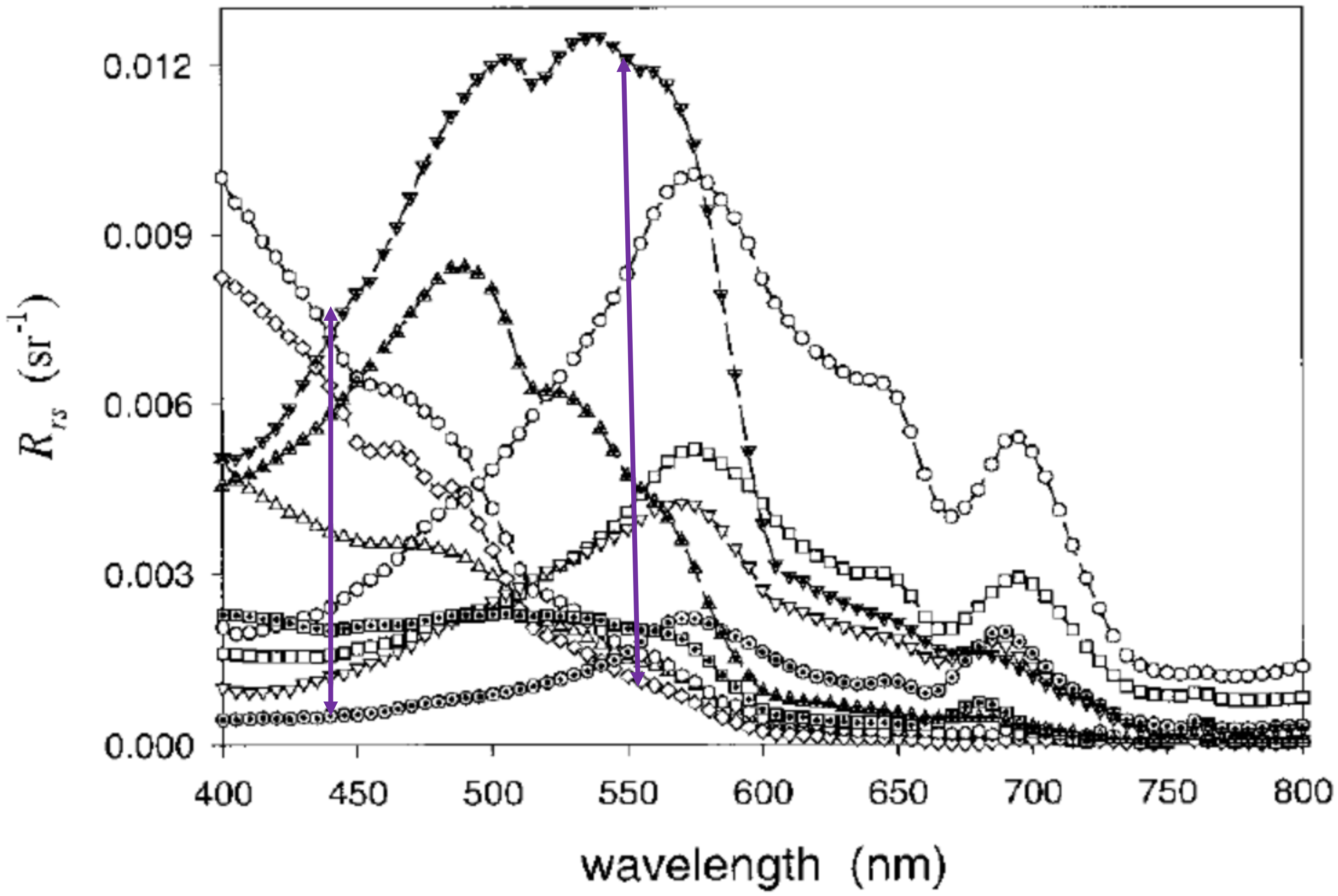
0.012
0.009
0.006
0.003
0.000
R_{rs} (sr^{-1})
400
450
500
550
600
650
700
750
800
wavelength (nm)

Chl based on band difference

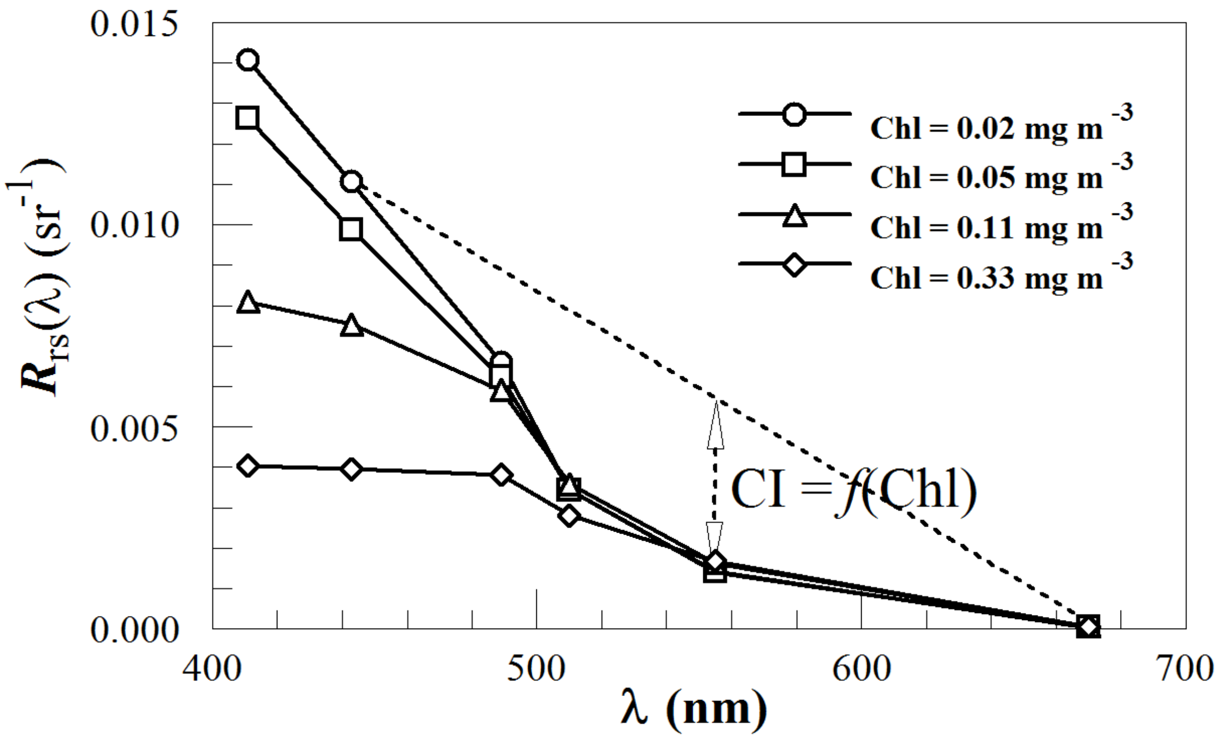

$$CI = R_{rs}(555) - \left\{ R_{rs}(443) + \frac{555-443}{670-443} \times \left[R_{rs}(670) - R_{rs}(443) \right] \right\}$$

$$Chl = 10^{-0.49+191.66\,CI}; \qquad CI \leq -0.0005\,\mathrm{sr}^{-1}$$

(Hu et al. 2012)

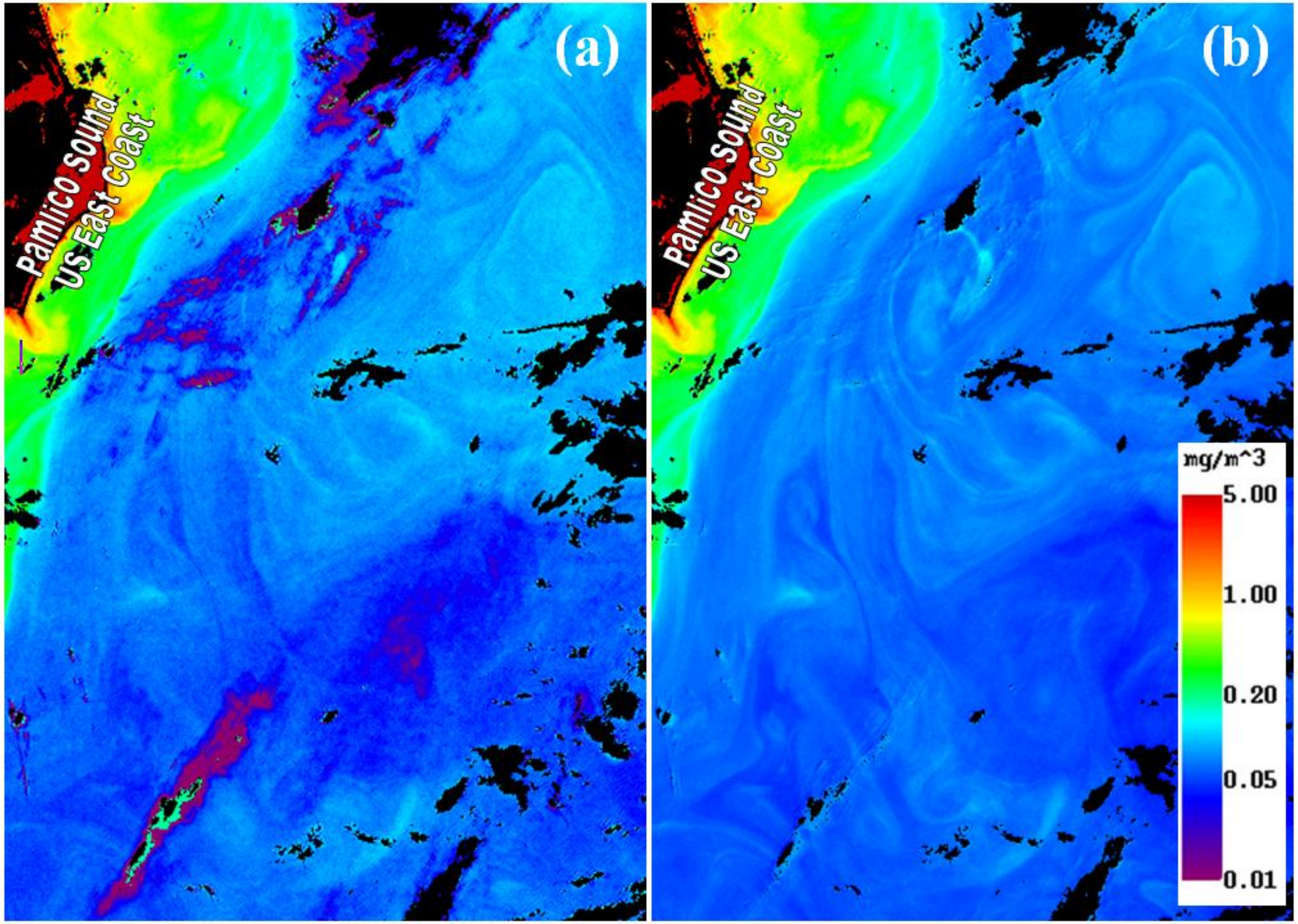
(a)
(b)
Pamlico Sound
US East Coast
Pamlico Sound
US East Coast
mg/m^3
5.00
1.00
0.20
0.05
0.01

(Hu et al. 2012)

$$R_{rs}^{Sat}(\lambda) = R_{rs}(\lambda) + \delta(\lambda) = R_{rs}(\lambda) + y\,\lambda + x$$

$$\boldsymbol{MBD_{Rrs440} = R_{rs}(555) - \left[R_{rs}(443) + \frac{555-443}{670-443}\big(R_{rs}(670) - R_{rs}(443)\big)\right]}$$

$$MBD(R_{rs}^{Sat}) = MBD_{Rrs}$$

Physics-based algorithms (mechanistic)

Remote-sensing reflectance (sr^{-1}):

$$R_{rs}(\lambda) = \frac{L_w(\lambda, 0^+)}{E_d(\lambda, 0^+)}$$

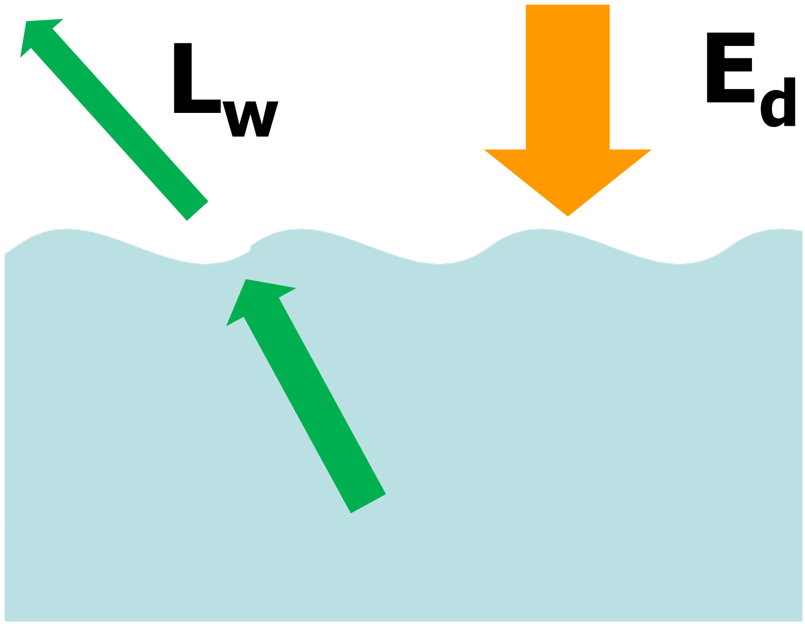

How is R_{rs} related to water's optical (biogeochemical) properties?

Physics-based algorithms (mechanistic)

$$r_{rs}(\lambda,\pi)=\sum_{i=1}^{2} g_i\left(\frac{b_b(\lambda)}{a(\lambda)+b_b(\lambda)}\right)^i;$$

$$g_1=0.0949,\ g_2=0.0794$$

(Gordon et al, 1988)

$r_{rs} \rightarrow R_{rs}$?

$$R_{rs} = \frac{L_w}{E_d(0^+)}$$

$$E_d(0^-) = t_E E_d(0^+) + \gamma E_u(0^-)$$

$$L_w = \frac{t_L}{n_w^{\ 2}} L_u(0^-)$$

$$R_{rs} = \frac{t_E\, t_L}{n_w^{\ 2}} \frac{r_{rs}}{1-\gamma R} \doteq \frac{0.52\, r_{rs}}{1-1.7\, r_{rs}}$$

Solve Rrs for IOPs or in-water constituents?

Two common strategies:

1. Bottom-up strategy (BUS):

    Assume we know the spectral shapes of the optically active components

2. Top-down strategy (TDS):

    Only need the spectral shape information when it is necessary

What are we facing in RS inversion?

$$R_{rs}(\lambda) = F(a(\lambda), b_b(\lambda))$$

$$\Downarrow$$

$$R_{rs}(\lambda) = F(a_w(\lambda), a_{ph}(\lambda), a_{dg}(\lambda), b_{bw}(\lambda), b_{bp}(\lambda))$$

$$\Downarrow$$

$$\begin{cases} R_{rs}(\lambda_1) = F(a_w(\lambda_1), a_{ph}(\lambda_1), a_{dg}(\lambda_1), b_{bw}(\lambda_1), b_{bp}(\lambda_1)) \\ R_{rs}(\lambda_2) = F(a_w(\lambda_2), a_{ph}(\lambda_2), a_{dg}(\lambda_2), b_{bw}(\lambda_2), b_{bp}(\lambda_2)) \\ \vdots \\ R_{rs}(\lambda_n) = F(a_w(\lambda_n), a_{ph}(\lambda_n), a_{dg}(\lambda_n), b_{bw}(\lambda_n), b_{bp}(\lambda_n)) \end{cases}$$

# of unknowns > # of equations!

An ill formulated math problem!

Have to increase # of equations or decrease # of unknowns!

1. Bottom-up strategy (BUS):

Build-up an Rrs spectrum block-by-block:

$$\boldsymbol{a(\lambda) = a_{w}(\lambda) + \sum a_{xi}(\lambda)} \qquad \boldsymbol{b_b(\lambda) = b_{bw}(\lambda) + \sum b_{bxi}(\lambda)}$$

$$a(\lambda) = a_w(\lambda) + a_{ph}(\lambda) + a_d(\lambda) + a_g(\lambda)$$

$$a(\lambda) = a_w(\lambda) + a_{ph}(\lambda) + a_{dg}(\lambda)$$

$$a(\lambda) = a_w(\lambda) + M_1 \left\langle a_{ph}(\lambda) \right\rangle + M_2 \left\langle a_{dg}(\lambda) \right\rangle$$

$$b_b(\lambda) = b_{bw}(\lambda) + b_{bp}(\lambda)$$

$$b_b(\lambda) = b_{bw}(\lambda) + M_3 \left\langle b_{bp}(\lambda) \right\rangle$$

Bio-optical models (forward model)

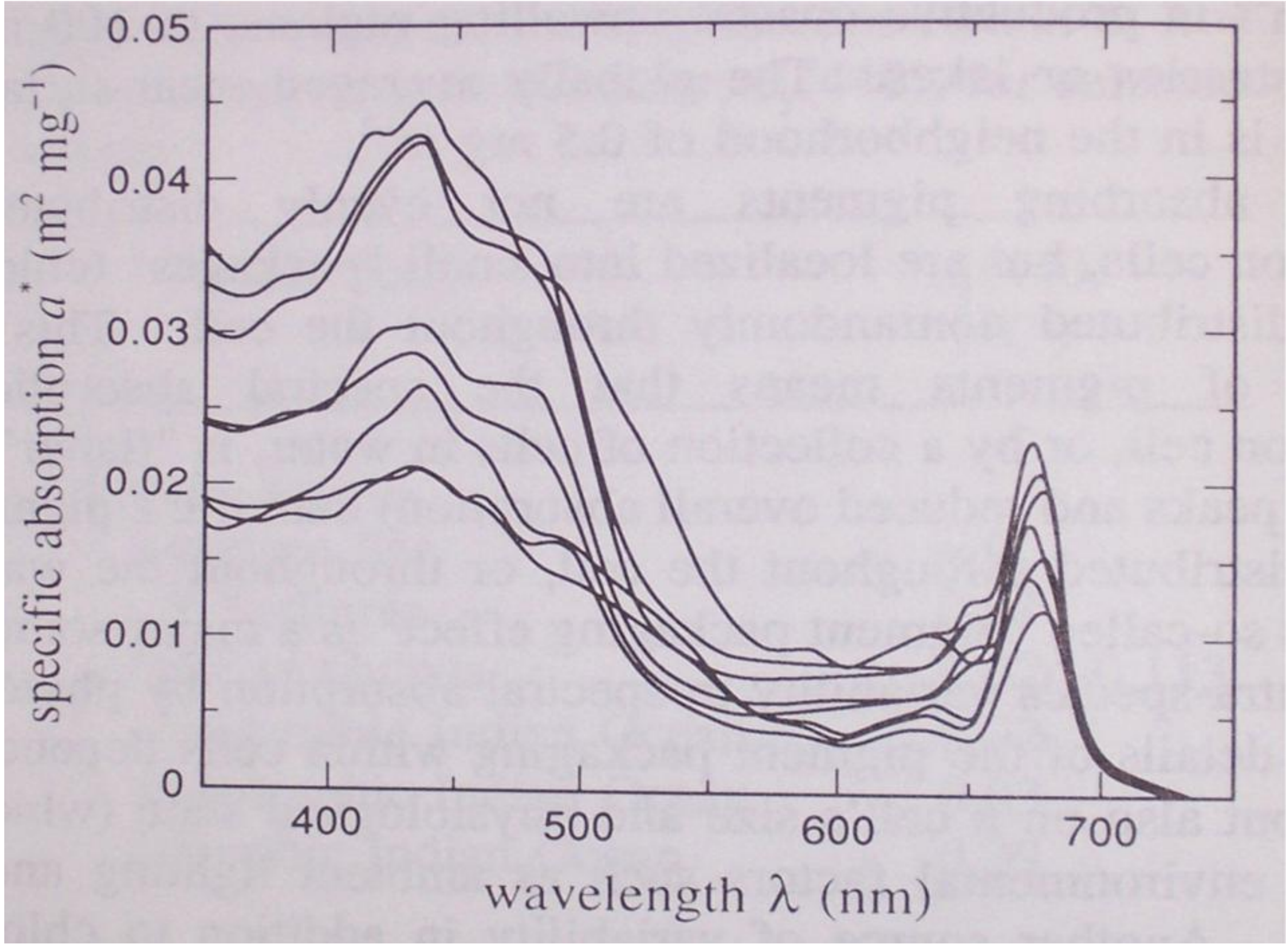

Modeling a_{ph} spectrum

Example of one parameter hyperspectral $a_{ph}(\lambda)$ model:

Bricaud et al (1995):

$$a_{ph}(\lambda) = A_{ph}(\lambda) Chl^{1-B_{ph}(\lambda)}$$

Lee (1994); Lee et al (1998):

$$a_{ph}(\lambda) = \left(a_0(\lambda) + a_1(\lambda)\ln(P)\right)P$$

$$\boldsymbol{P = a_{ph}(440)}$$

Table 2. Spectral Values of the Constants Obtained When Fitting the Variations of $a^*_{ph}(\lambda)$ Versus the (chl a + di a) Concentration ⟨Chl⟩ to Power Laws of the Form $a^*_{ph}(\lambda) = A(\lambda)\langle\text{Chl}\rangle^{-B(\lambda)}$ and Determination Coefficients on th Log-Transformed Data r^2

λ, nm	A	B	r^2	λ, nm	A	B
400	0.0263	0.282	0.702	402	0.0271	0.281
404	0.0280	0.282	0.706	406	0.0290	0.281
408	0.0301	0.282	0.710	410	0.0313	0.283
412	0.0323	0.286	0.718	414	0.0333	0.291
416	0.0342	0.293	0.725	418	0.0349	0.296
420	0.0356	0.299	0.733	422	0.0359	0.306
424	0.0362	0.313	0.746	426	0.0369	0.316
428	0.0376	0.317	0.749	430	0.0386	0.314
432	0.0391	0.318	0.750	434	0.0395	0.324
436	0.0399	0.328	0.757	438	0.0401	0.332
440	0.0403	0.332	0.762	442	0.0398	0.339
444	0.0390	0.348	0.774	446	0.0383	0.355
448	0.0375	0.360	0.783	450	0.0371	0.359
452	0.0365	0.362	0.783	454	0.0358	0.366
456	0.0354	0.367	0.789	458	0.0351	0.368
460	0.0350	0.365	0.789	462	0.0347	0.366
464	0.0343	0.368	0.792	466	0.0339	0.369
468	0.0335	0.369	0.793	470	0.0332	0.368
472	0.0325	0.371	0.792	474	0.0318	0.375
476	0.0312	0.378	0.793	478	0.0306	0.379
480	0.0301	0.377	0.791	482	0.0296	0.377
484	0.0290	0.376	0.788	486	0.0285	0.373
488	0.0279	0.369	0.783	490	0.0274	0.361
492	0.0267	0.356	0.774	494	0.0258	0.349
496	0.0249	0.341	0.763	498	0.0240	0.332
500	0.0230	0.321	0.747	502	0.0220	0.311
504	0.0209	0.300	0.722	506	0.0199	0.288
508	0.0189	0.275	0.686	510	0.0180	0.260
512	0.0171	0.249	0.641	514	0.0163	0.237
516	0.0156	0.224	0.578	518	0.0149	0.211
520	0.0143	0.196	0.498	522	0.0137	0.184
524	0.0131	0.173	0.417	526	0.0126	0.162
528	0.0121	0.151	0.332	530	0.0117	0.139
532	0.0113	0.129	0.248	534	0.0108	0.119
536	0.0104	0.109	0.176	538	0.0100	0.100
540	0.0097	0.090	0.116	542	0.0093	0.081

Table 2. Parameters for the Empirical $a_\phi(\lambda)$ Simulation by Eq. (12)[a]

Wavelength	$a_0(\lambda)$	$a_1(\lambda)$
390	0.5813	0.0235
400	0.6843	0.0205
410	0.7782	0.0129
420	0.8637	0.006
430	0.9603	0.002
440	1.0	0
450	0.9634	0.006
460	0.9311	0.0109
470	0.8697	0.0157
480	0.789	0.0152
490	0.7558	0.0256
500	0.7333	0.0559
510	0.6911	0.0865
520	0.6327	0.0981
530	0.5681	0.0969
540	0.5046	0.09
550	0.4262	0.0781
560	0.3433	0.0659
570	0.295	0.06
580	0.2784	0.0581

Example of two-parameters model:

(Ciotti et al 2002)

$$a_\phi(\lambda) = a_\phi(505)\{[S_f \cdot \bar{a}_{<pico>}(\lambda)] + [(1 - S_f)\cdot \bar{a}_{<micro>}(\lambda)]\}$$

Table 3. Basis vectors representing the normalized absorption for the smallest ($\bar{a}_{(pico)}(\lambda)$, *Prochlorococcus*) and biggest ($\bar{a}_{(micro)}(\lambda)$, average microplankton) cell sizes in our data set. Wavelength (λ) in nm. Basis vectors for $a^*_{ph}(\lambda)$ can be constructed by setting $\bar{a}_{(pico)}(676)$ to 0.023 $m^2\ mg^{-1}$, $\bar{a}_{(micro)}(674)$ to 0.0086 $m^2\ mg^{-1}$, and scaling for the other wavelengths accordingly.

λ	Pico	Micro	λ	Pico	Micro	λ	Pico	Micro	λ	Pico	Micro	λ	Pico	Micro
400	1.682	1.574												
402	1.734	1.584	462	2.526	1.623	522	0.544	1.013	582	0.111	0.459	642	0.191	0.528
404	1.800	1.600	464	2.455	1.616	524	0.522	0.992	584	0.072	0.452	644	0.174	0.526
406	1.890	1.617	466	2.402	1.606	526	0.486	0.977	586	0.073	0.452	646	0.197	0.528
408	1.978	1.633	468	2.331	1.592	528	0.448	0.959	588	0.073	0.449	648	0.176	0.538
410	2.057	1.654	470	2.281	1.568	530	0.391	0.944	590	0.099	0.443	650	0.168	0.549
412	2.162	1.669	472	2.205	1.542	532	0.375	0.927	592	0.070	0.433	652	0.160	0.574
414	2.269	1.674	474	2.136	1.509	534	0.336	0.909	594	0.095	0.424	654	0.217	0.605
416	2.327	1.684	476	2.063	1.481	536	0.305	0.888	596	0.085	0.416	656	0.244	0.655
418	2.398	1.697	478	2.049	1.459	538	0.292	0.868	598	0.090	0.406	658	0.286	0.720
420	2.457	1.708	480	1.998	1.437	540	0.288	0.847	600	0.086	0.401	660	0.381	0.798
422	2.533	1.710	482	1.930	1.415	542	0.261	0.826	602	0.068	0.400	662	0.437	0.889
424	2.614	1.716	484	1.918	1.399	544	0.245	0.806	604	0.078	0.403	664	0.520	0.979
426	2.663	1.737	486	1.897	1.387	546	0.214	0.785	606	0.069	0.408	666	0.660	1.068
428	2.749	1.763	488	1.867	1.377	548	0.194	0.764	608	0.090	0.416	668	0.716	1.147
430	2.804	1.793	490	1.812	1.367	550	0.187	0.737	610	0.096	0.429	670	0.824	1.207
432	2.840	1.812	492	1.776	1.349	552	0.138	0.711	612	0.094	0.443	672	0.846	1.243
434	2.915	1.827	494	1.701	1.338	554	0.137	0.682	614	0.084	0.458	674	0.816	1.249
436	2.947	1.830	496	1.648	1.319	556	0.111	0.653	616	0.105	0.473	676	0.891	1.227
438	2.978	1.834	498	1.522	1.301	558	0.094	0.626	618	0.128	0.487	678	0.869	1.174
440	3.014	1.824	500	1.439	1.271	560	0.095	0.604	620	0.119	0.495	680	0.812	1.096
442	3.032	1.800	502	1.373	1.242	562	0.070	0.580	622	0.126	0.499	682	0.741	1.004
444	3.011	1.771	504	1.270	1.222	564	0.053	0.555	624	0.138	0.504	684	0.605	0.893

Multiple-parameters model:

$$a_{ph}(\lambda) = \sum_{j=1}^{l} C_j a_j^*(\lambda_{mj}) \exp\left[\frac{(\lambda - \lambda_{mj})^2}{2\sigma_j^2}\right] \qquad (7)$$

TABLE 2. Input Values and Mean Characteristics of Gaussian Bands Reflecting Absorption by Chlorophylls and Carotenoids

Characteristic	Gaussian Band Number and Associated Pigment Species												
	1 chl *a*	2 chl *a*	3 chl *a*	4 chl *c*	5 chl *b*	6 carot.	7 carot.	8 chl *c*	9 chl *a*	10 chl *c*	11 chl *b*	12 chl *a*	13 chl *a*
Input parameters													
Half width, nm	53.8	21.3	32.1	27.2	45.0	45.4	45.9	46.3	35.0	28.9	24.4	21.6	33.5
Center, nm	384	413	435	461	464	490	532	583	623	644	655	676	700
Output parameters													
Half width, nm	43.2	22.7	34.5	29.3	36.0	46.8	49.6	46.8	38.0	24.9	25.4	24.7	29.0
Center, nm	381.5	410.8	433.5	459.2	466.6	487.8	532.0	585.6	620.6	640.7	652.9	675.6	699.8
Specific absorption coefficient, m^2 (mg pigment)$^{-1}$	0.042	0.019	0.047	0.110	0.115	0.035	0.019	0.044	0.005	0.044	0.029	0.021	0.002

Specific absorption coefficients of each pigment are ratios of Gaussian band absorptions (in reciprocal meters) to high-performance liquid chromatography concentrations (in milligrams per cubic meter) of that pigment. Chl, chlorophyll; Carot., carotenoid.

(Hoepffner and Sathyendranath, 1993)

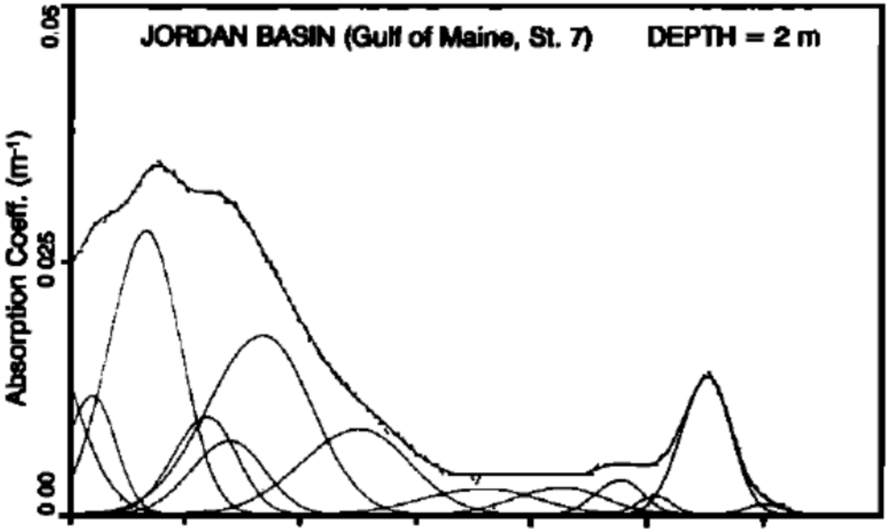

Absorption components: a_{dg} spectrum shapes

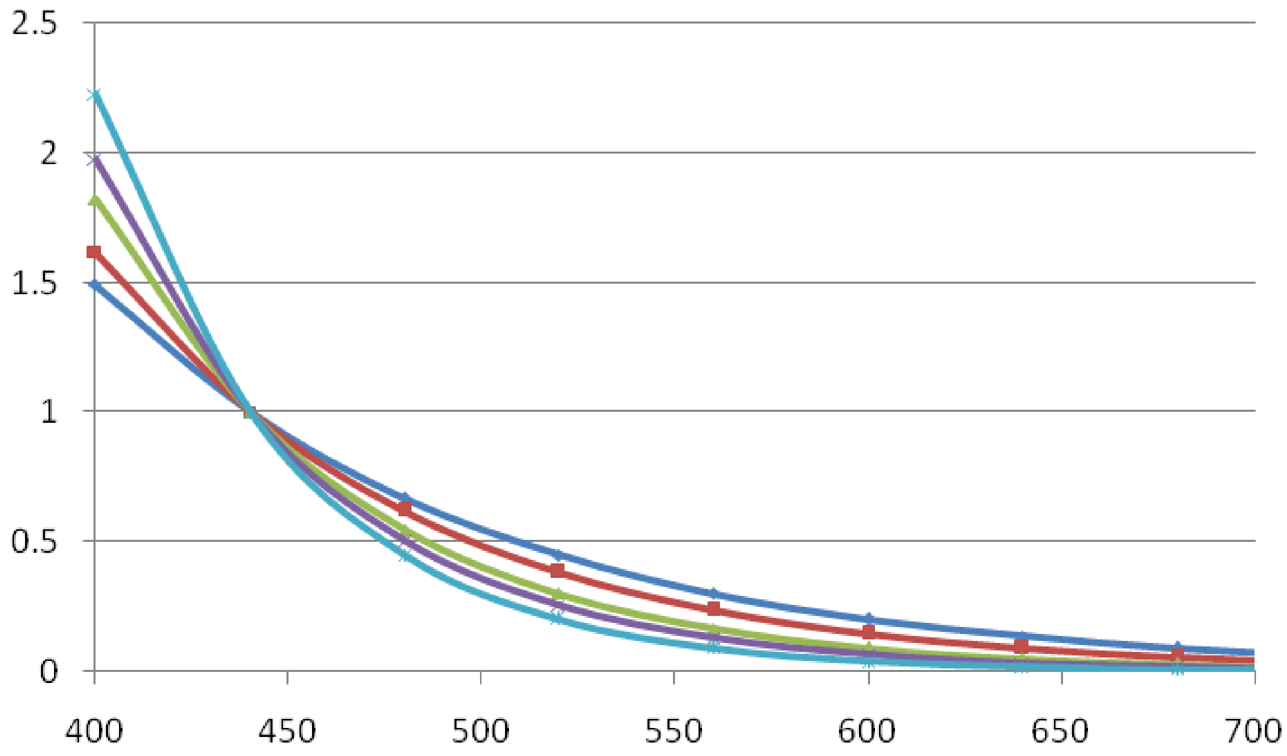

$$\left\langle a_{dg}(\lambda) \right\rangle = e^{-S(\lambda - 440)}$$

S: 0.01 – 0.02 nm^{-1}

(Bricaud et al 1981)

$$\left\langle b_{bp}(\lambda) \right\rangle = \left(\frac{440}{\lambda} \right)^{\eta}$$

$$R_{rs}(\lambda) = G \frac{b_b(\lambda)}{a(\lambda) + b_b(\lambda)}$$

$$R_{rs}(\lambda) = G \frac{b_{bw}(\lambda) + M_3 \langle b_{bp}(\lambda) \rangle}{a_w(\lambda) + M_1 \langle a_{ph}(\lambda) \rangle + M_2 \langle a_{dg}(\lambda) \rangle + b_{bw}(\lambda) + M_3 \langle b_{bp}(\lambda) \rangle}$$

3-variable model to describe an Rrs spectrum

(Sathyendranath et al 1989)

$M_{1\text{-}3}$ are wavelength independent variables.

Then they could be derived by comparing the modeled Rrs spectrum with the measured Rrs spectrum.

Spectral ranges used for solutions (e.g. examples of BUS):

The **blue-green** domain: e.g., Hoge and Lyon (1996), Carder et al (1999)
The **red-infrared** domain: e.g., Binding et al (2012)
The **entire spectrum** (**spectral optimization**): e.g., Bukata et al (1995), Lee et al (1994,1996,1999), Maritorena et al (2002), Boss and Roesler (2006), Brando et al (2012)， Werdell et al (2013)

Look-Up-Tables (LUT): e.g., Carder et al (1991); Mobley et al (2005)

Spectral Optimization

Matching between measured and modeled R_{rs} spectra

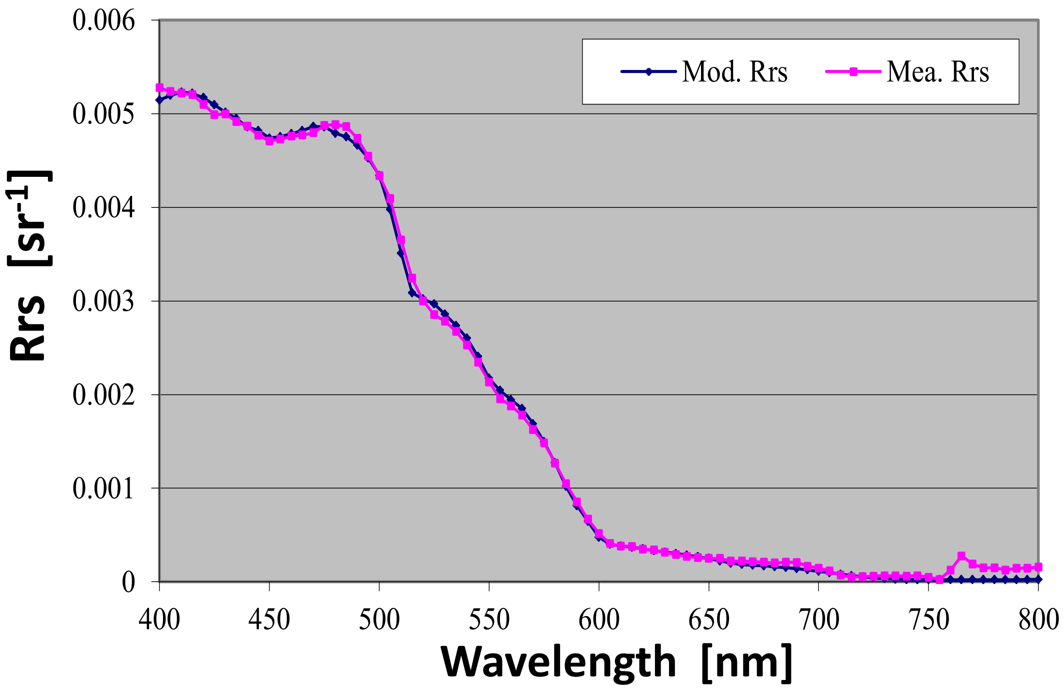

Quantitative measure of the closure (**error function**):

$$\delta_{R_{rs}} = \frac{\sqrt{\Lambda_{\lambda 1}^{\lambda 2}\left(\tilde{R}_{rs}(\lambda) - R_{rs}(\lambda)\right)^2}}{\Lambda_{\lambda 1}^{\lambda 2} R_{rs}(\lambda)} = \sqrt{n}\,\frac{\sqrt{\sum_{\lambda 1}^{\lambda 2}\left(\tilde{R}_{rs}(\lambda) - R_{rs}(\lambda)\right)^2}}{\sum_{\lambda 1}^{\lambda 2} R_{rs}(\lambda)}$$

Logic (assumption) behind SOA:

A unique set of bio-optical properties for each Rrs spectrum.

Algorithms using information in the red-infrared bands

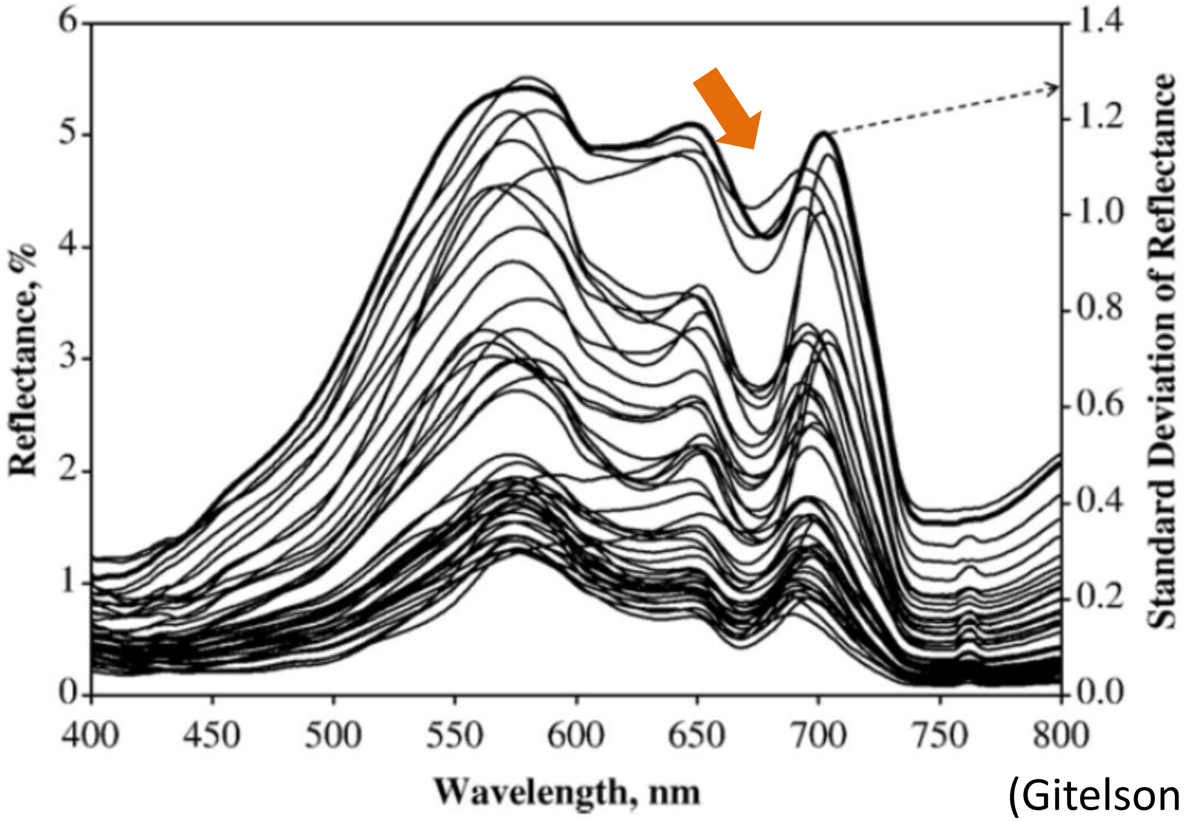

(Gitelson et al 2007)

Two bands

$$Chl = f\left(\frac{Rrs(75x)}{Rrs(67x)}\right)$$

Three bands

$$Chl = f\left(\frac{Rrs(75x)}{Rrs(67x)} - \frac{Rrs(75x)}{Rrs(70x)}\right)$$

a_{ph}

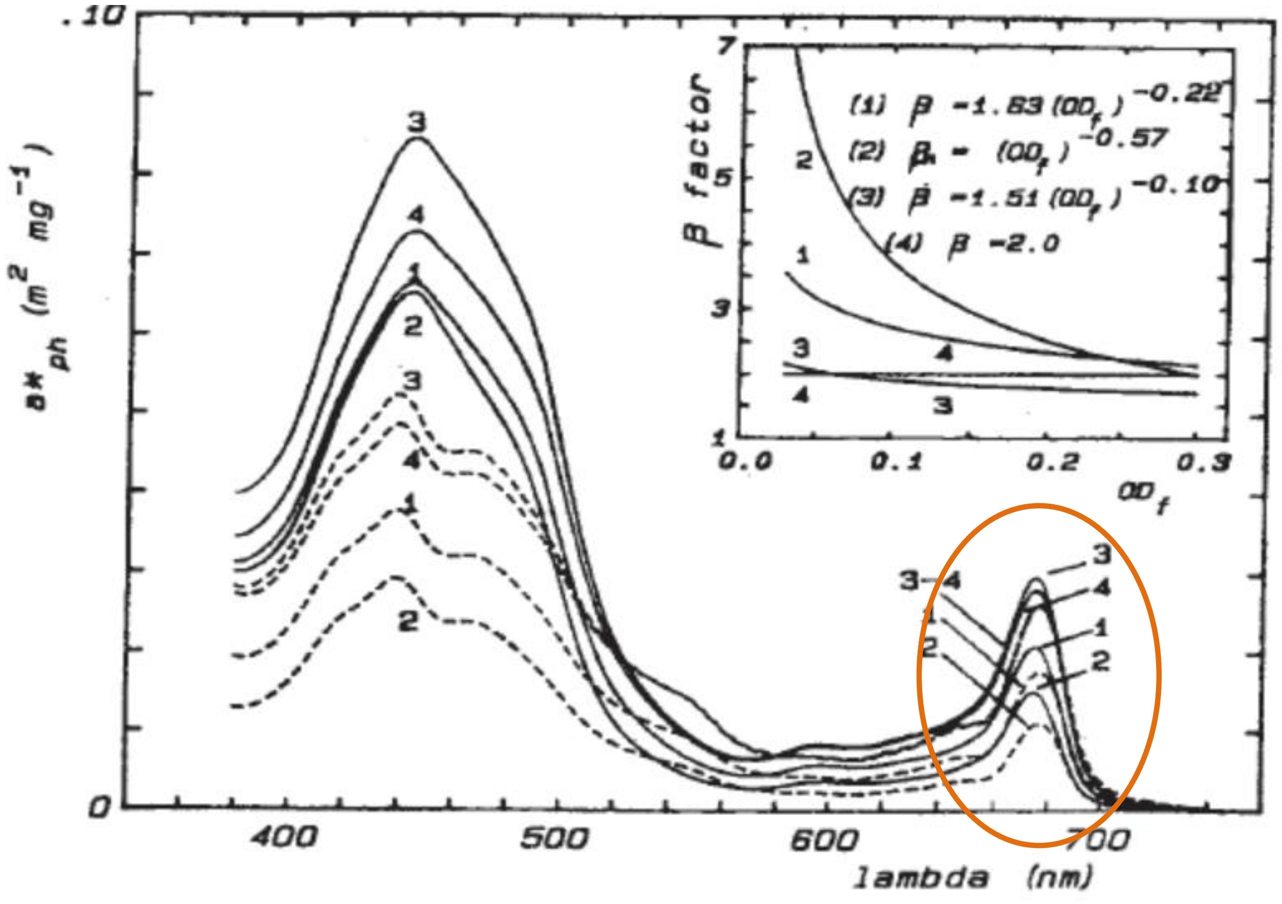

.10
0
400
500
600
700
lambda (nm)
a*ph (m2 mg-1)
β factor
OD f
0.0
0.1
0.2
0.3
(1) β =1.83 (OD f) -0.22
(2) β = (OD f) -0.57
(3) β =1.51 (OD f) -0.10
(4) β =2.0

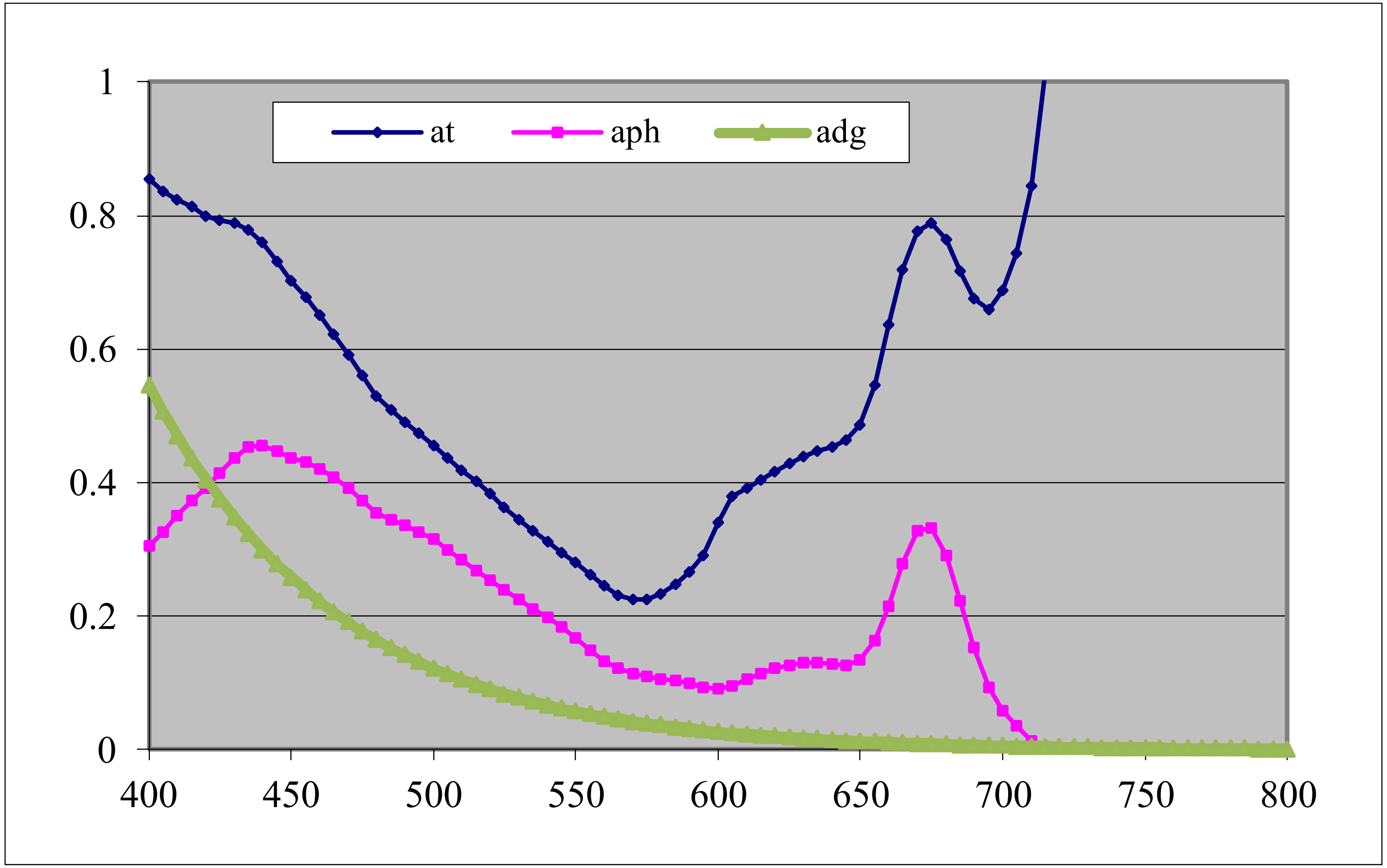
1
0.8
0.6
0.4
0.2
0
400
450
500
550
600
650
700
750
800
at
aph
adg

$$R_{rs}(\lambda) = G\frac{b_{bw}(\lambda) + M_3\left\langle b_{bp}(\lambda)\right\rangle}{a_w(\lambda) + M_1\left\langle a_{ph}(\lambda)\right\rangle + M_2\left\langle a_{dg}(\lambda)\right\rangle + b_{bw}(\lambda) + M_3\left\langle b_{bp}(\lambda)\right\rangle}$$

$$R_{rs}(\lambda) \approx G\frac{M_3\left\langle b_{bp}(\lambda)\right\rangle}{a_w(\lambda) + M_1\left\langle a_{ph}(\lambda)\right\rangle}$$

$$\frac{R_{rs}(\lambda_{red1})}{R_{rs}(\lambda_{red2})} = \frac{\left\langle b_{bp}(\lambda_{red1})\right\rangle}{\left\langle b_{bp}(\lambda_{red2})\right\rangle}\frac{a_w(\lambda_{red2}) + M_1\left\langle a_{ph}(\lambda_{red2})\right\rangle}{a_w(\lambda_{red1}) + M_1\left\langle a_{ph}(\lambda_{red1})\right\rangle}$$

Proper contrast of Rrs at λ_1 and λ_2 then leads to M_1.

2. Top-down strategy (TDS):

$$R_{rs} = G\frac{b_b}{a+b_b}$$

$$\boldsymbol{R_{rs} \rightarrow b_b \& a \rightarrow a_x}$$

$$\Downarrow$$

Clarity (Secchi depth, light depth, SPM, etc)

Remote sensing measures the *total* effect:

Water clarity (or turbidity) is also a measure of total effect.

Examples of TDS:

Loisel & Stramski (2000), QAA (Lee et al, 2002); Smyth et al (2006); Doran et al (2007).

The Quasi-Analytical Algorithm (QAA)

Forward modeling:

$(a, b_b, \text{etc}) \Longrightarrow Rrs$

$$R_{rs} \approx 0.05 \frac{b_b}{a + b_b}$$

QAA:

$(a, b_b) \Longleftarrow Rrs$

The data flow of QAA:

$$r_{rs}(\lambda)$$

$$\boxed{\eta}$$

$$\boxed{a(\lambda_0) = a_w(\lambda_0) + \Delta a(\lambda_0)}$$

$$b_{bp}(\lambda_0) = \mathrm{F}_2\left(r_{rs}(\lambda_0), \boxed{a(\lambda_0)}, b_{bw}(\lambda_0)\right)$$

$$b_{bp}(\lambda) = b_{bp}(\lambda_0)\left(\frac{\lambda_0}{\lambda}\right)^{\boxed{\eta}}$$

$$a(\lambda) = \mathrm{F}_3\left(r_{rs}(\lambda), b_{bp}(\lambda), b_{bw}(\lambda)\right)$$

$$\begin{cases} a(411) = a_w(411) + \boxed{\zeta}\, a_{ph}(443) + \boxed{\xi}\, a_{dg}(443) \\ a(443) = a_w(443) + a_{ph}(443) + a_{dg}(443) \end{cases}$$

$$\zeta = \frac{a_{ph}(411)}{a_{ph}(443)}$$

$$\xi = \frac{a_{dg}(411)}{a_{dg}(443)}$$

(Lee et al 2002)

Logic behind QAA (and its updated versions):

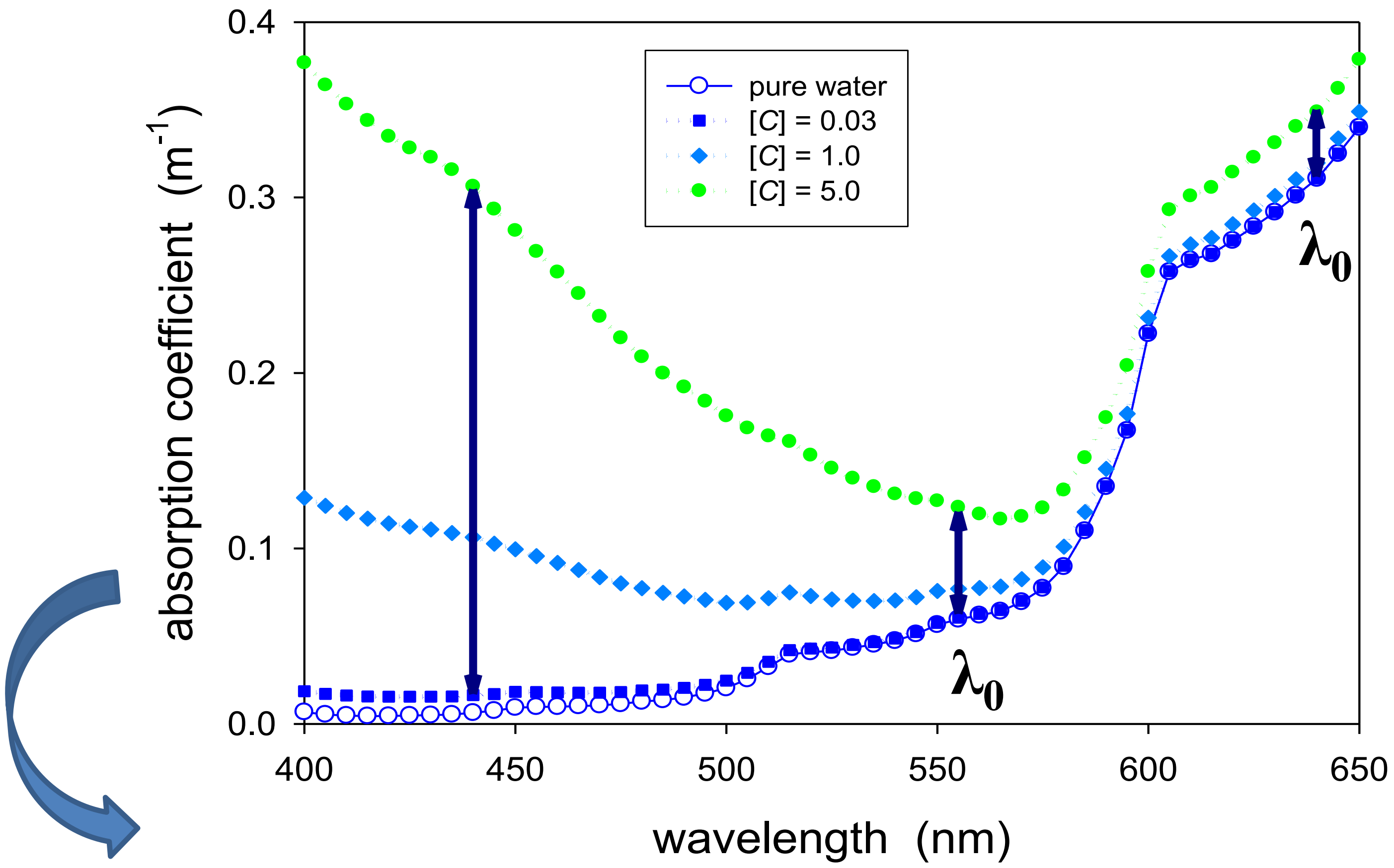

For a reference wavelength, λ_0, variation of $a(\lambda_0)$ is limited.

Known $a(\lambda_0)$, enables calculation of $b_b(\lambda_0)$ from $R_{rs}(\lambda_0)$; propagate $b_b(\lambda_0)$ to $b_b(\lambda)$, then enables calculation of $a(\lambda)$ from $R_{rs}(\lambda)$.

No need of spectral model of $a_x(\lambda)$ in this process!

When 550 nm as the reference wavelength (λ_0)

$$a(550) = a_w(550) + 10^{-1.146-1.366\chi-0.469\chi^2}$$

$$\chi = \log\left(\frac{r_{rs}(443) + r_{rs}(490)}{r_{rs}(\lambda_0) + 5\,\frac{r_{rs}(667)}{r_{rs}(490)}\,r_{rs}(667)}\right)$$

$a_w(550) = 0.0565\ \text{m}^{-1}$

Empirical!

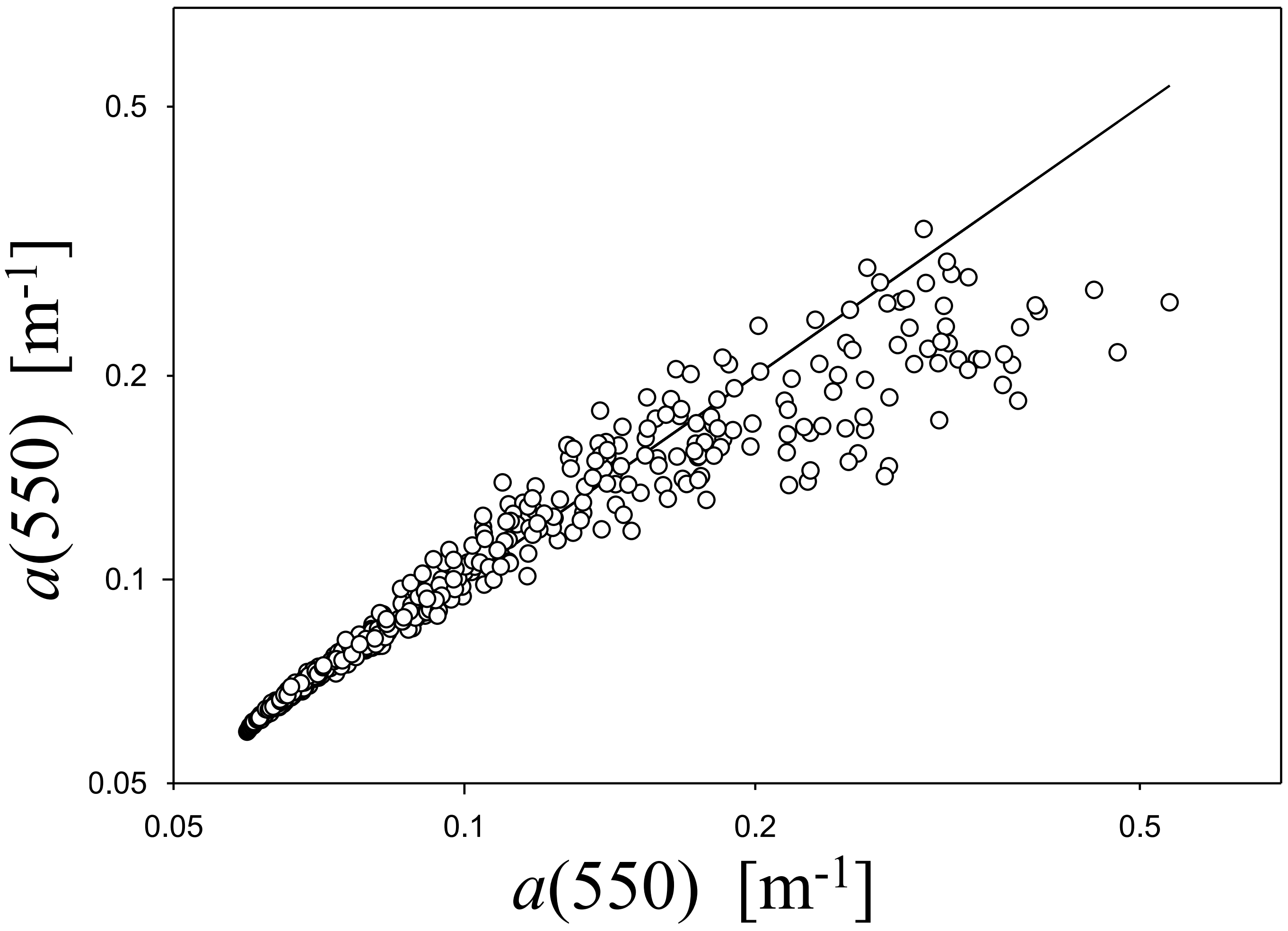

0.5
0.2
0.1
0.05
0.05
0.1
0.2
0.5
a(550) [m-1]
a(550) [m-1]

Invert Rrs:

$$R_{rs} \Rightarrow r_{rs} \Rightarrow \{a \& b_b\}$$

$r_{rs}(\lambda) = R_{rs}(\lambda)/(0.52 + 1.7\, R_{rs}(\lambda))$

$$r_{rs} = g_0\left(\frac{b_b}{a+b_b}\right) + g_1\left(\frac{b_b}{a+b_b}\right)^2$$

$g_0=0.089, g_1=0.125$

$$u(\lambda) = \frac{b_b(\lambda)}{a(\lambda)+b_b(\lambda)} = \frac{-g_0 + \sqrt{(g_0)^2 + 4g_1 * r_{rs}(\lambda)}}{2g_1}$$

$$a(550) = a_w(550) + 10^{-1.146 - 1.366\,\chi - 0.469\,\chi^2}$$

$$\Rightarrow \quad b_{bp}(550) = \frac{u(550)\,a(550)}{1 - u(550)} - b_{bw}(550)$$

$$b_{bp}(\lambda) = b_{bp}(550)\left(\frac{550}{\lambda}\right)^{\eta}$$

Empirical:

$$\eta = 2.0\left(1 - 1.2\ \exp\left(-0.9\frac{r_{rs}(443)}{r_{rs}(55x)}\right)\right)$$

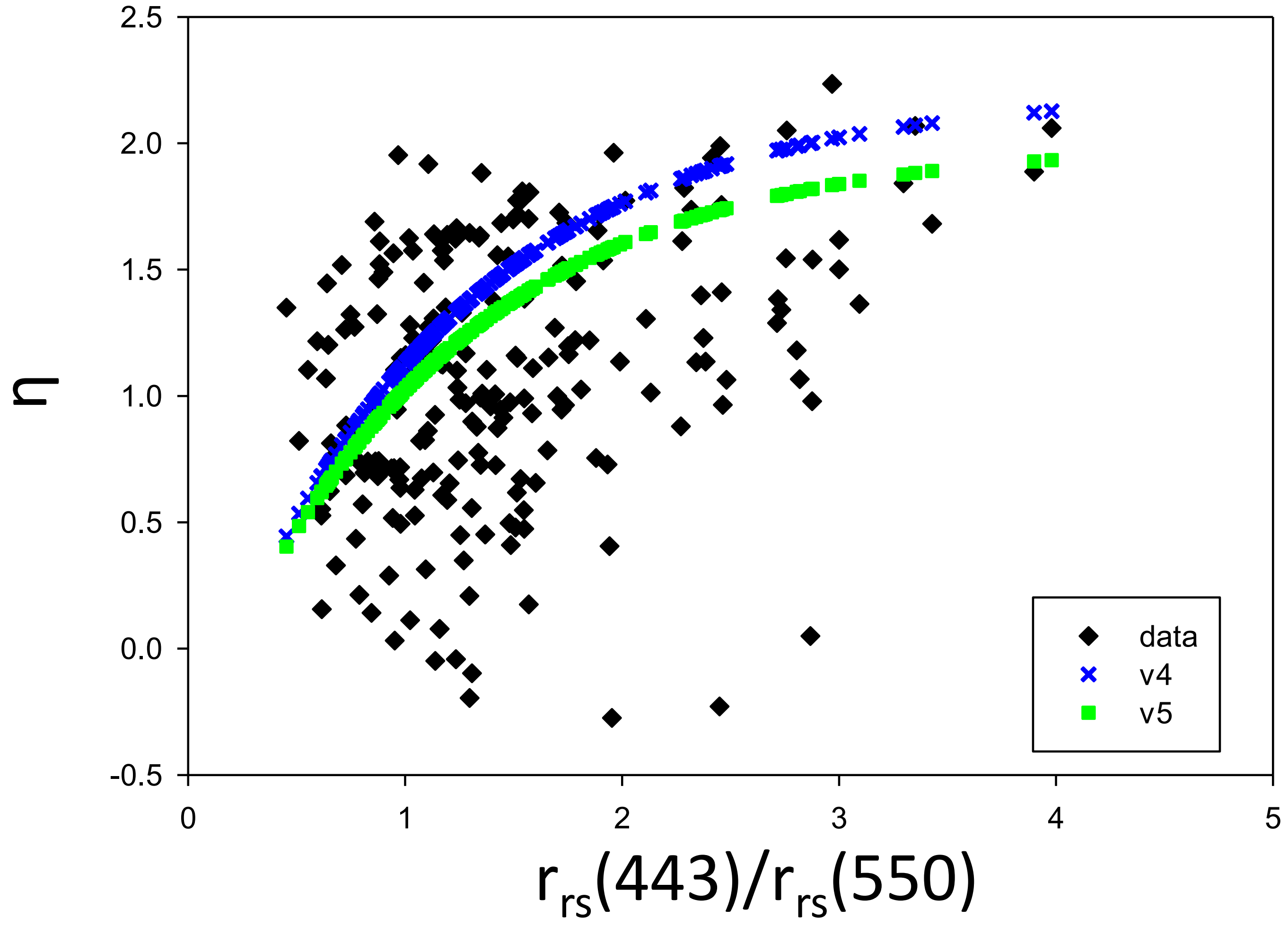

$$b_b(\lambda) = b_{bw}(\lambda) + b_{bp}(\lambda)$$

$$a(\lambda) = \frac{(1 - u(\lambda))\, b_b(\lambda)}{u(\lambda)}$$

$$a(\lambda) = a_w(\lambda) + a_{ph}(\lambda) + a_{dg}(\lambda)$$

$$\begin{cases} a(410) = a_w(410) + a_{ph}(410) + a_{dg}(410), \\ a(440) = a_w(440) + a_{ph}(440) + a_{dg}(440). \end{cases}$$

$$\zeta = \frac{a_{ph}(410)}{a_{ph}(440)} \qquad \xi = \frac{a_{dg}(410)}{a_{dg}(440)}$$

$$\begin{cases} a(410) = a_w(410) + \zeta\, a_{ph}(440) + \xi\, a_{dg}(440), \\ a(440) = a_w(440) + a_{ph}(440) + a_{dg}(440). \end{cases}$$

$$\begin{cases} a(410) = a_w(410) + \zeta\, a_{ph}(440) + \xi\, a_{dg}(440), \\ a(440) = a_w(440) + a_{ph}(440) + a_{dg}(440). \end{cases}$$

$$\begin{cases} a_g(440) = \dfrac{\big(a(410) - \zeta\, a(440)\big) - \big(a_w(410) - \zeta\, a_w(440)\big)}{\xi - \zeta}, \\ a_{ph}(440) = a(440) - a_w(440) - a_{dg}(440). \end{cases}$$

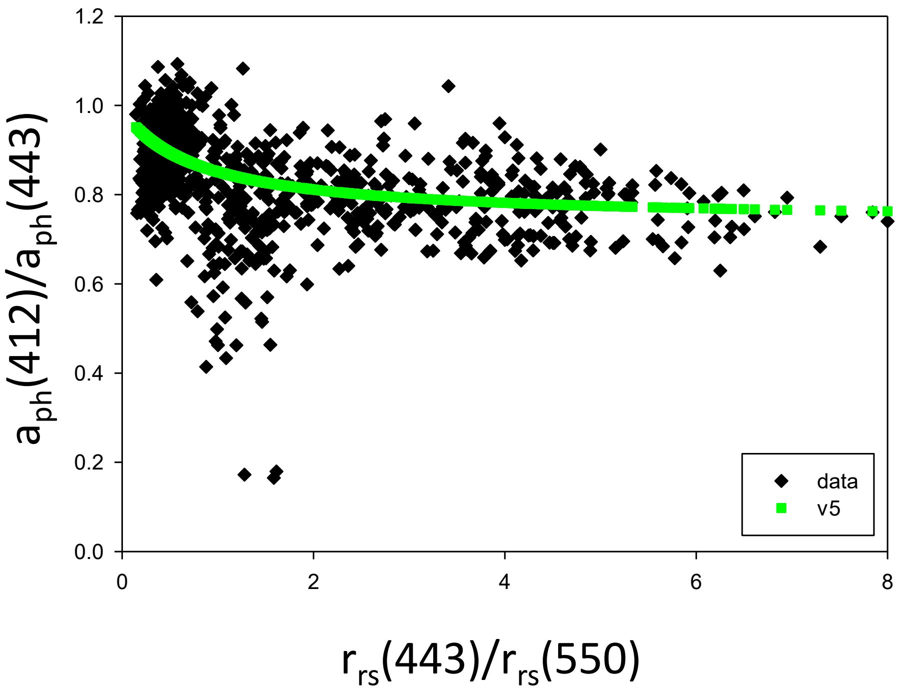

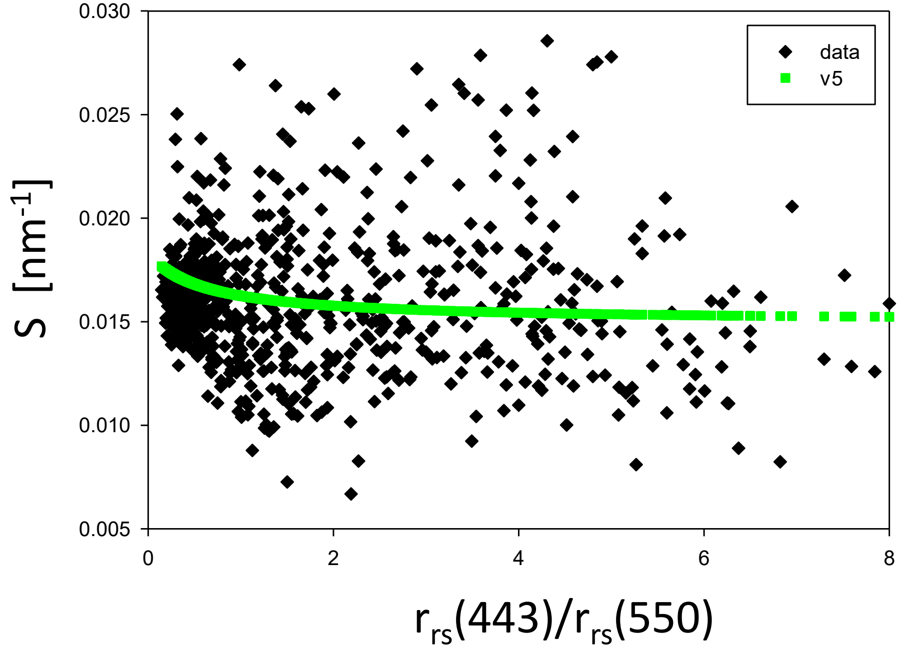

$$\zeta = 0.74 + \frac{0.2}{0.8 + r_{rs}(443)/r_{rs}(550)}$$

$$\xi = e^{S(443-411)},$$

$$S = 0.015 + \frac{0.002}{0.6 + r_{rs}(443)/r_{rs}(550)}$$

Empirical!

Ensemble solutions:

Wang et al. 2006; Zheng et al. 2015

$$a(\lambda) = a_w(\lambda) + \mathrm{M}_1 \left\langle a_{ph}(\lambda) \right\rangle + M_2 \left\langle a_{dg}(\lambda) \right\rangle$$

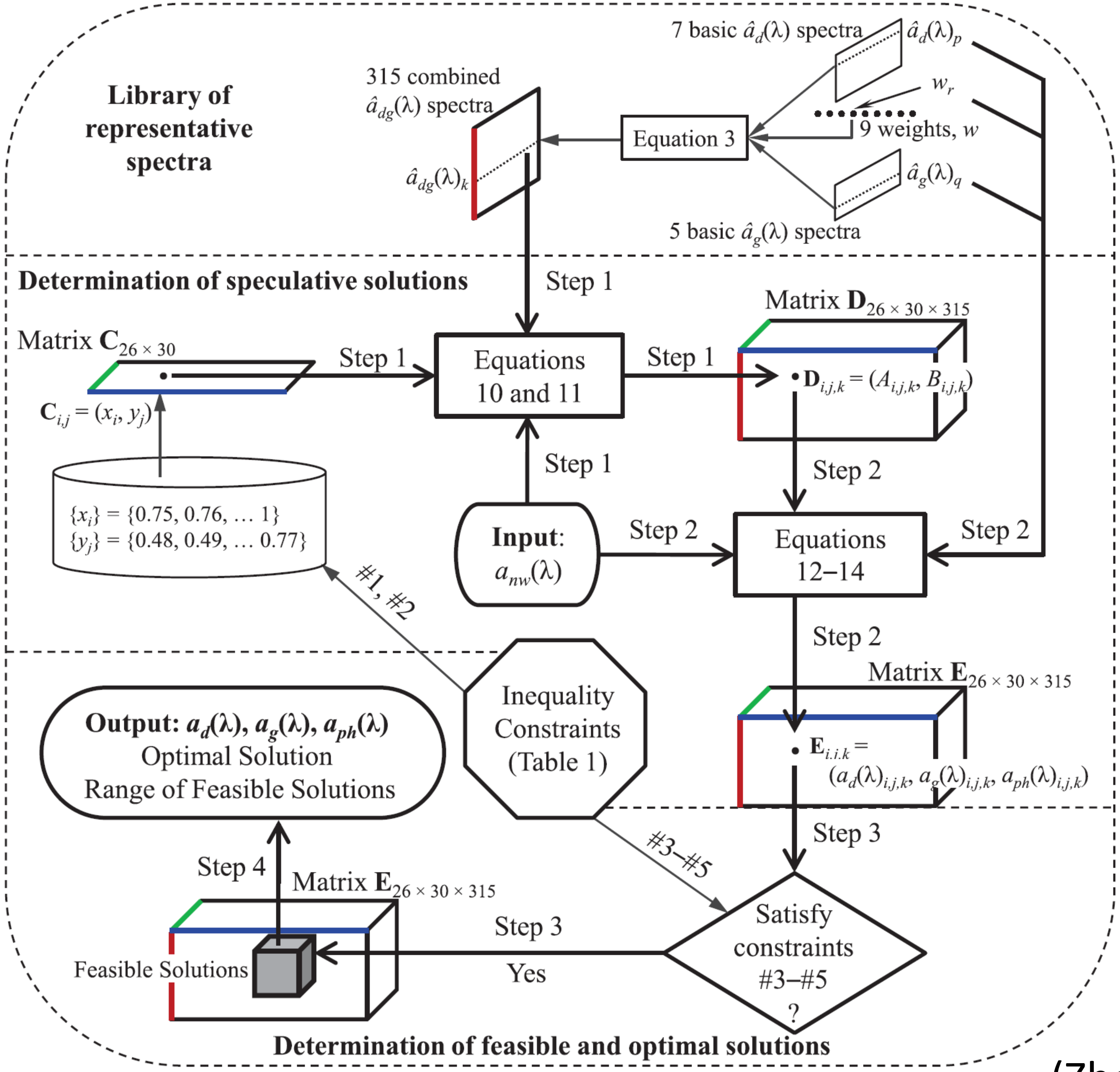

(Zheng et al. 2015)

What is band-ratio derived [Chl]?

$$[Chl] = f_1\left(R_{rs}(\lambda_i)/R_{rs}(\lambda_j)\right)$$

$$R_{rs}(\lambda_i)/R_{rs}(\lambda_j) = f_2\left(\frac{b_{bw}(\lambda_i)+b_{bp}(\lambda_i)}{b_{bw}(\lambda_j)+b_{bp}(\lambda_j)}\,\frac{a_w(\lambda_j)+a_{ph}(\lambda_j)+a_{dg}(\lambda_j)}{a_w(\lambda_i)+a_{ph}(\lambda_i)+a_{dg}(\lambda_i)}\right)$$

[Chl] is actually an IOP product

Key Points:

1. Various inversion algorithms for IOPs have been developed; but more/better ones are also expected.

2. BUS derives every component first, then (simultaneously) derives the total optical property.

Assume the spectral shapes of the optically active components are well characterized!
BUS relies more on the accuracy of forward bio-optical model.

3. TDS derives total first, then decompose to separate components.

TDS relies more on the accuracy of Rrs measurement.

II. Applications of inverted IOPs

$Rrs(\lambda) \Rightarrow$ **IOPs**

What to do with the retrieved IOPs?

Traditional strategy: [chl] centered system

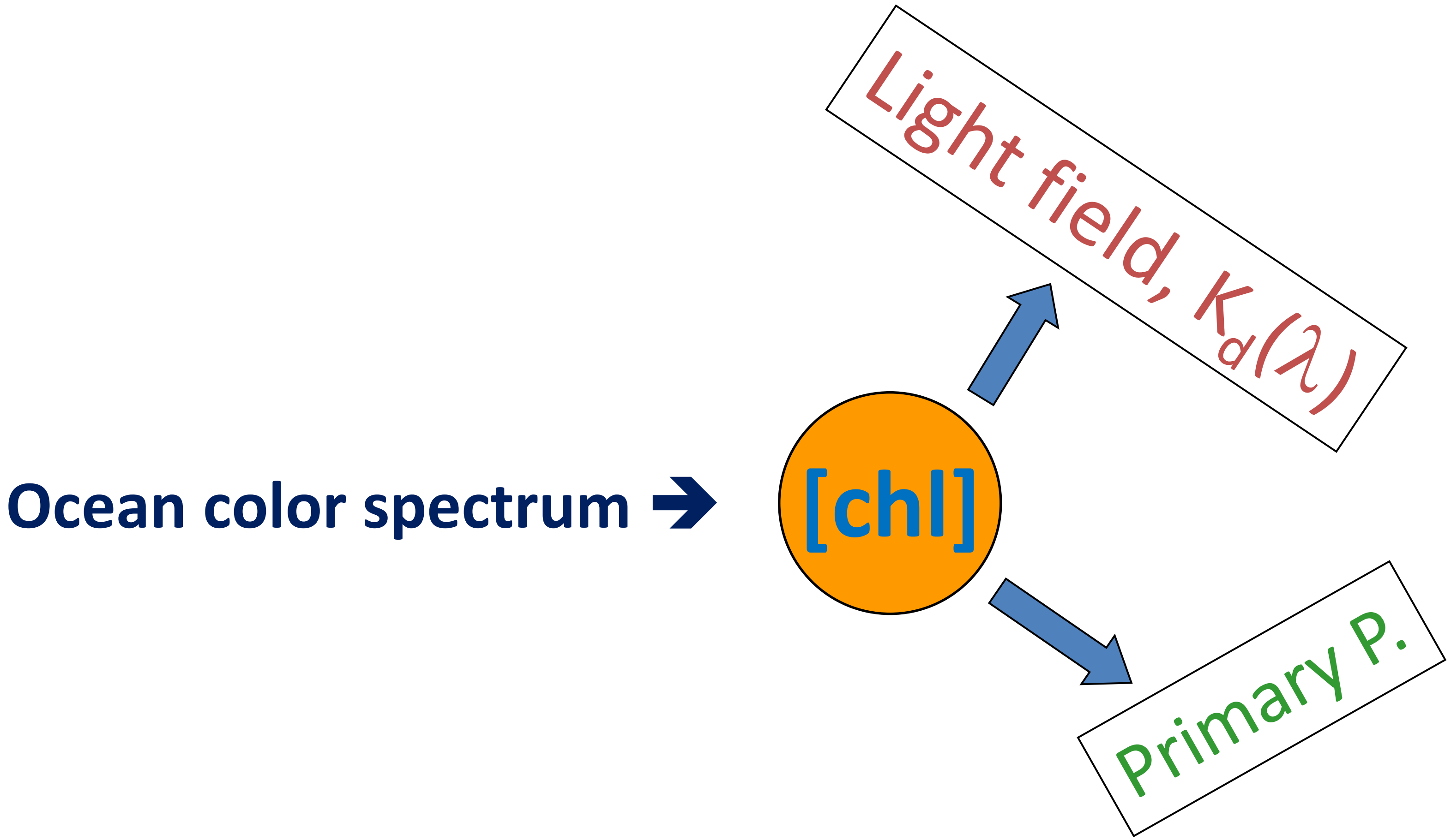

Works for waters where IOPs co-vary with [Chl].

Application examples of IOP products

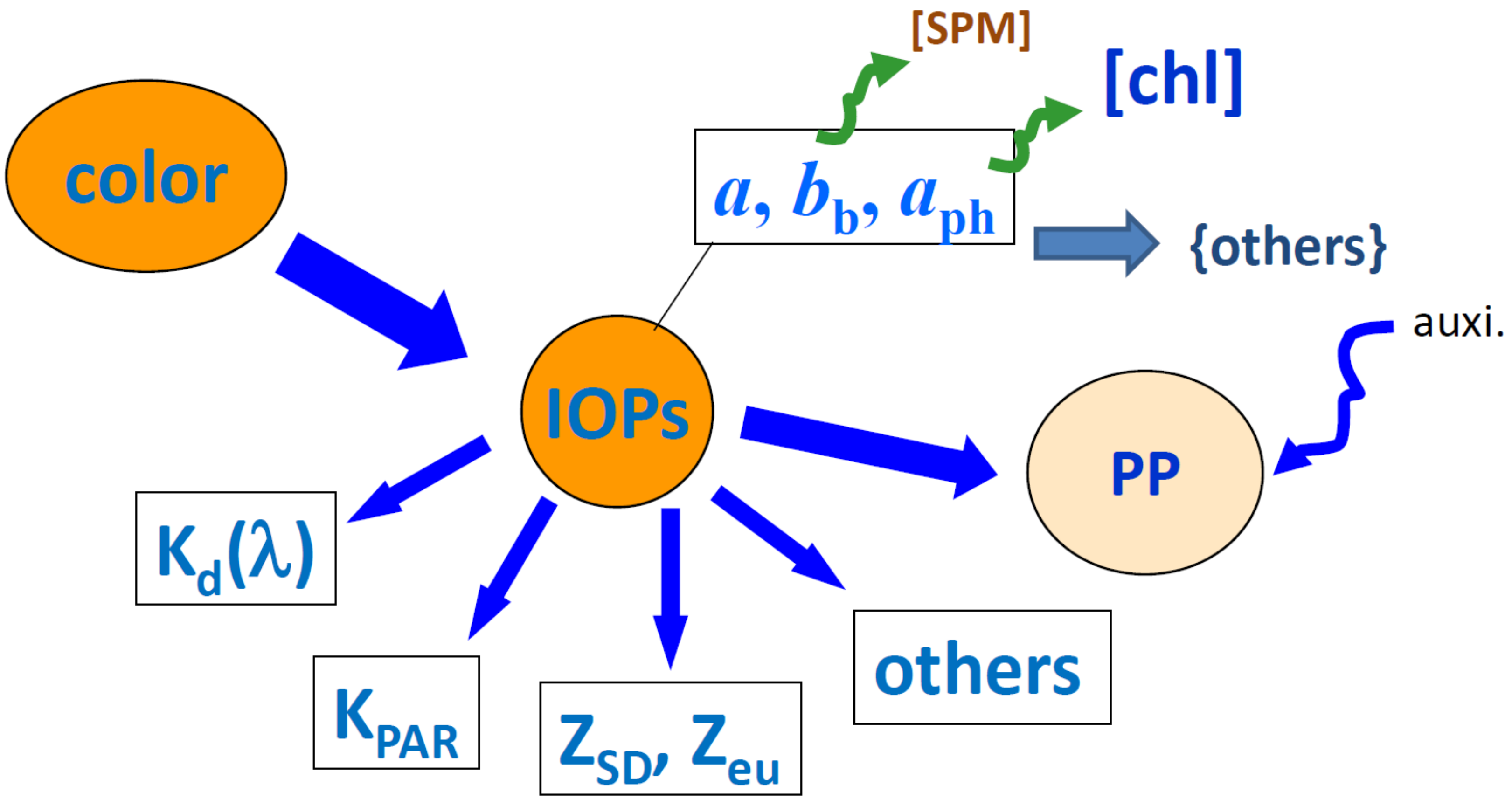

No division of "Case-1" vs "Case-2" waters.

1. Estimation of diffuse attenuation coefficient ($K_d(\lambda)$)

2. Estimation of Kd(PAR) and euphotic-zone depth

3. Estimation of water clarity (Secchi disk depth)

4. Estimation of primary production

5. A few other examples

1. Estimation of diffuse attenuation coefficient ($K_d(\lambda)$)

Traditionally,

$$K_d(490) = A\left(\frac{L_w(\lambda_{blue})}{L_w(\lambda_{green})}\right)^B$$

Austin and Petzold （1981）

Or,

$$\mathrm{K_d}(\lambda, [\mathrm{Chl}]) = \mathrm{K_w}(\lambda) + \chi(\lambda)[\mathrm{Chl}]^{\mathrm{e}(\lambda)} \quad (2)$$

(Morel and Maritorena 2001)

For “Case-1” waters

$$\log_{10}(K_{bio}(490)) = a_0 + \sum_{i=1}^{4} a_i \log_{10}\left(\frac{R_{rs}(\lambda_{\text{blue}})}{R_{rs}(\lambda_{\text{green}})}\right)$$

$$Kd\_490 = K_{bio}(490) + 0.0166$$

$$log_{10}(chlor\_a) = a_0 + \sum_{i=1}^{4} a_i log_{10}\left(\frac{R_{rs}(\lambda_{blue})}{R_{rs}(\lambda_{green})}\right)^i,$$

$Rrs(\lambda_{blue}) = Rrs(443) > Rrs(486)$

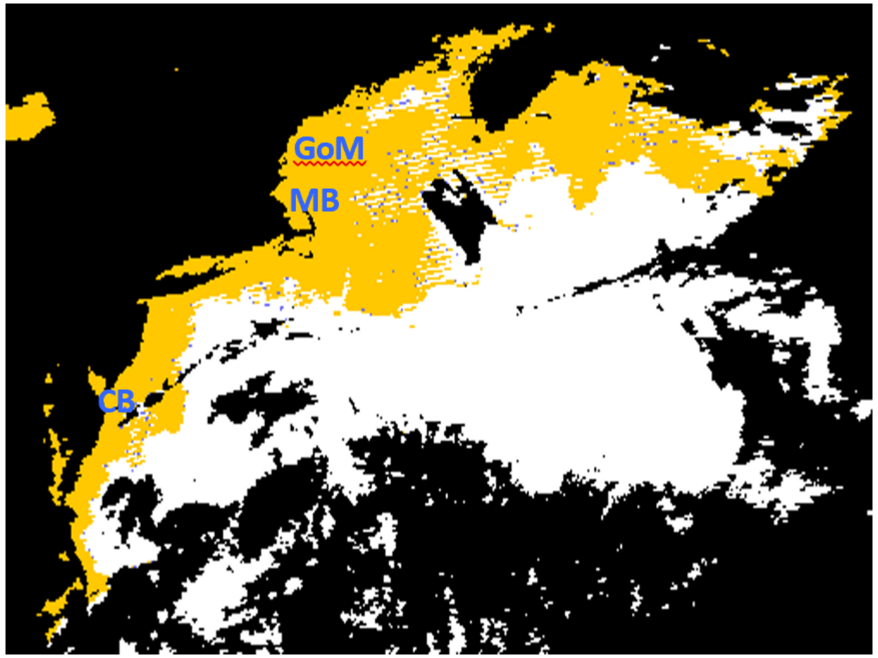

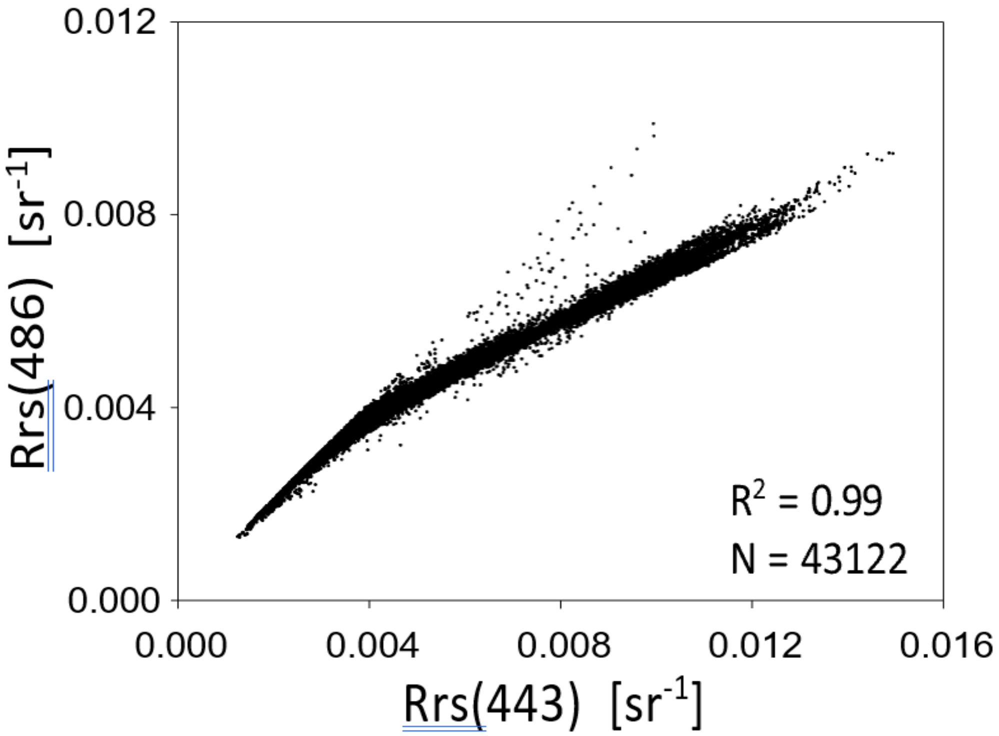

The standard $K_d(490)$ and Chl products are 100% co-vary in coastal waters; further

$$K_d(490) = Fun\left(\frac{R_{rs}(490)}{R_{rs}(555)}\right)$$

AOP: sun angle dependent

Nearly independent of sun angle.

The two sides do not match in optical nature.

In addition, ratio-derived K_d has large uncertainties or errors in coastal waters.

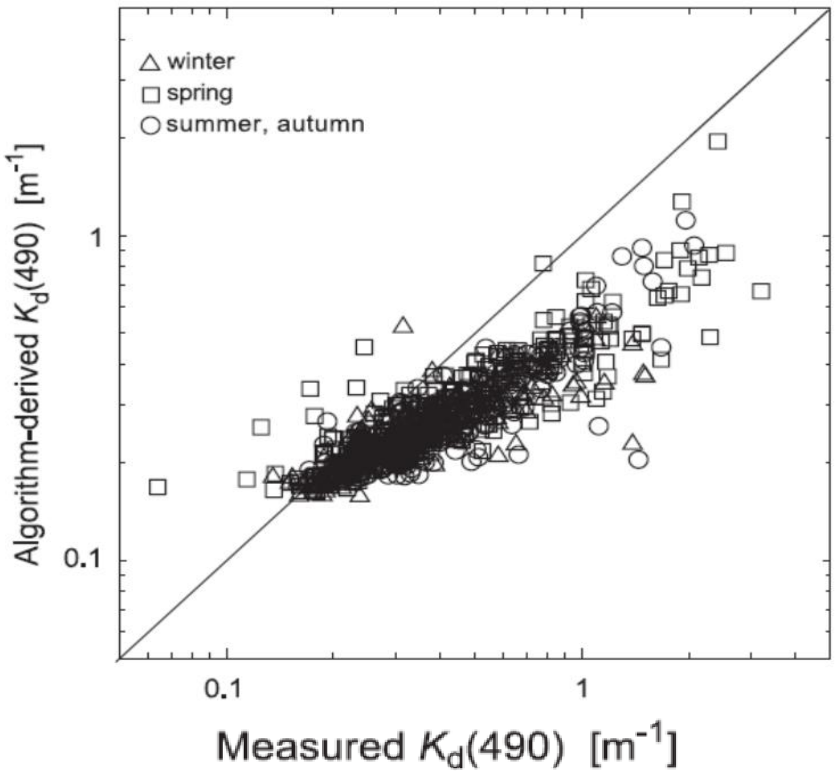

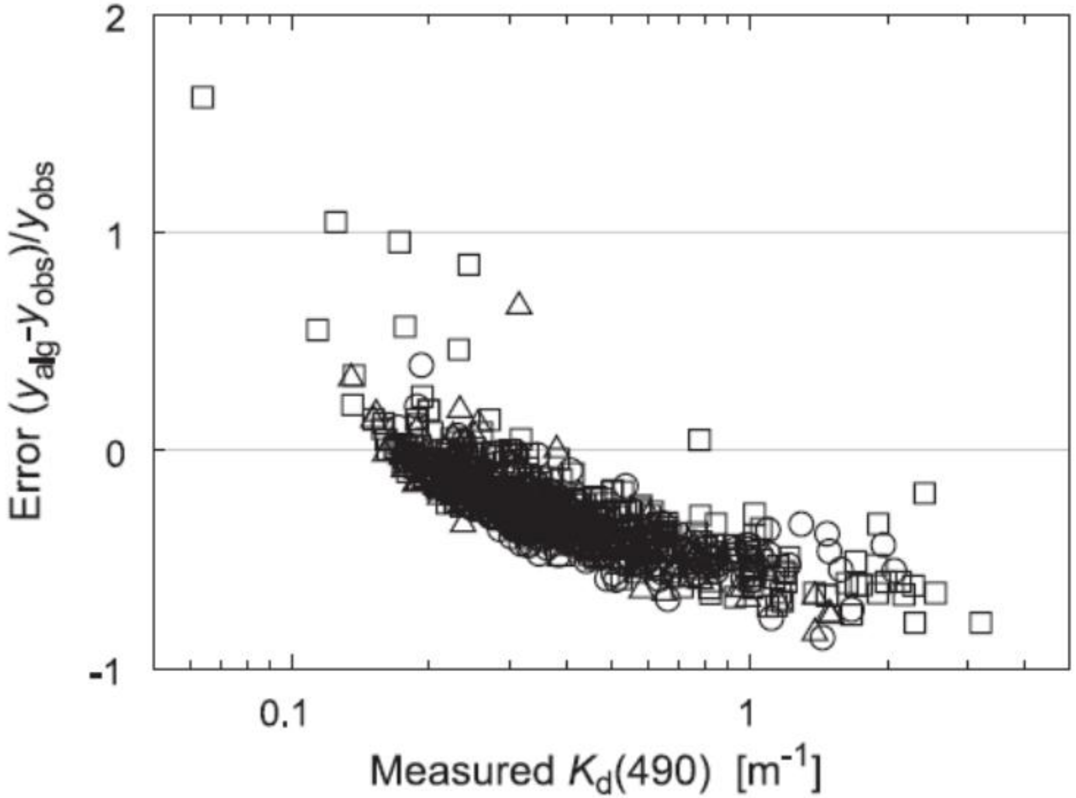

(Darecki and Stramisk, 2004)

IOPs-based system:

$$K_d = \mathrm{m}_0\, a + \mathrm{v}\ b_b$$

$$\mathrm{v} = m_1(1 - m_2 e^{-m_3 a})$$

($m_{0,1,2}$ are wavelength independent)

No division of “Case 1” vs “Case 2” waters.

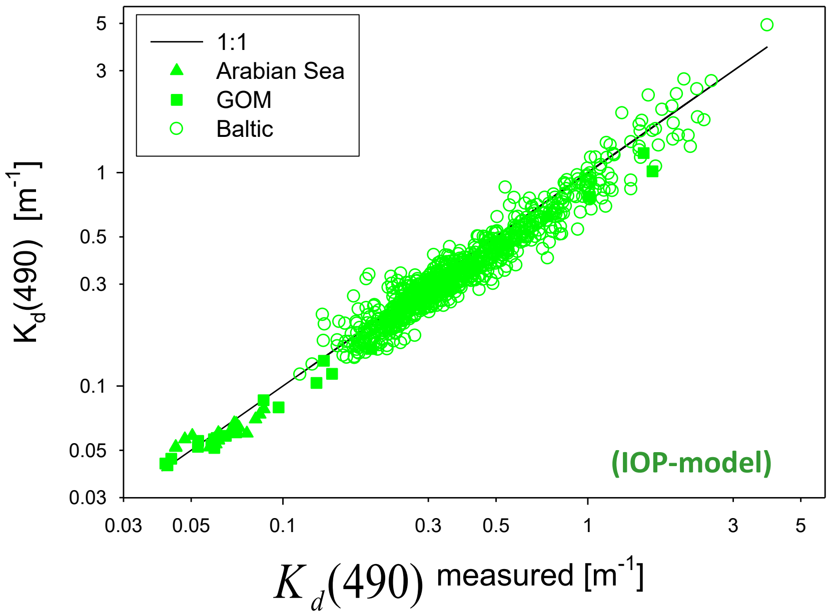

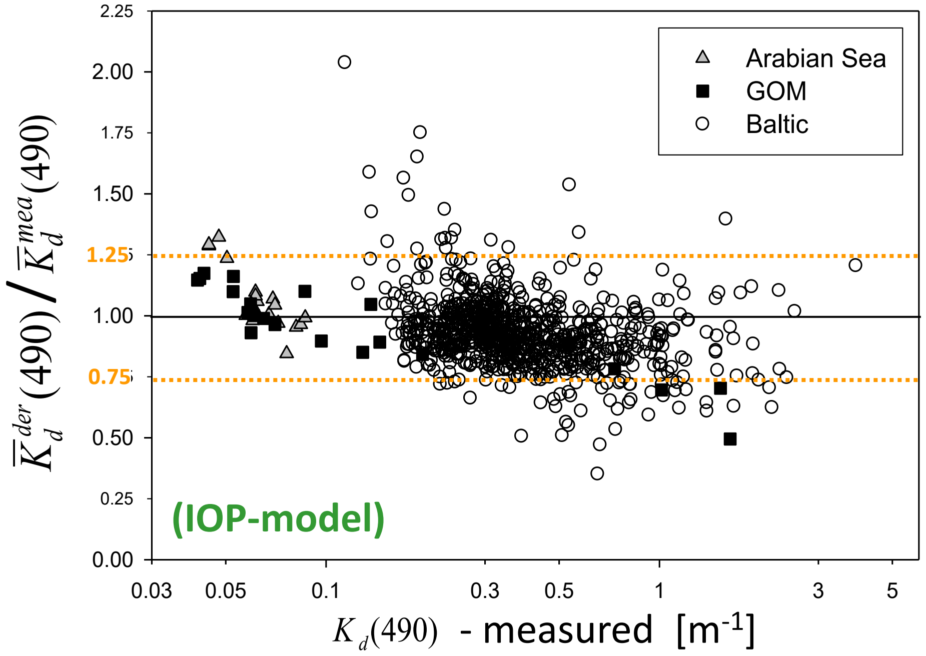

Oceanic & Coastal waters

(*Lee et al. 2005*)

hyperspectral

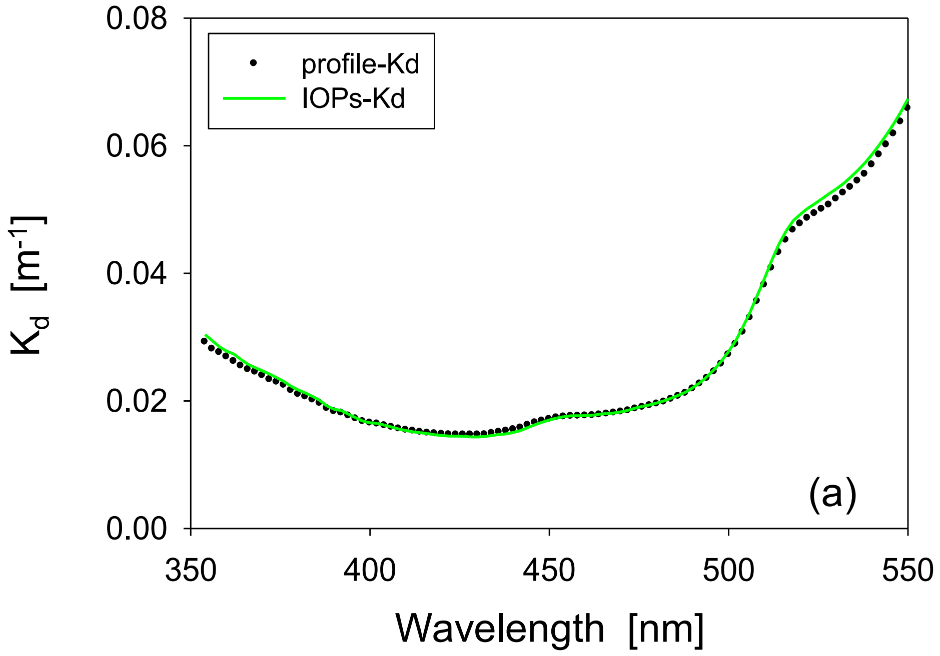

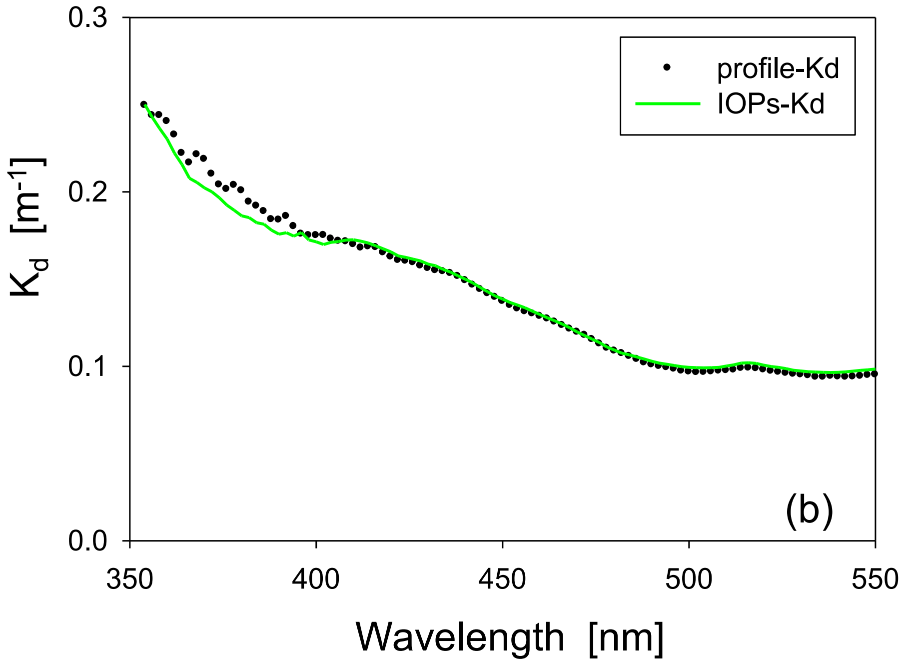

(Lee et al. 2013)

Through a semi-analytical system, a K_d spectrum, not at a single band, can be derived.

2. Estimation of K_{PAR} and euphotic depth

$$PAR(z) = PAR(0)\, e^{-K_{PAR}\, z}$$

$$K_{PAR} = K_w + k_c C + K_x$$

Good for earlier days,
Not so good for the 21st century

hence of K_{PAR}.

1. K_w is a value averaged over the whole spectrum. It is computed for a layer extending from zero to a certain depth Z within an ideally optically pure ocean. When computing this depth-averaged value, denoted $\bar{K}_w(0, Z)$, the spectral distribution of the light at the surface, $E_0(\lambda)$, and at the depth Z, $E_z(\lambda)$, intervenes according to

$$\bar{K}_w(0, Z) = -Z^{-1} \log \left\{ \int_{400}^{700} E_0(\lambda) \exp\left[-K_w(\lambda) Z\right] d\lambda \Big/ \int_{400}^{700} E_0(\lambda)\, d\lambda \right\} \quad (7)$$

In other words, $\bar{K}_w(0, Z)$ is no longer a constant as soon as it is computed for a layer of variable thickness. When Z increases, the remnant light tends to become monochromatic, with the irradiance maximum centered on the minimum of K_w, and the averaged value $\bar{K}_w(0, Z)$ decreases accordingly (see Figure 4; $E_0(\lambda)$ is taken from Figure 8).

2. The constant coefficient k_c is also a doubly averaged value, over the spectrum and over the layer considered. The result of such averaging depends on the spectral composition of the underwater light and on its change with depth. Since the phytoplankton concentration depicted by C governs both

(Morel, 1988, JGR)

$$K_{PAR} = \frac{-1}{z} \ln\left(\frac{PAR(z)}{PAR(0)}\right) \qquad PAR(z) = \int_{400}^{700} E_0(\lambda,0)\, e^{-K(\lambda,z)z} d\lambda$$

K_{PAR} is light-quality weighted.

Change of light with depth:

(Kirk 1994)

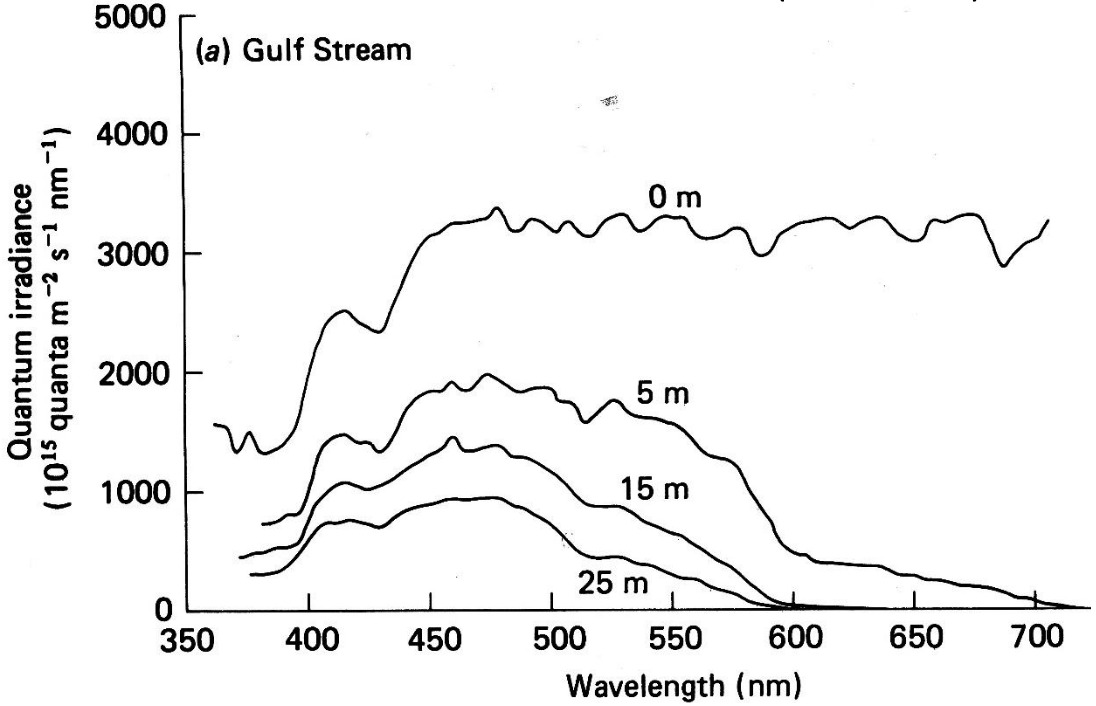

➔ Light at deeper depth is associated with lower attenuation coefficient

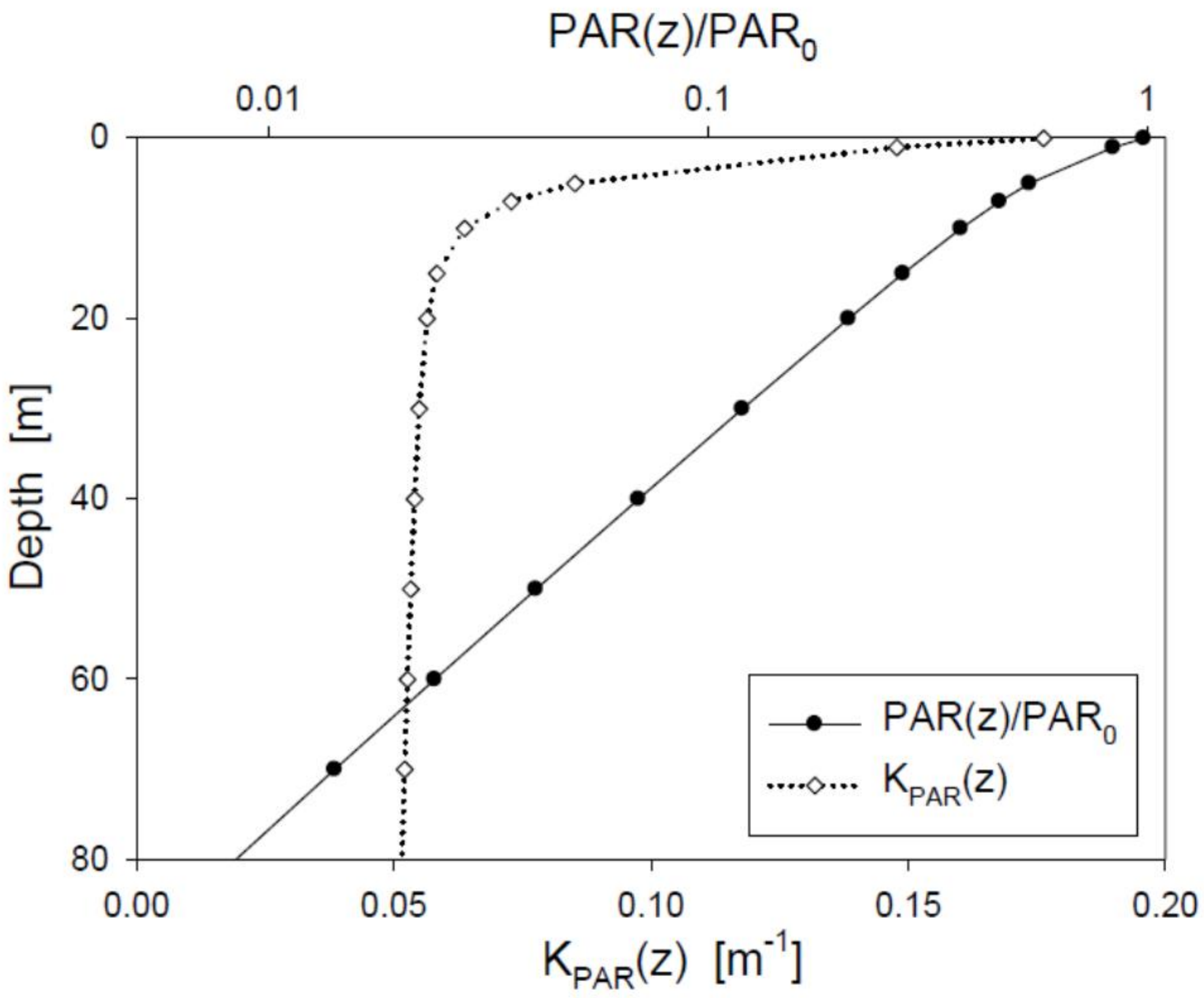

PAR(z)/PAR0
0.01
0.1
1
0
20
40
60
80
Depth [m]
PAR(z)/PAR0
KPAR(z)
0.00
0.05
0.10
0.15
0.20
KPAR(z) [m-1]

$$PAR(z) = PAR(0)\, e^{-K_{par}(z)\, z}$$

$$K_{PAR}(z) \approx K_1 + \frac{K_2}{(1+z)^{0.5}}$$

$$K_1 = f_1(a(490), b_b(490) \qquad K_2 = f_2(a(490), b_b(490)$$

Key:

K_{PAR} varies with depth, especially in the upper water column!

Euphotic depth (z_{eu}), based on 1% definition:

$$z_{eu} = \frac{4.6}{K_{PAR}(z_{eu})}$$

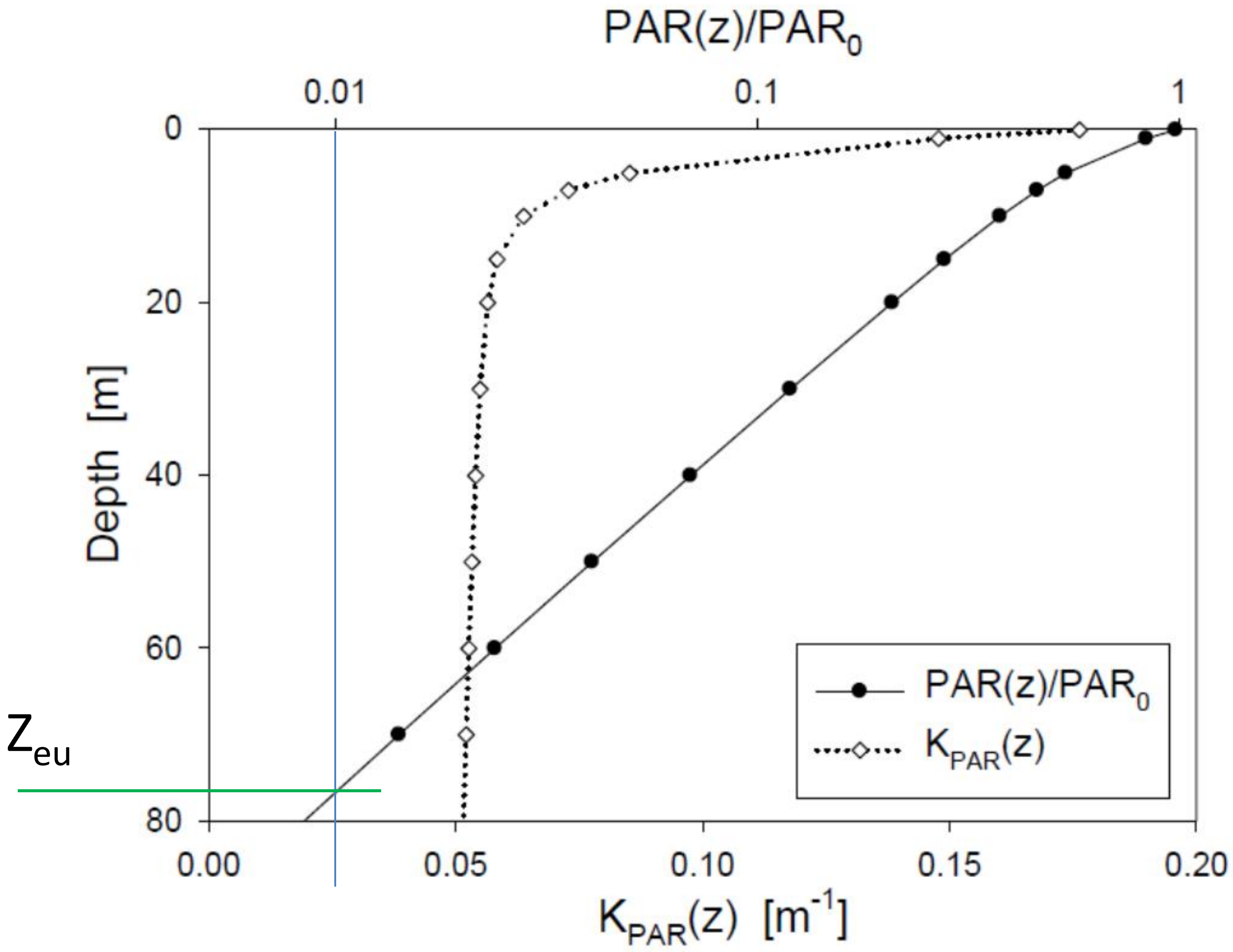

$$\frac{PAR(z_{eu})}{PAR(0)} = 1\% \text{ (or } 0.5\%)$$

$$\left\{K_1(a(490)\&b_b(490)) + \frac{K_2(a(490)\&b_b(490))}{(1+z_{eu})^{0.5}}\right\} z_{eu} = 4.6$$

(or 5.3 if defined as 0.5%)

$R_{rs}(\lambda) \rightarrow a(\lambda)\&b_b(\lambda) \rightarrow K_{PAR}(z) \rightarrow z_{eu}$

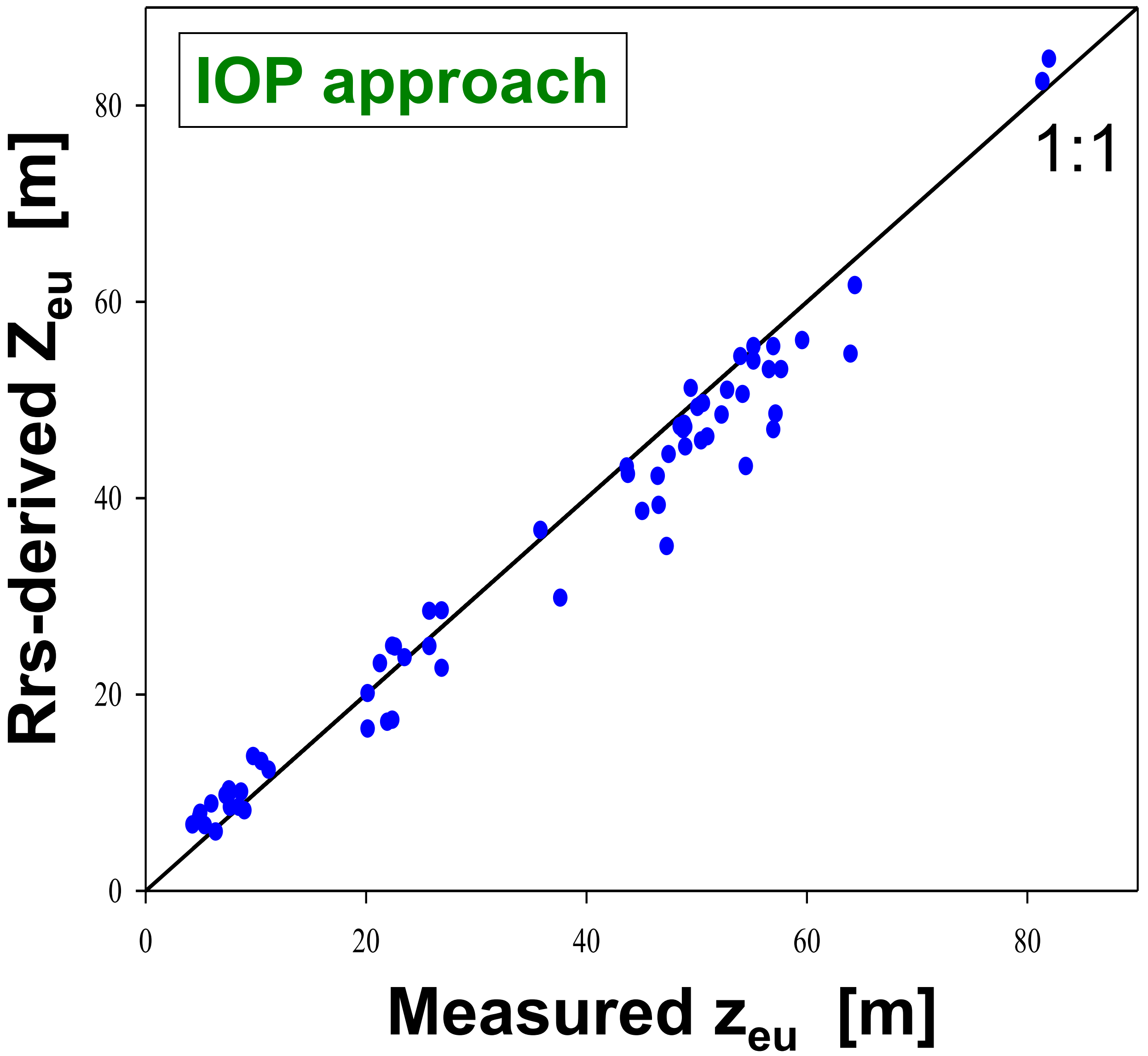

(Lee et al 2007)

Global distribution of Z_{eu}

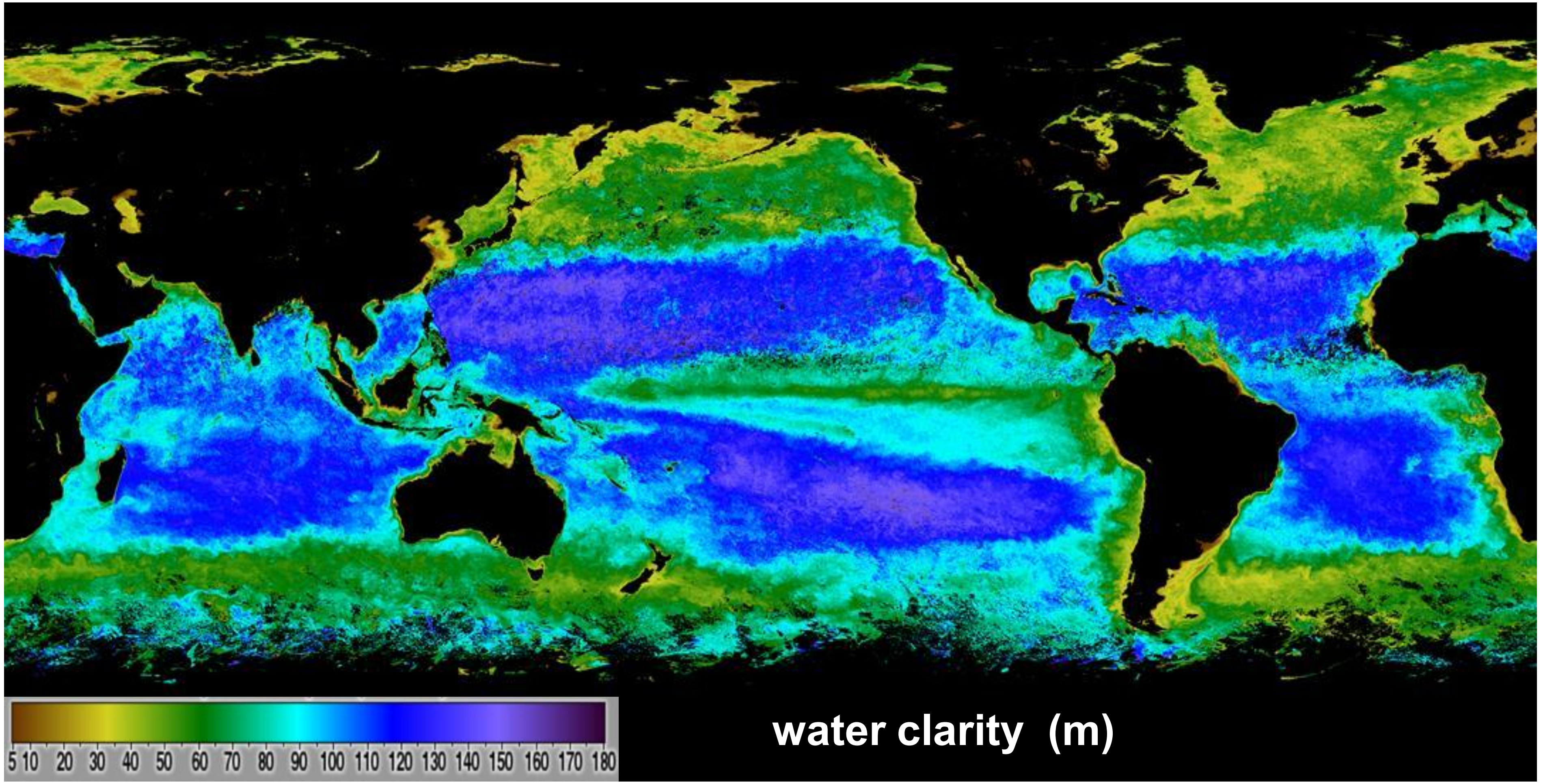

3. Estimation of water clarity (Secchi disk depth)

Water clarity

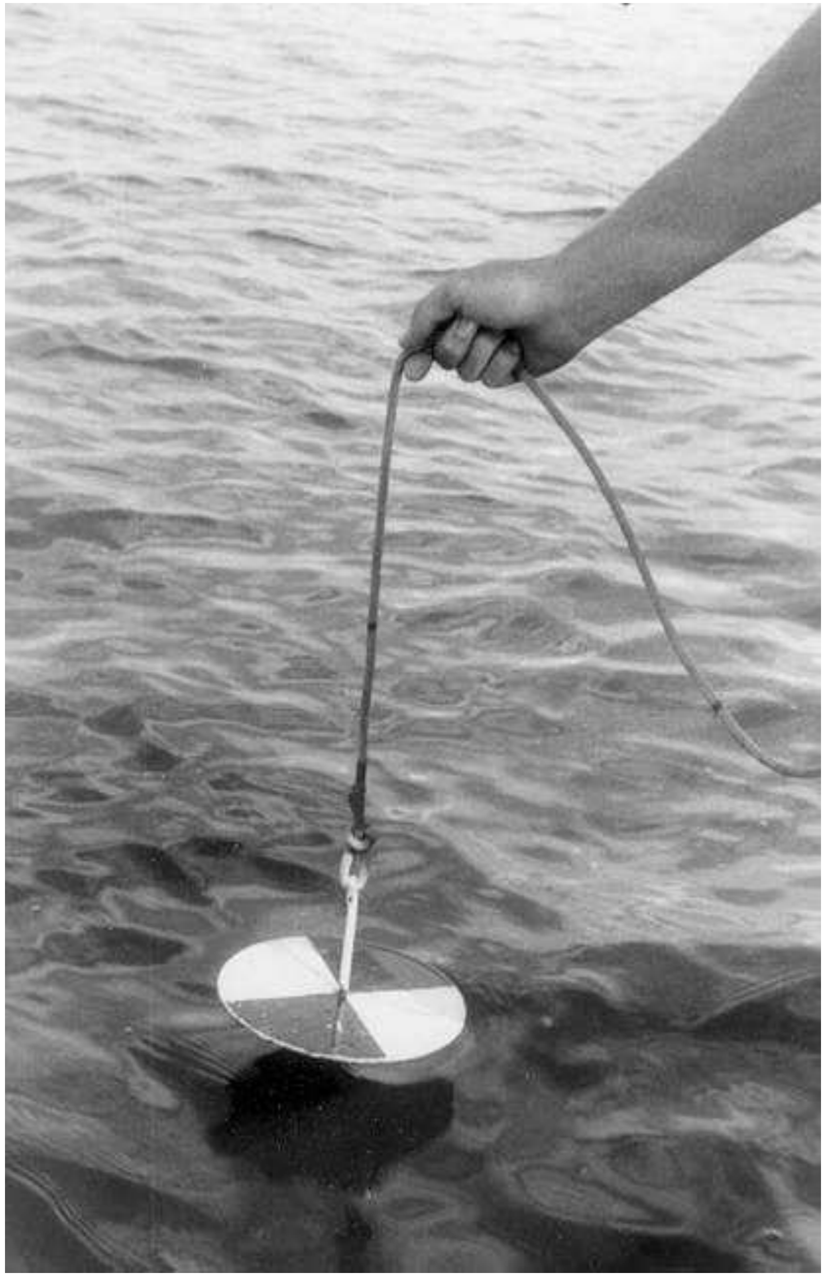

Empirical relationships for Z_{SD} derived from measurements:

Formula	Z_{SD} range (m)	Reference
$Z_{SD} = 1.7/K_{PAR}$	1.9 - 35	Poole and Atkins (1929)
$Z_{SD} = 1.44/K_{PAR}$	2 - 12	Holmes (1970)
$Z_{SD} = 1.7/K_{PAR}$	0.1 - 35	Idso (1974)
$Z_{SD} = 1.54/K_{PAR}$	6 - 46	Megard and Berman (1989)
$Z_{SD} = 1.27/K_{PAR}$	0.2 – 2.2	Gallegos et al. (1990)
$Z_{SD} = 1.86/K_{PAR}$	2.3 – 14.7	Kolengings et al. (1991)
$Z_{SD}^{1.16} = 1.48/K_{PAR}$	1.2 - 5	Montes-Hugo et al. (2005)
$Z_{SD} = 1.36/K_{PAR}$	0.1 - 42	Lugo-Fernandez (2008)
$Z_{SD}^{0.76} = 2/K_{PAR}$	0.2 - 6	Padial and Thomaz (2008)
$Z_{SD} = 1.8/K_{PAR}$	0.6 – 4.2	Bracchini et al. (2009)
$Z_{SD}^{0.85} = 1.76/K_{PAR}$	1.7 – 7.0	Ficek and Zapadka (2010)
$Z_{SD} = 1.4/K_{PAR}$	0.5 – 2.5	Gallegos et al. (2011)
$Z_{SD} = 1.37/K_{PAR}$	0.1 – 2.4	Zhang et al. (2012)

$$Z_{SD} = (1.4\text{-}1.7)/K_{PAR}$$

New theoretical relationship for Z_{SD}:

$$Z_{SD} \approx \frac{1}{2.5K_d^{tr}} \ln\left(\frac{\left|r_T - r_w^{tr}\right|}{0.013}\right)$$

(Lee et al 2015)

K_d^{tr} **: attenuation coefficient in the transparent window**

$$Z_{SD} \approx \frac{1}{K_d^{tr}} \approx \frac{1.4}{K_{PAR}}$$

(Lee et al 2018)

Now theory and measurements are consistent.

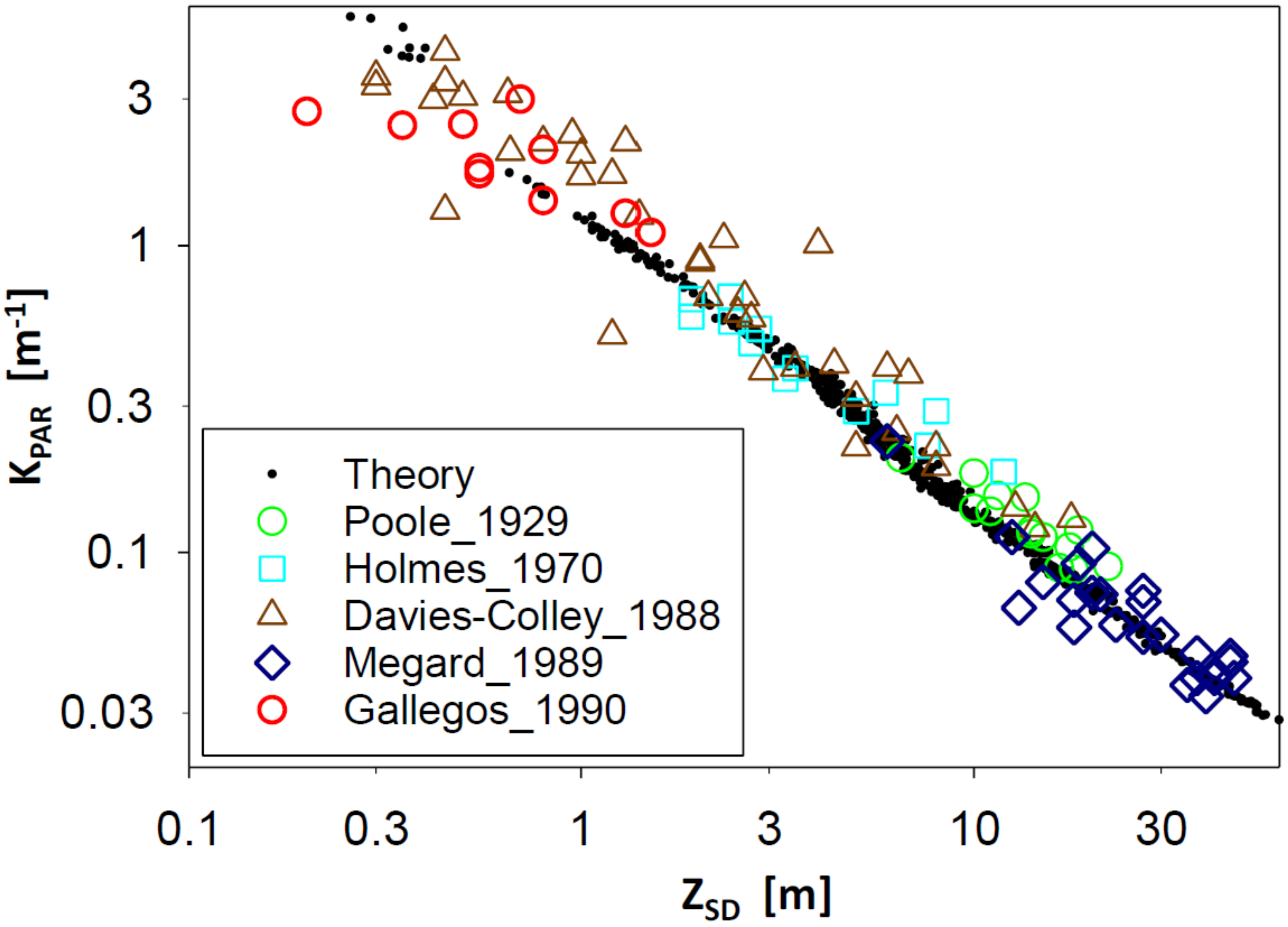

(Lee et al. 2018)

Verification of the new Secchi disk theory

$R_{rs} \Rightarrow a\&b_b \Rightarrow K_d \Rightarrow Z_{SD}$

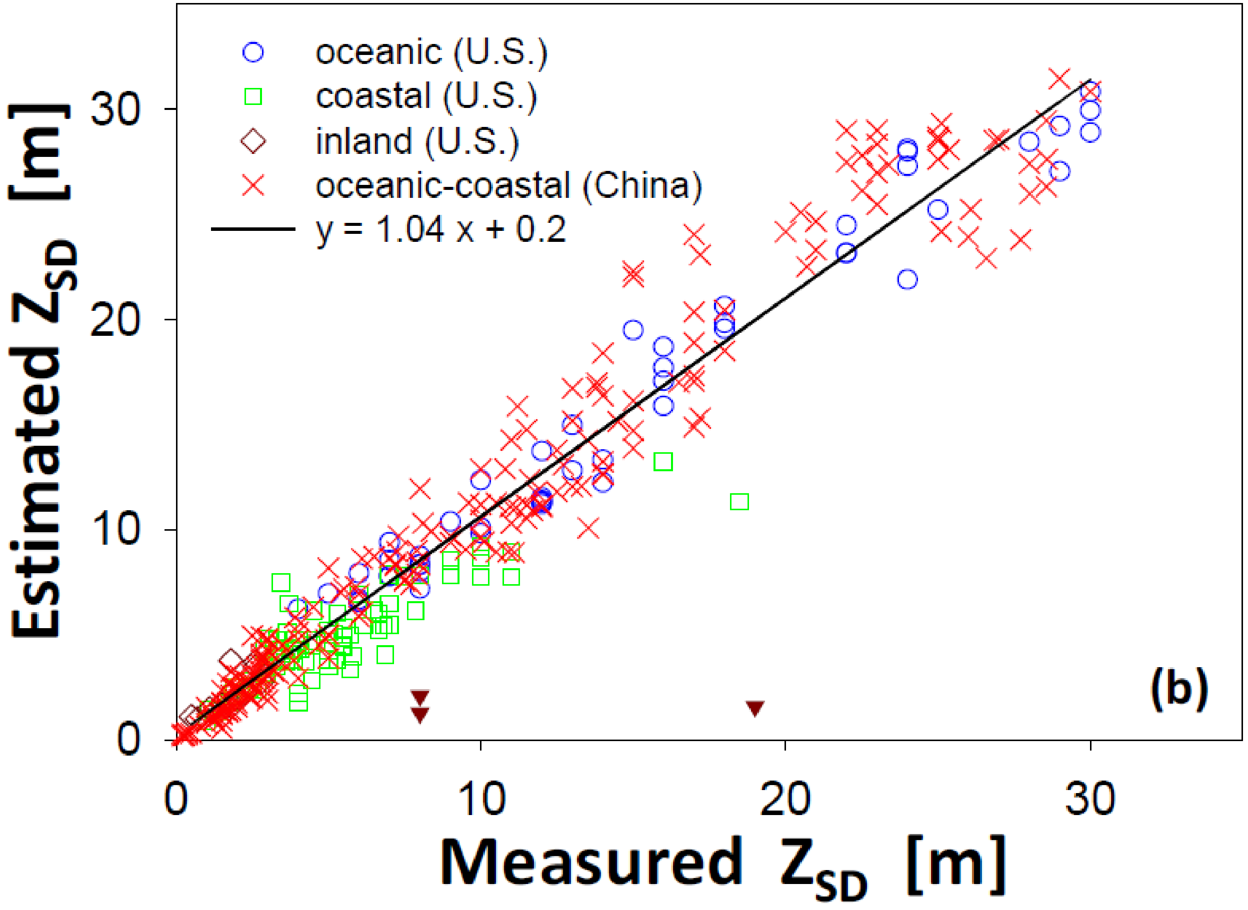

(Lee et al 2015)

4. Estimation of primary production

Protocol. A primary goal of ocean-colour remote sensing is to produce synoptic fields of chlorophyll pigment, an index of phytoplankton biomass. It is the single most

(IOCCG Report #2, 1999)

"One of the principal applications of satellite ocean color data is to derive **net primary production** (NPP)."

--- McClain (Annu. Rev. Mar. Sci., 2009)

Traditionally Chl is used to represent phytoplankton

I. Wavelength-resolved models (WRMs)

$$\sum PP = \int_{\lambda=400}^{700} \int_{t=\text{sunrise}}^{\text{sunset}} \int_{z=0}^{Z_{eu}} \Phi(\lambda, t, z) \times \text{PAR}(\lambda, t, z) \times a^*(\lambda, z) \times \boxed{\text{Chl}(z)}\, d\lambda\, dt\, dz - R$$

II. Wavelength-integrated models (WIMs)

$$\sum PP = \int_{t=\text{sunrise}}^{\text{sunset}} \int_{z=0}^{Z_{eu}} \varphi(t, z) \times \text{PAR}(t, z) \times \boxed{\text{Chl}(z)}\, dt\, dz - R$$

II. Time-integrated models (TIMs)

$$\sum PP = \int_{z=0}^{Z_{eu}} P^b(z) \times \text{PAR}(z) \times DL \times \boxed{\text{Chl}(z)}\, dz$$

IV. Depth-integrated models (DIMs)

$$\sum PP = P^b_{opt} \times f[\text{PAR}(0)] \times DL \times \boxed{\text{Chl}} \times Z_{eu}$$

VGPM:

$$PP_{eu} = 0.66125 \times P^B_{opt} \times [E_0/(E_0 + 4.1)] \times Z_{eu} \times C_{opt} \times D_{irr}.$$

(Behrenfeld and Falkowski, 1997)

Quantum yield of photosynthesis

I. Wavelength-resolved models (WRMs)

$$\sum PP = \int_{\lambda=400}^{700} \int_{t=\text{sunrise}}^{\text{sunset}} \int_{z=0}^{Z_{eu}} \boxed{\Phi(\lambda, t, z)} \times \text{PAR}(\lambda, t, z) \times \boxed{a^*(\lambda, z)} \times \text{Chl}(z)\, d\lambda\, dt\, dz - R$$

$$a^* = \frac{a_{ph}}{Chl}$$

a_{ph}: phytoplankton absorption coefficient

$$\sum PP = \int_{t=\text{sunrise}}^{\text{sunset}} \int_{z=0}^{Z_{eu}} \varphi(t, z) \times \text{PAR}(t, z) \times \text{Chl}(z)\, dt\, dz - R$$

$$\sum PP = \int \iint \phi \times PAR(\lambda, t, z) \times a_{ph}(\lambda, z) dt\, dz\, d\lambda - R$$

Centered on a_{ph}

5. Conclusions and Expectations

(1) It is not necessary to know B for the calculation of P with remote-sensing methods. What is

(Lee et al., 1996, Appl Opt)

$$\sum PP = \int_{t=\text{sunrise}}^{\text{sunset}} \int_{z=0}^{Z_{eu}} \varphi(t, z) \times \mathrm{PAR}(t, z) \times \mathrm{Chl}(z)\, \mathrm{d}t\, \mathrm{d}z - R$$

$$\sum PP = \int \iint \phi \times PAR(\lambda, t, z) \times a_{ph}(\lambda, z) dt\, dz\, d\lambda\ - R$$

Contrast in mathematics and physics of the two approaches:

φ vs ϕ:

φ involves both ϕ and a^*.

Chl vs a_{ph}:

Chl is a biological property; could not be directly obtained from OC remote sensing.

a_{ph} is an optical property; ocean color measures optical property.

Absorption based on PP model

$$PP(z) = \iint \phi \times E_0(\lambda, t, z) \times a_{ph}(\lambda, z)\, d\lambda\, dt$$

A more direct representation of photosynthesis.

$$\boxed{\text{Ocean color}} \longrightarrow \boxed{K_d,\ a_{ph}} \xrightarrow{\ \phi\ } \boxed{\text{PP}}$$

$$\phi(E_o) = \frac{\phi_m K_\phi}{K_\phi + E_o} \qquad (2)$$

(Kiefer and Mitchell, 1983, L&O)

Remotely-estimated PP compared with measured PP

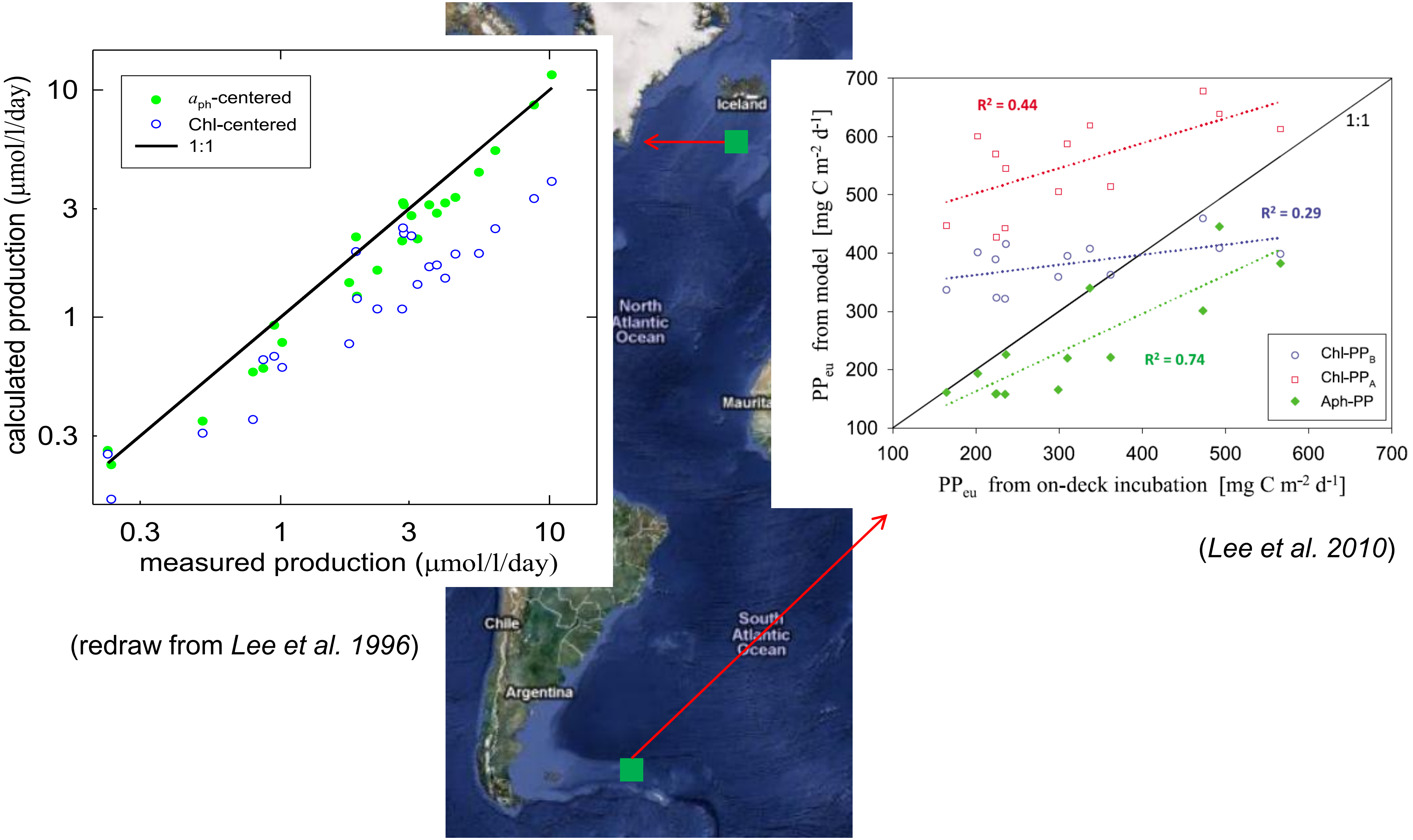

(redraw from *Lee et al. 1996*)

(*Lee et al. 2010*)

Labrador Sea

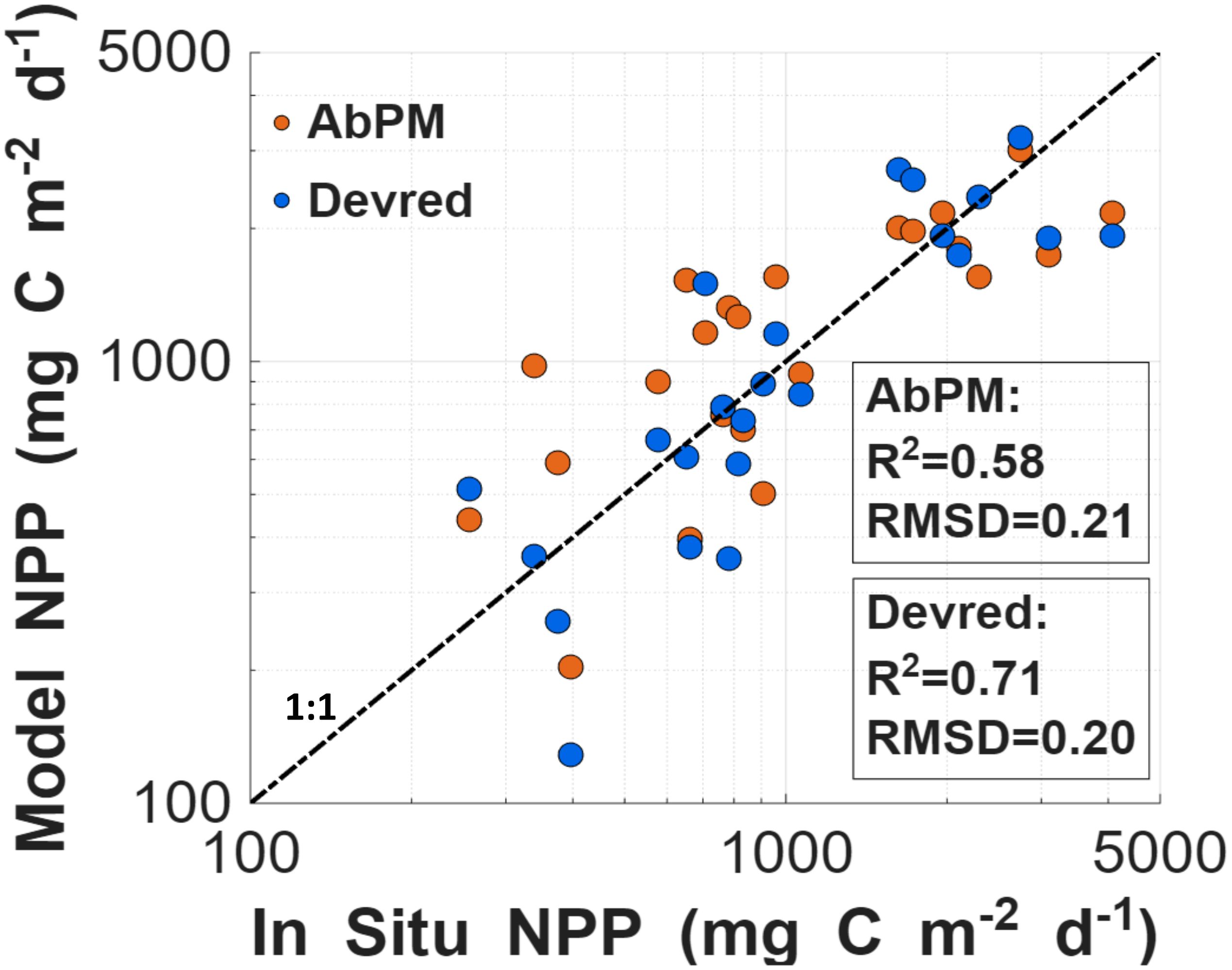

(Lee et al., under revision)

Why a_{ph} based approach is likely better?

Essence of present satellite Chl product:

$$Chl = fun\left(\frac{R_{rs}(\lambda_1)}{R_{rs}(\lambda_2)}\right)$$

$$R_{rs} \approx G\frac{b_b}{a+b_b}$$

$$\frac{R_{rs}(440)}{R_{rs}(550)} \approx \frac{a(550)}{a(440)}\frac{b_{bw}(440)+b_{bp}(440)}{b_{bw}(550)+b_{bp}(550)}$$

$$\Rightarrow \quad \frac{R_{rs}(440)}{R_{rs}(550)} \propto \frac{a(550)}{a(440)} = \frac{a_w(550)+a_{dg}(550)+a_{ph}^*(550)Chl}{a_w(440)+a_{dg}(440)+a_{ph}^*(440)Chl}$$

Change of R_{rs} band ratio not necessarily represents change of [Chl].

5. A few other examples

5a. Water mass classification

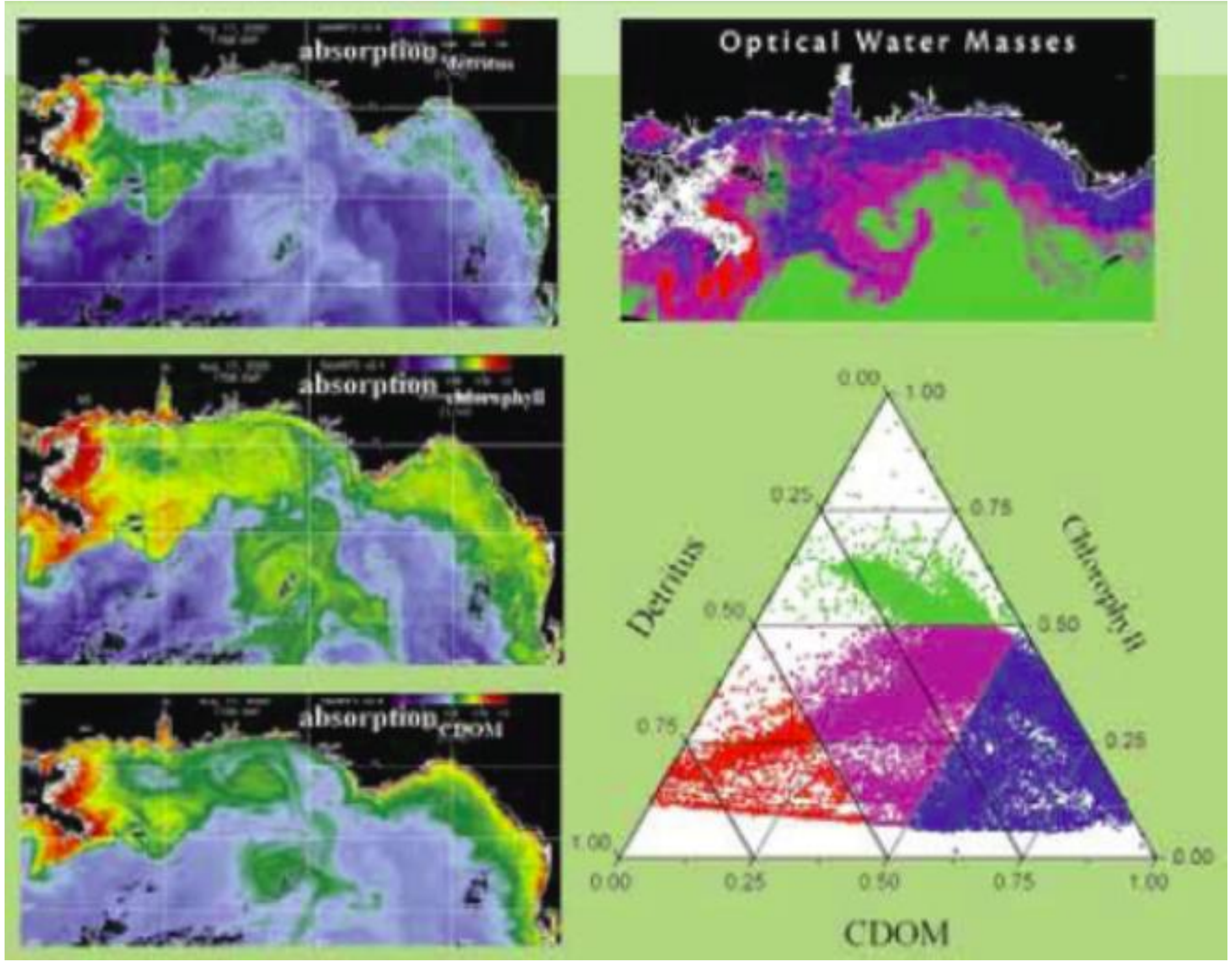

(Arnone et al. 2004)

5b. HAB identification-1

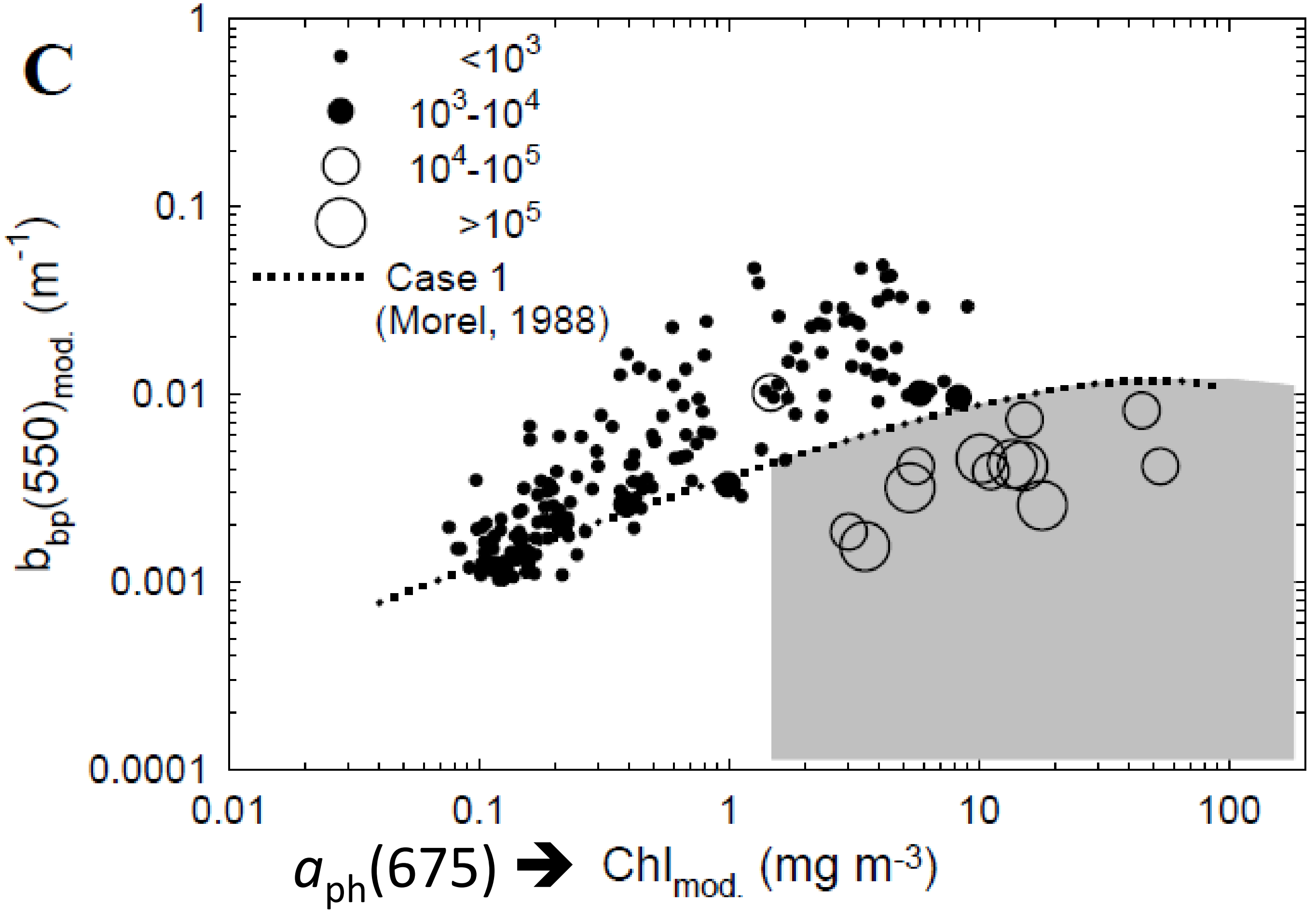

(Carnizzaro et al. 2008)

5b. HAB identification-2

QAA

$$R_{rs}(\lambda) \xrightarrow{\text{QAA}} a_{ph}(\lambda) = a(\lambda) - a_{dg}(\lambda) - a_w(\lambda)$$

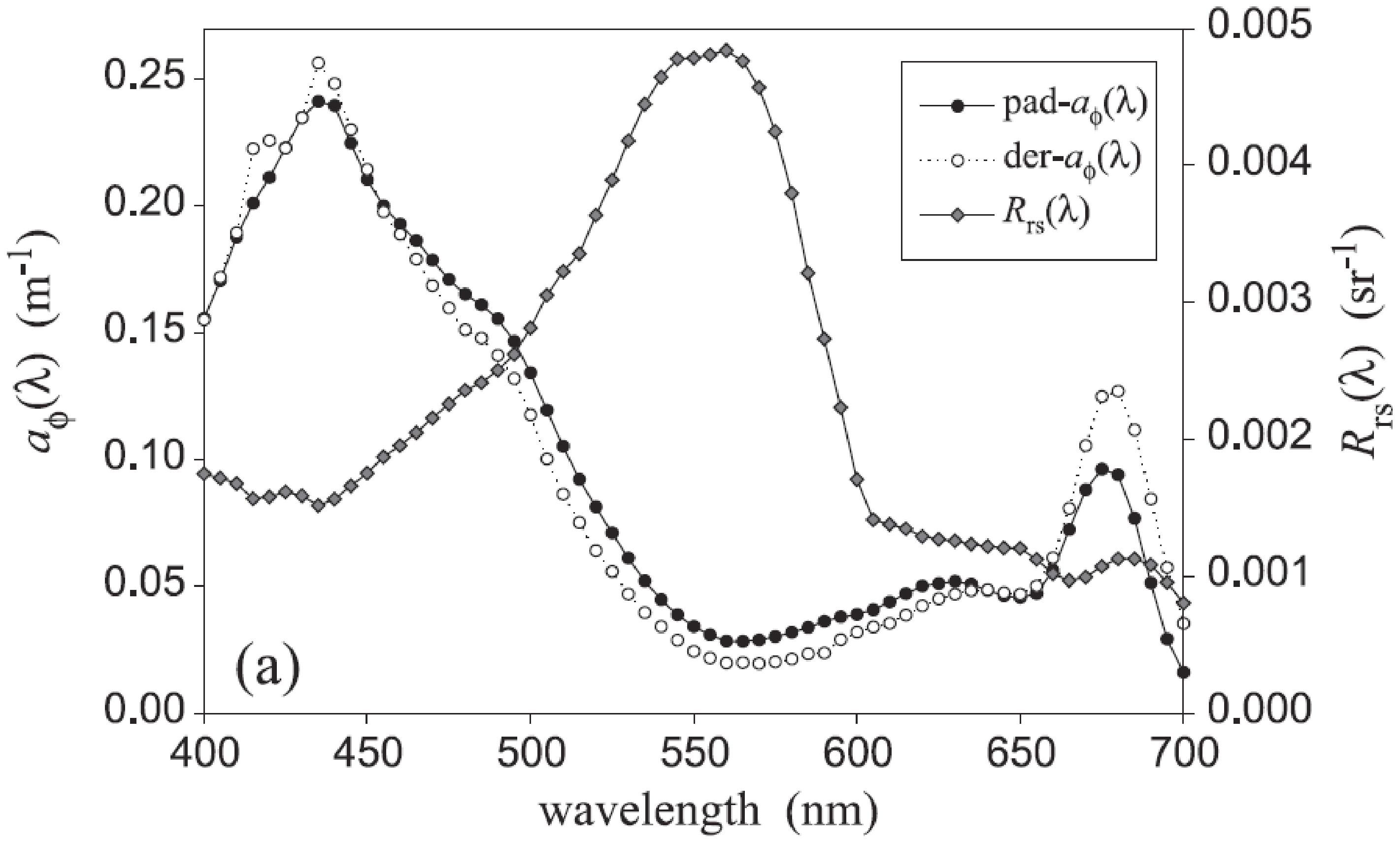

(Lee and Carder 2004)

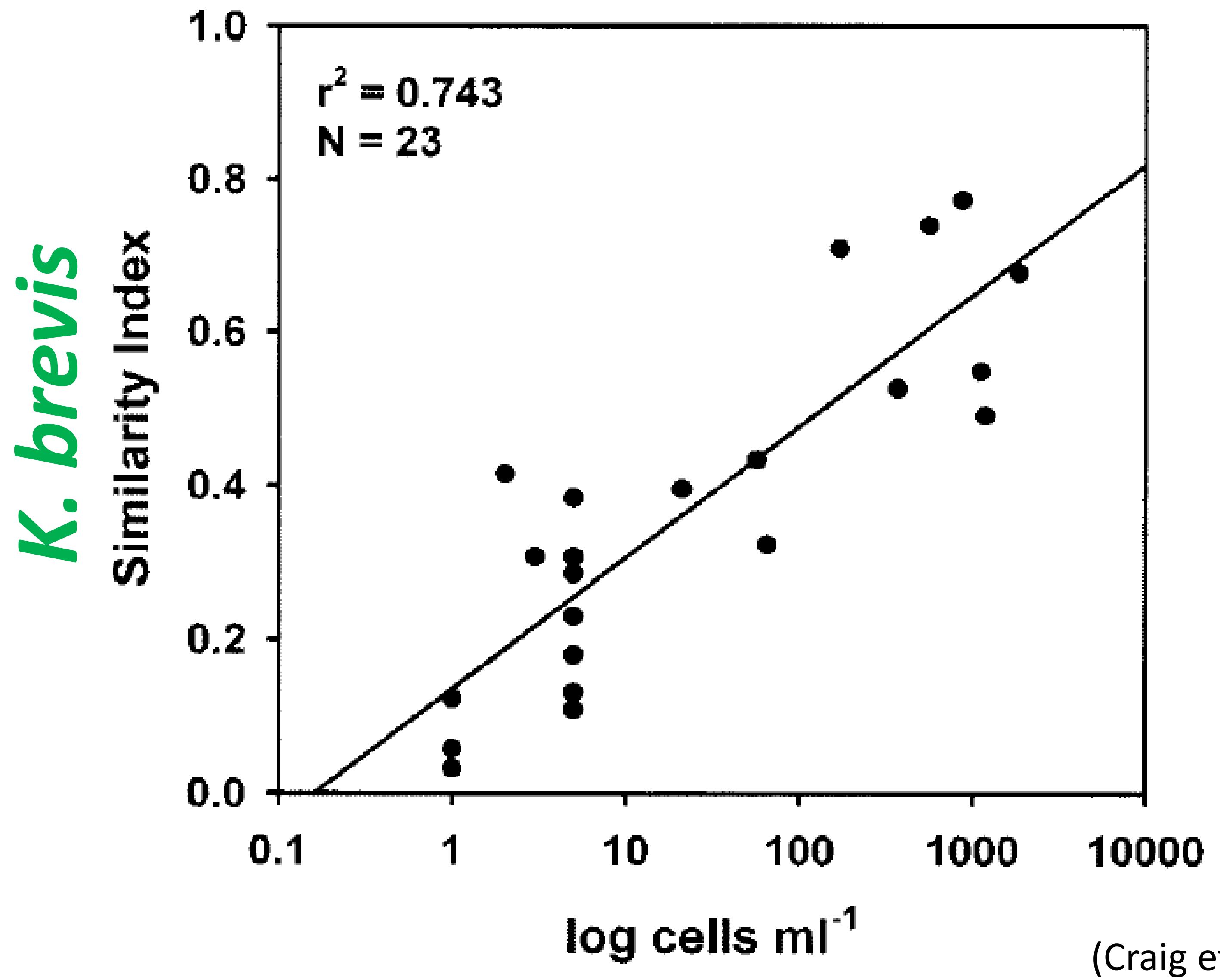

(Craig et al 2006)

5c. Bloom dynamics

Distribution of $a_{ph}(440)$ at Luzon Street

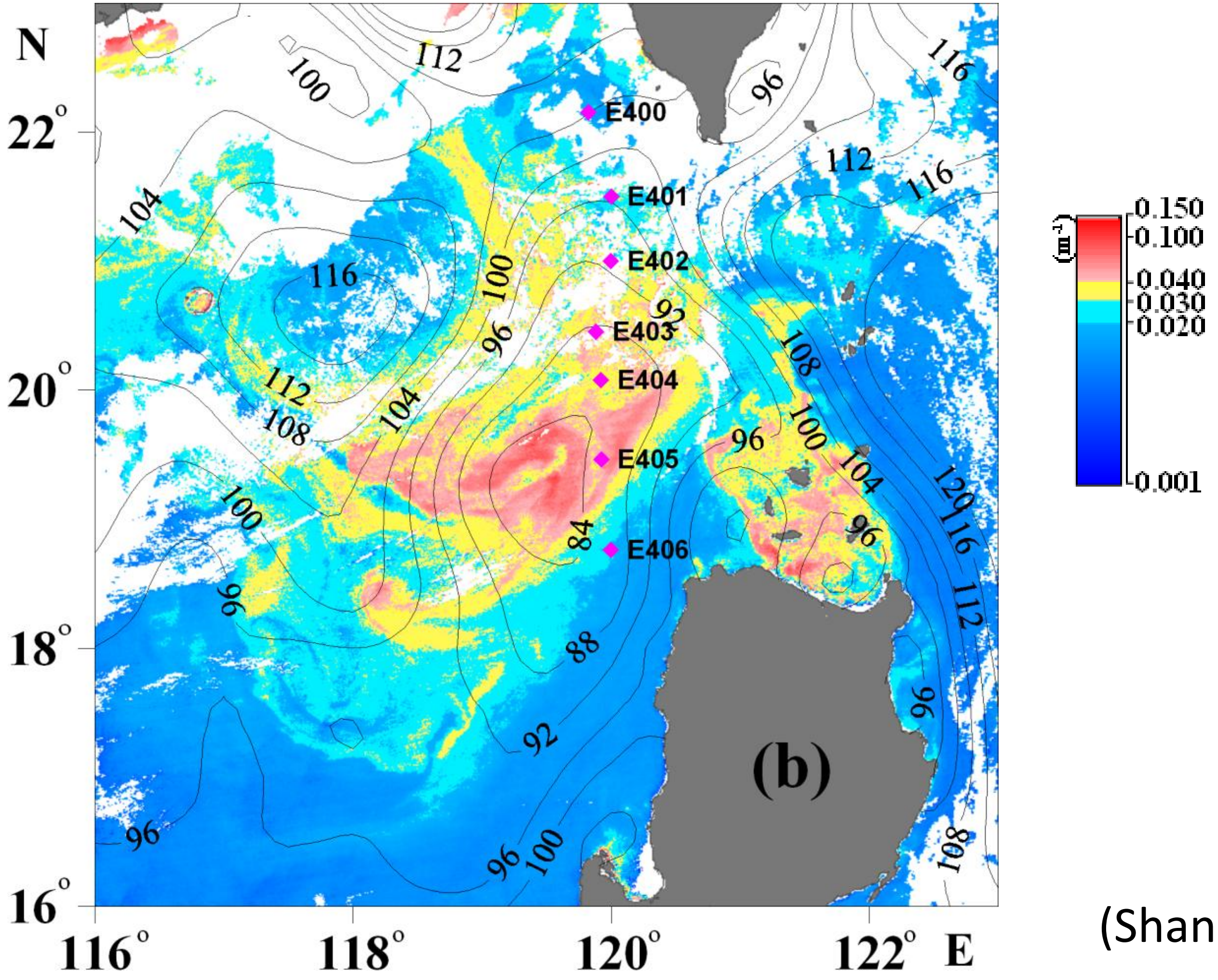

(Shang et al, 2012)

Monthly distribution of $a_{ph}(440)$ at Luzon Street

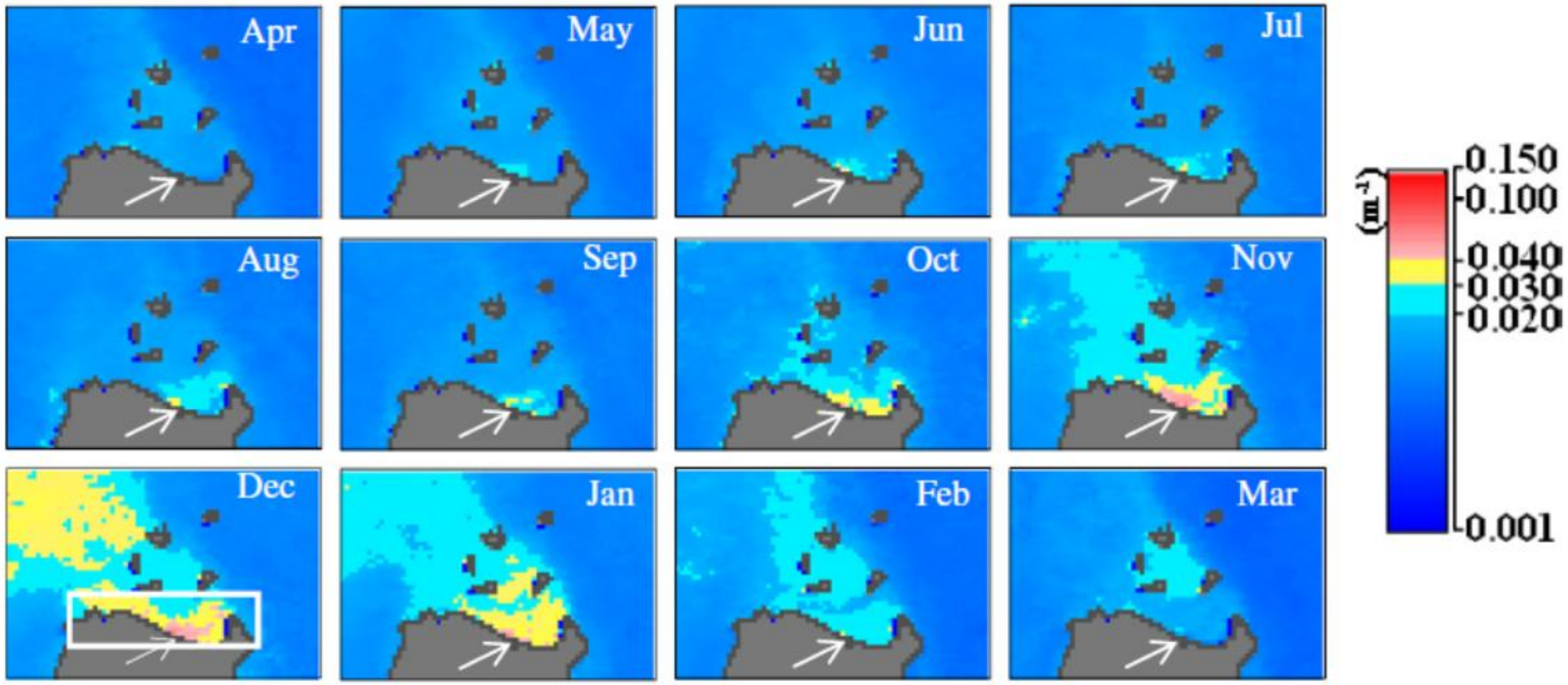

(Shang et al, 2012)

5d. Global physiology of ocean phytoplankton

IOP

$$F_{\text{sat}} = Chl_{\text{sat}} \times <a^*_{ph}> \times \phi \times S, \qquad (2)$$

ϕ: quantum yield of fluorescence

(Behrenfeld et al 2009)

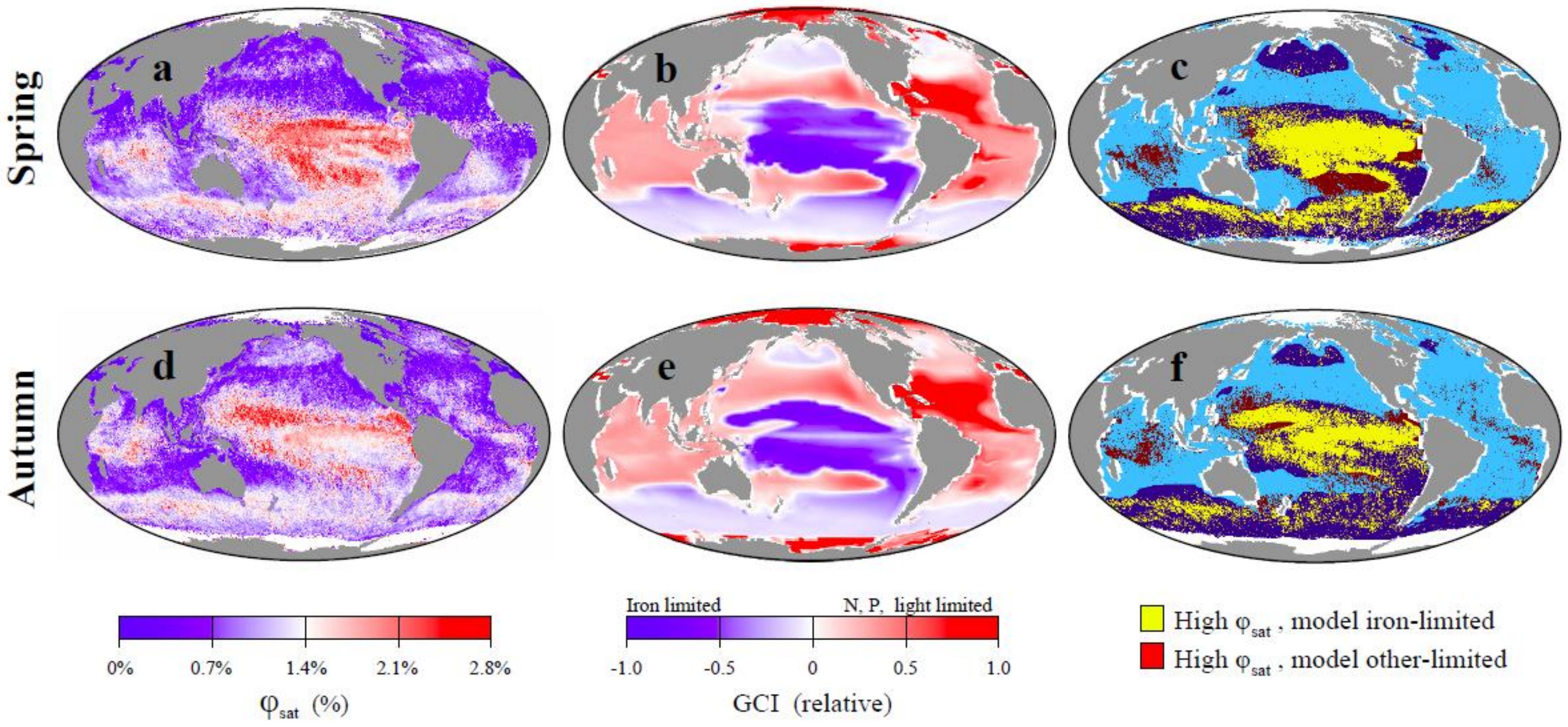

(Behrenfeld et al 2009)

5e. Salinity estimation

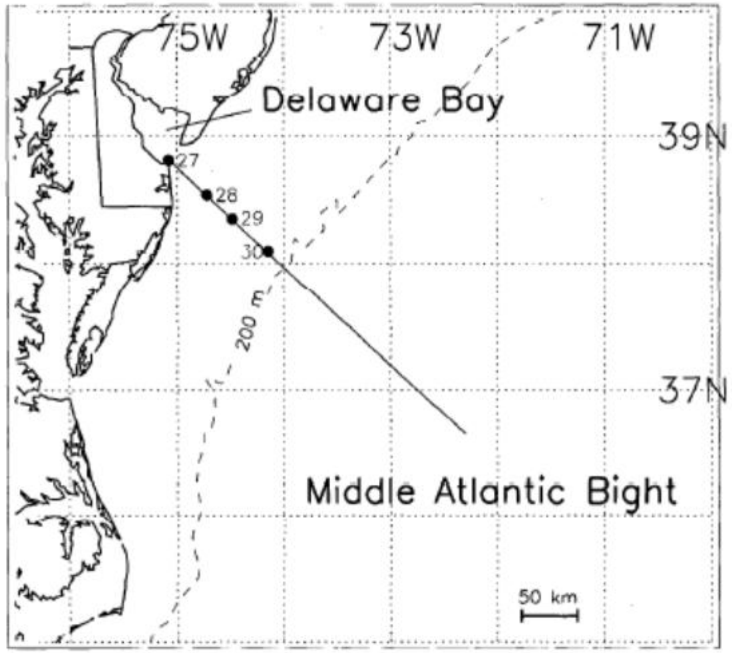

Fig. 1. Locations of the transect and hydrocast stations in the Middle Atlantic Bight.

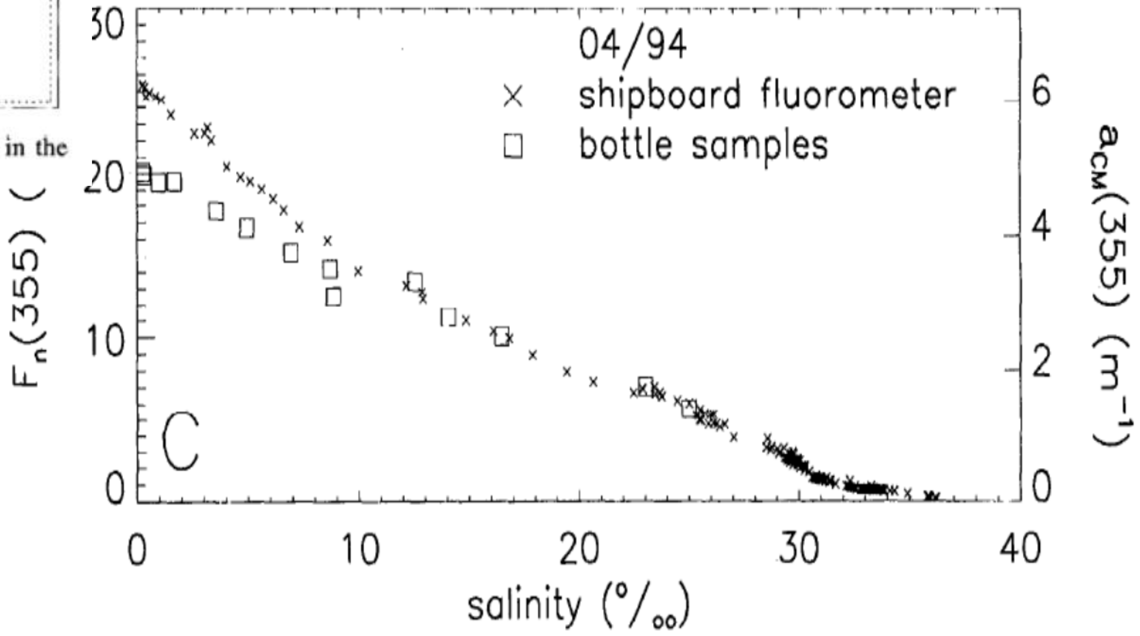

(Vodacek et al 1997)

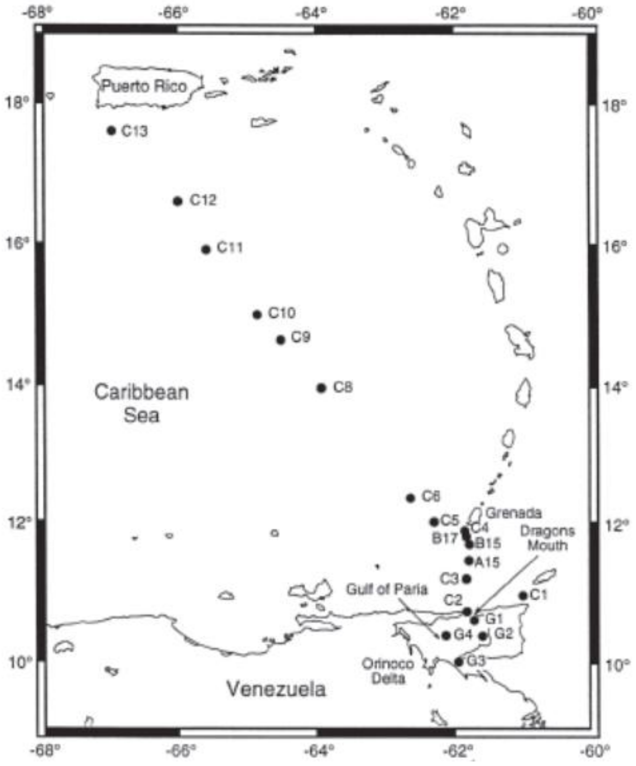

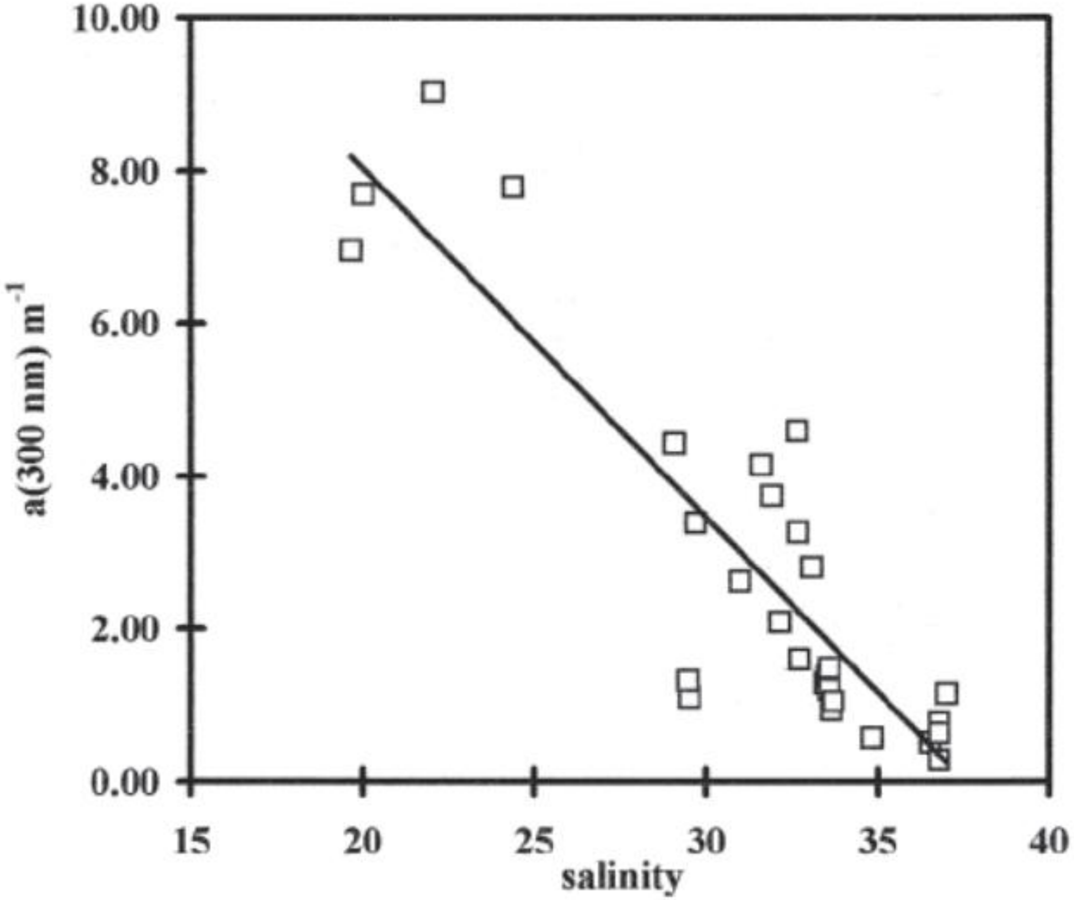

$$\mathrm{SSS} = \mathrm{x}\, a_{\mathrm{CDOM}} + \mathrm{y}$$

(Castellio et al 1999)

5f. pCO2 estimation

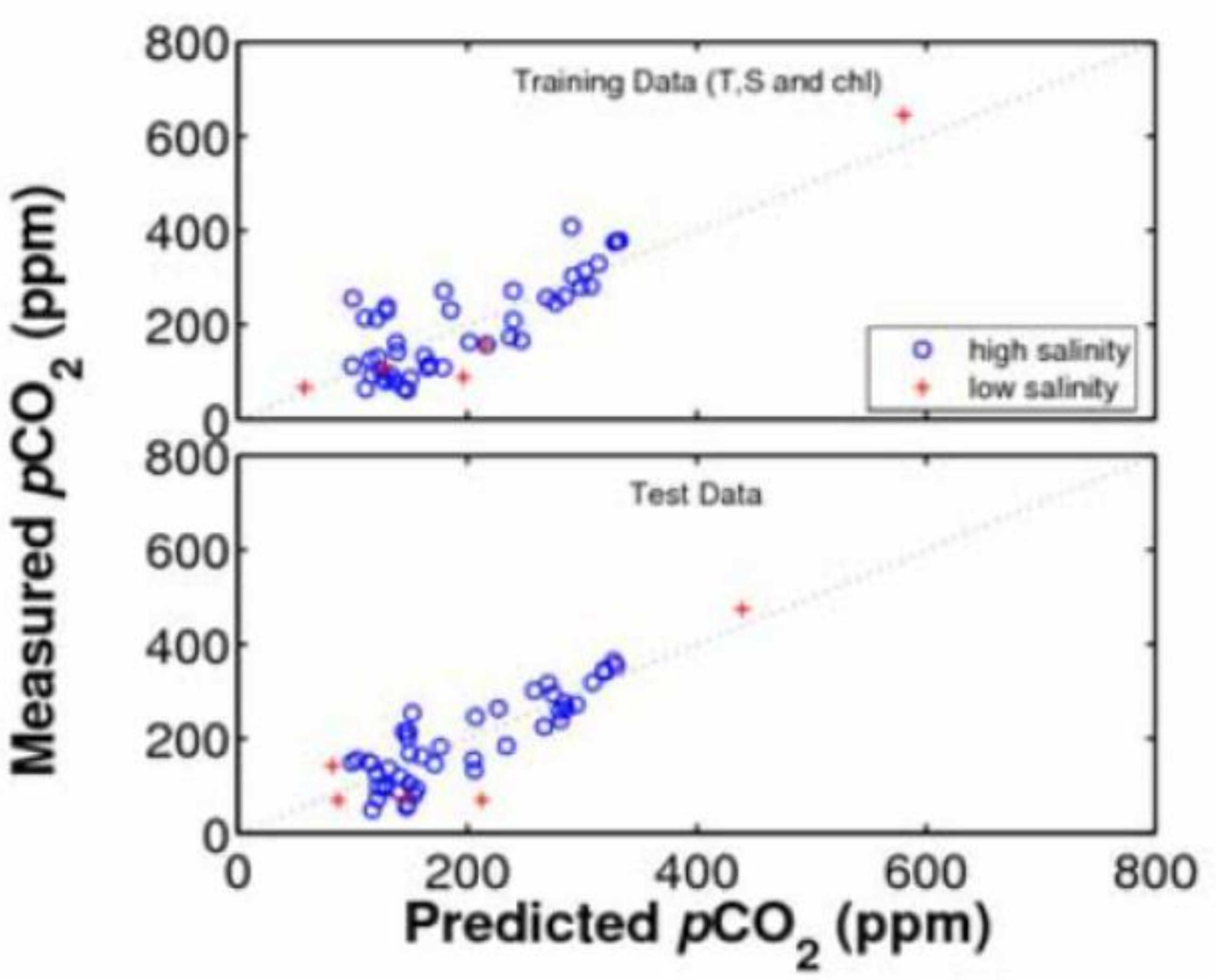

Lohrenz and Cai (2006)

pCO2 = f(T, S, Chl)

Key Points:

1. Many applications traditionally built around [Chl] can be built around IOPs.

2. Remote sensing and applications centered around IOPs avoided, when necessary, concentration-normalized optical properties.

3. With IOPs as inputs, many products, e.g. Kd, Zeu, Zsd, PP, could be estimated easily and more accurately.

4. When IOPs are known, many other applications could be carried out.
Be creative.

References:

Ocean color chlorophyll algorithms for SeaWiFS

John E. O'Reilly,[1] Stéphane Maritorena,[2] B. Greg Mitchell,[3] David A. Siegcl,[4]
Kendall L. Carder,[5] Sara A. Garver,[6] Mati Kahru,[3] and Charles McClain[7]

JOURNAL OF GEOPHYSICAL RESEARCH, VOL. 103, NO. C11, PAGES 24,937–24,953, OCTOBER 15, 1998

Chlorophyll *a* algorithms for oligotrophic oceans: A novel approach based on three-band reflectance difference

Chuanmin Hu,[1] Zhongping Lee,[2] and Bryan Franz[3]

JOURNAL OF GEOPHYSICAL RESEARCH, VOL. 117, C01011, doi:10.1029/2011JC007395, 2012

An empirical algorithm for light absorption by ocean water based on color

Z. P. Lee, K. L. Carder, R. G. Steward, and T. G. Peacock
Department of Marine Science, University of South Florida, St. Petersburg

JOURNAL OF GEOPHYSICAL RESEARCH, VOL. 103, NO. C12, PAGES 27,967–27,978, NOVEMBER 15, 1998

Absorption Coefficient and Chlorophyll Concentration of Oceanic Waters Estimated from Band Difference of Satellite-Measured Remote Sensing Reflectance

Zhongping Lee[1*], Longteng Zhao[1], Chuanmin Hu[2], Daosheng Wang[1], Junfang Lin[3], and Shaoling Shang[1]

Journal of Remote Sensing
A SCIENCE PARTNER JOURNAL

Lee et al. 2023 | https://doi.org/10.34133/remotesensing.0063

Variability in the chlorophyll-specific absorption coefficients of natural phytoplankton: Analysis and parameterization

Annick Bricaud, Marcel Babin, André Morel, and Hervé Claustre

JOURNAL OF GEOPHYSICAL RESEARCH, VOL. 100, NO. C7, PAGES 13,321–13,332, JULY 15, 1995

Hyperspectral remote sensing for shallow waters. I. A semianalytical model

Zhongping Lee, Kendall L. Carder, Curtis D. Mobley, Robert G. Steward, and Jennifer S. Patch

20 September 1998 / Vol. 37, No. 27 / APPLIED OPTICS 6329

Assessment of the relationships between dominant cell size in natural phytoplankton communities and the spectral shape of the absorption coefficient

Áurea M. Ciotti,[1] Marlon R. Lewis, and John J. Cullen[2]

Limnol. Oceanogr., 47(2), 2002, 404–417

Determination of the Major Groups of Phytoplankton Pigments From the Absorption Spectra of Total Particulate Matter

NICOLAS HOEPFFNER[1] AND SHUBHA SATHYENDRANATH[2]

JOURNAL OF GEOPHYSICAL RESEARCH, VOL. 98, NO. C12, PAGES 22,789–22,803, DECEMBER 15, 1993

Absorption by dissolved organic matter of the sea (yellow substance) in the UV and visible domains[1]

Annick Bricaud, André Morel, and Louis Prieur

Limnol. Oceanogr., 26(1), 1981, 43–53

A three-component model of ocean colour and its application to remote sensing of phytoplankton pigments in coastal waters

S. SATHYENDRANATH†, L. PRIEUR and A. MOREL

INT. J. REMOTE SENSING, 1989, VOL. 10, NO. 8, 1373–1394

Satellite retrieval of inherent optical properties by linear matrix inversion of oceanic radiance models: An analysis of model and radiance measurement errors

Frank E. Hoge
NASA Goddard Space Flight Center, Wallops Flight Facility, Wallops Island, Virginia

Paul E. Lyon

JOURNAL OF GEOPHYSICAL RESEARCH, VOL. 101, NO. C7, PAGES 16,631–16,648, JULY 15, 1996

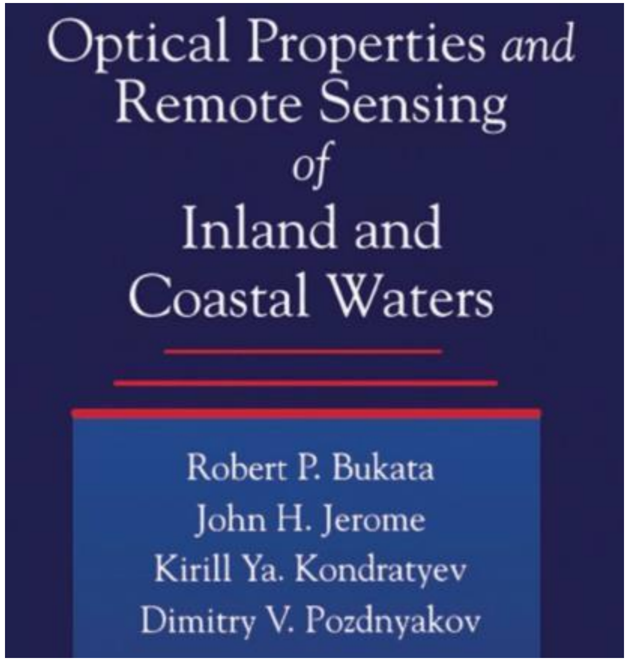

1994

Semianalytic Moderate-Resolution Imaging Spectrometer algorithms for chlorophyll *a* and absorption with bio-optical domains based on nitrate-depletion temperatures

K. L. Carder, F. R. Chen, Z. P. Lee, and S. K. Hawes

JOURNAL OF GEOPHYSICAL RESEARCH, VOL. 104, NO. C3, PAGES 5403–5421, MARCH 15, 1999

Optimization of a semianalytical ocean color model for global-scale applications

Stéphane Maritorena, David A. Siegel, and Alan R. Peterson

20 May 2002 / Vol. 41, No. 15 / APPLIED OPTICS 2705

Generalized ocean color inversion model for retrieving marine inherent optical properties

P. Jeremy Werdell,[1,2,*] Bryan A. Franz,[1] Sean W. Bailey,[1,3] Gene C. Feldman,[1] Emmanuel Boss,[2] Vittorio E. Brando,[4] Mark Dowell,[5] Takafumi Hirata,[6] Samantha J. Lavender,[7] ZhongPing Lee,[8] Hubert Loisel,[9] Stéphane Maritorena,[10] Fréderic Mélin,[5] Timothy S. Moore,[11] Timothy J. Smyth,[12] David Antoine,[13] Emmanuel Devred,[14] Odile Hembise Fanton d'Andon,[15] and Antoine Mangin[15]

1 April 2013 / Vol. 52, No. 10 / APPLIED OPTICS 2019

Interpretation of hyperspectral remote-sensing imagery by spectrum matching and look-up tables

Curtis D. Mobley, Lydia K. Sundman, Curtiss O. Davis, Jeffrey H. Bowles,
Trijntje Valerie Downes, Robert A. Leathers, Marcos J. Montes, William Paul Bissett,
David D. R. Kohler, Ruth Pamela Reid, Eric M. Louchard, and Arthur Gleason

3576 APPLIED OPTICS / Vol. 44, No. 17 / 10 June 2005

Remote chlorophyll-*a* retrieval in turbid, productive estuaries: Chesapeake Bay case study

Anatoly A. Gitelson [a,*], John F. Schalles [b], Christine M. Hladik [c,1]

Remote Sensing of Environment 109 (2007) 464–472

Estimation of the inherent optical properties of natural waters from the irradiance attenuation coefficient and reflectance in the presence of Raman scattering

Hubert Loisel and Dariusz Stramski

20 June 2000 / Vol. 39, No. 18 / APPLIED OPTICS 3001

Deriving inherent optical properties from water color: a multiband quasi-analytical algorithm for optically deep waters

ZhongPing Lee, Kendall L. Carder, and Robert A. Arnone

20 September 2002 / Vol. 41, No. 27 / APPLIED OPTICS 5755

Semianalytical model for the derivation of ocean color inherent optical properties: description, implementation, and performance assessment

Timothy J. Smyth, Gerald F. Moore, Takafumi Hirata, and James Aiken

8116 APPLIED OPTICS / Vol. 45, No. 31 / 1 November 2006

Estimation of light penetration, and horizontal and vertical visibility in oceanic and coastal waters from surface reflectance

Maéva Doron,[1,2,3] Marcel Babin,[2,3] Antoine Mangin,[1] and Odile Hembise[1]

JOURNAL OF GEOPHYSICAL RESEARCH, VOL. 112, C06003, doi:10.1029/2006JC004007, 2007

Uncertainties of inherent optical properties obtained from semianalytical inversions of ocean color

Peng Wang, Emmanuel S. Boss, and Collin Roesler

4074 APPLIED OPTICS / Vol. 44, No. 19 / 1 July 2005

A model for partitioning the light absorption coefficient of natural waters into phytoplankton, nonalgal particulate, and colored dissolved organic components: A case study for the Chesapeake Bay

Guangming Zheng[1,2,3], Dariusz Stramski[4], and Paul M. DiGiacomo[1]

10.1002/2014JC010604

Influence of Raman scattering on ocean color inversion models

Toby K. Westberry,[1,*] Emmanuel Boss,[2] and Zhongping Lee[3]

5552 APPLIED OPTICS / Vol. 52, No. 22 / 1 August 2013

THE DETERMINATION OF THE DIFFUSE ATTENUATION COEFFICIENT

OF SEA WATER USING THE COASTAL ZONE COLOR SCANNER

R.W. Austin and T.J. Petzold

J. F. R. Gower (ed.), *Oceanography from Space*
© Plenum Press, New York 1981

Bio-optical properties of oceanic waters: A reappraisal

André Morel
Laboratoire de Physique et Chimie Marines, Université Pierre et Marie Curie, CNRS-INSU
Villefranche-sur-mer, France

Stéphane Maritorena

JOURNAL OF GEOPHYSICAL RESEARCH, VOL. 106, NO. C4, PAGES 7163–7180, APRIL 15, 2001

An evaluation of MODIS and SeaWiFS bio-optical algorithms in the Baltic Sea

Miroslaw Darecki[a,*], Dariusz Stramski[b]

Remote Sensing of Environment 89 (2004) 326–350

Limnol. Oceanogr., 29(2), 1984, 350–356

Dependence of relationship between inherent and apparent optical properties of water on solar altitude

J. T. O. Kirk

Limnol. Oceanogr., 34(8), 1989, 1389–1409

Can the Lambert-Beer law be applied to the diffuse attenuation coefficient of ocean water?

Howard R. Gordon

A model for the diffuse attenuation coefficient of downwelling irradiance

Zhong-Ping Lee[1]
Naval Research Laboratory, Stennis Space Center, Mississippi, USA

Ke-Ping Du
State Key Laboratory of Remote Sensing Science, Research Center for Remote Sensing and GIS, School of Geography, Beijing Normal University, Beijing, China

Robert Arnone

JOURNAL OF GEOPHYSICAL RESEARCH, VOL. 110, C02016, doi:10.1029/2004JC002275, 2005

Penetration of UV-visible solar radiation in the global oceans: Insights from ocean color remote sensing

Zhongping Lee,[1] Chuanmin Hu,[2] Shaoling Shang,[3] Keping Du,[4] Marlon Lewis,[5] Robert Arnone,[6] and Robert Brewin[7]

JOURNAL OF GEOPHYSICAL RESEARCH: OCEANS, VOL. 118, 4241–4255, doi:10.1002/jgrc.20308, 2013

Diffuse attenuation coefficient of downwelling irradiance: An evaluation of remote sensing methods

Zhong-Ping Lee,[1,2] Miroslaw Darecki,[3] Kendall L. Carder,[4] Curtiss O. Davis,[5] Dariusz Stramski,[6] and W. Joseph Rhea[5]

JOURNAL OF GEOPHYSICAL RESEARCH, VOL. 110, C02017, doi:10.1029/2004JC002573, 2005

Optical Modeling of the Upper Ocean in Relation to Its Biogenous Matter Content (Case I Waters)

ANDRÉ MOREL

JOURNAL OF GEOPHYSICAL RESEARCH, VOL. 93, NO. C9, PAGES 10,749–10,768, SEPTEMBER 15, 1988

Penetration of solar radiation in the upper ocean: A numerical model for oceanic and coastal waters

ZhongPing Lee,[1,2] KePing Du,[3] Robert Arnone,[1] SooChin Liew,[4] and Bradley Penta[1]

JOURNAL OF GEOPHYSICAL RESEARCH, VOL. 110, C09019, doi:10.1029/2004JC002780, 2005

JOURNAL OF GEOPHYSICAL RESEARCH, VOL. 112, C03009, doi:10.1029/2006JC003802, 2007

Click Here for Full Article

Euphotic zone depth: Its derivation and implication to ocean-color remote sensing

ZhongPing Lee,[1] Alan Weidemann,[1] John Kindle,[1] Robert Arnone,[1] Kendall L. Carder,[2] and Curtiss Davis[3]

Reconciling Between Optical and Biological Determinants of the Euphotic Zone Depth

Jinghui Wu[1,3], Zhongping Lee[2], Yuyuan Xie[1,5], Joaquim Goes[3], Shaoling Shang[1], John F. Marra[4], Gong Lin[1], Lei Yang[1], and Bangqin Huang[1]

RESEARCH ARTICLE
10.1029/2020JC016874

Light Penetration in the Coastal Waters Off Goa

SHUBHA SATHYENDRANATH & V V R VARADACHARI

Indian Journal of Marine Sciences
Vol. 11, June 1982, pp. 148-152

Resolving the long-standing puzzles about the observed Secchi depth relationships

Zhongping Lee,[1*] Shaoling Shang,[2*] Keping Du,[3] Jianwei Wei[1]

Limnol. Oceanogr. 00, 2018, 00–00

SCRIPPS INSTITUTION OF OCEANOGRAPHY UC San Diego

Title:
The Visibility of Submerged Objects (Chapters 1 through 4)

Author:
Duntley, Seibert Q

Originally issued: August 1952
Reissued: October 1960

Secchi disk science: Visual optics of natural waters[1]

Rudolph W. Preisendorfer

Limnol. Oceanogr., 31(5), 1986, 909–926

Robust underwater visibility parameter

J. Ronald V. Zaneveld
WET Labs, Inc., P.O. Box 518, Philomath, OR 97370
ron@wetlabs.com

W. Scott Pegau

17 November 2003 / Vol. 11, No. 23 / OPTICS EXPRESS 2997

Secchi depth in the Oslofjord–Skagerrak area: theory, experiments and relationships to other quantities

E. Aas[1], J. Høkedal[2], and K. Sørensen[3]

Ocean Sci., 10, 177–199, 2014

Ocean transparency from space: Validation of algorithms estimating Secchi depth using MERIS, MODIS and SeaWiFS data

Maéva Doron [a,b,c,*], Marcel Babin [b,c], Odile Hembise [a], Antoine Mangin [a], Philippe Garnesson [a]

Remote Sensing of Environment 115 (2011) 2986–3001

Secchi disk depth: A new theory and mechanistic model for underwater visibility

CrossMark

ZhongPing Lee [a,*], Shaoling Shang [b,*], Chuanmin Hu [c], Keping Du [d], Alan Weidemann [e], Weilin Hou [e], Junfang Lin [a], Gong Lin [b]

Remote Sensing of Environment 169 (2015) 139–149

A Decade of Satellite Ocean Color Observations*

Charles R. McClain

Annu. Rev. Mar. Sci. 2009. 1:19–42

IOCCG Report Number 2, 1999

Status and plans for Satellite Ocean-Colour Missions: Considerations for Complementary Missions.

A consumer's guide to phytoplankton primary productivity models

Michael J. Behrenfeld and Paul G. Falkowski

Limnol. Oceanogr., 42(7), 1997, 1479–1491

Limnol. Oceanogr., 28(4), 1983, 770–776

A simple, steady state description of phytoplankton growth based on absorption cross section and quantum efficiency[1]

Estimating primary production at depth from remote sensing

Z. P. Lee, K. L. Carder, J. Marra, R. G. Steward, and M. J. Perry

20 January 1996 / Vol. 35, No. 3 / APPLIED OPTICS 463

An assessment of optical properties and primary production derived from remote sensing in the Southern Ocean (SO GasEx)

Zhongping Lee,[1] Veronica P. Lance,[2,3] Shaoling Shang,[4] Robert Vaillancourt,[5]

JOURNAL OF GEOPHYSICAL RESEARCH, VOL. 116, C00F03, doi:10.1029/2010JC006747, 2011

COASTAL OCEAN OPTICS AND DYNAMICS

The Evolution of Optical Water Mass Classification

BY ROBERT A. ARNONE, A. MICHELLE WOOD, AND RICHARD W. GOULD, JR.

Oceanography | June 2004 15

A novel technique for detection of the toxic dinoflagellate, *Karenia brevis*, in the Gulf of Mexico from remotely sensed ocean color data

Jennifer P. Cannizzaro[a,*], Kendall L. Carder[a], F. Robert Chen[a], Cynthia A. Heil[b], Gabriel A. Vargo[a]

Continental Shelf Research 28 (2008) 137–158

Absorption spectrum of phytoplankton pigments derived from hyperspectral remote-sensing reflectance

ZhongPing Lee[a,*], Kendall L. Carder[b]

Remote Sensing of Environment 89 (2004) 361–368

Use of hyperspectral remote sensing reflectance for detection and assessment of the harmful alga, *Karenia brevis*

Susanne E. Craig, Steven E. Lohrenz, Zhongping Lee, Kevin L. Mahoney, Gary J. Kirkpatrick, Oscar M. Schofield, and Robert G. Steward

5414 APPLIED OPTICS / Vol. 45, No. 21 / 20 July 2006

Phytoplankton bloom during the northeast monsoon in the Luzon Strait bordering the Kuroshio

Shaoling Shang [a,b,*], Li Li [c], Jun Li [a], Yonghong Li [a], Gong Lin [a], Jun Sun [d]

Remote Sensing of Environment 124 (2012) 38–48

Satellite-detected fluorescence reveals global physiology of ocean phytoplankton

M. J. Behrenfeld[1], T. K. Westberry[1], E. S. Boss[2], R. T. O'Malley[1], D. A. Siegel[3], J. D. Wiggert[4], B. A. Franz[5], C. R. McClain[5], G. C. Feldman[5], S. C. Doney[6], J. K. Moore[7], G. Dall'Olmo[1], A. J. Milligan[1], I. Lima[6], and N. Mahowald[8]

Biogeosciences, 6, 779–794, 2009

Seasonal variation of CDOM and DOC in the Middle Atlantic Bight: Terrestrial inputs and photooxidation

Anthony Vodacek[1] *and Neil V. Blough*[1]
Department of Chemistry and Biochemistry, University of Maryland, College Park, Maryland 20742

Michael D. DeGrandpre,[2] *Edward T. Peltzer, and Robert K. Nelson*

Limnol. Oceanogr., 42(4), 1997, 674–686

Analysis of the optical properties of the Orinoco River plume by absorption and fluorescence spectroscopy

Carlos E. Del Castillo [a,*], Paula G. Coble [a], Julio M. Morell [b], José M. López [b], Jorge E. Corredor [b]

Marine Chemistry 66 (1999) 35–51

Satellite ocean color assessment of air-sea fluxes of CO_2 in a river-dominated coastal margin

Steven E. Lohrenz
Department of Marine Science, University of Southern Mississippi, Stennis Space Center, Mississippi, USA

Wei-Jun Cai

GEOPHYSICAL RESEARCH LETTERS, VOL. 33, L01601, doi:10.1029/2005GL023942, 2006

[Chl] (empirical) approach:

Rrs(λ) → [Chl] → z_{eu}

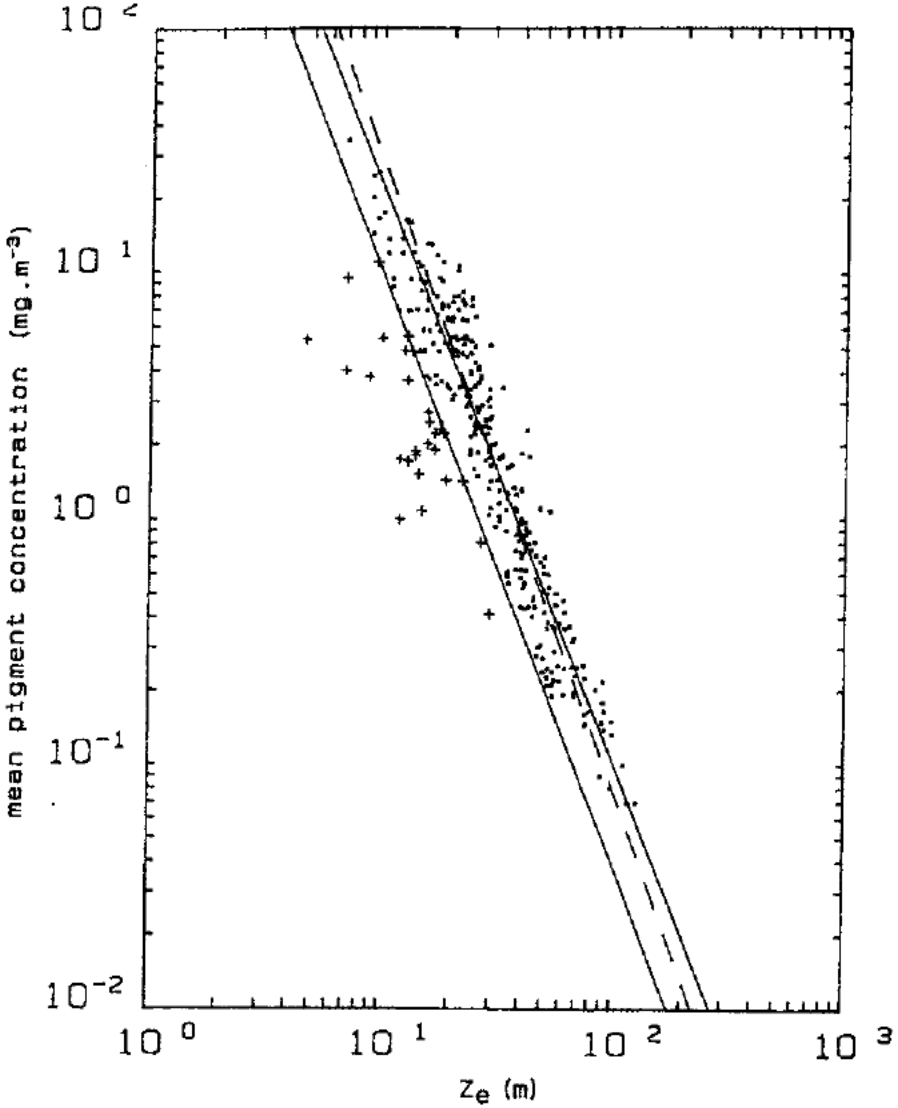

$$Z_e = 38.0C^{-0.428}$$

(Morel 1988)

Global Z_{SD}

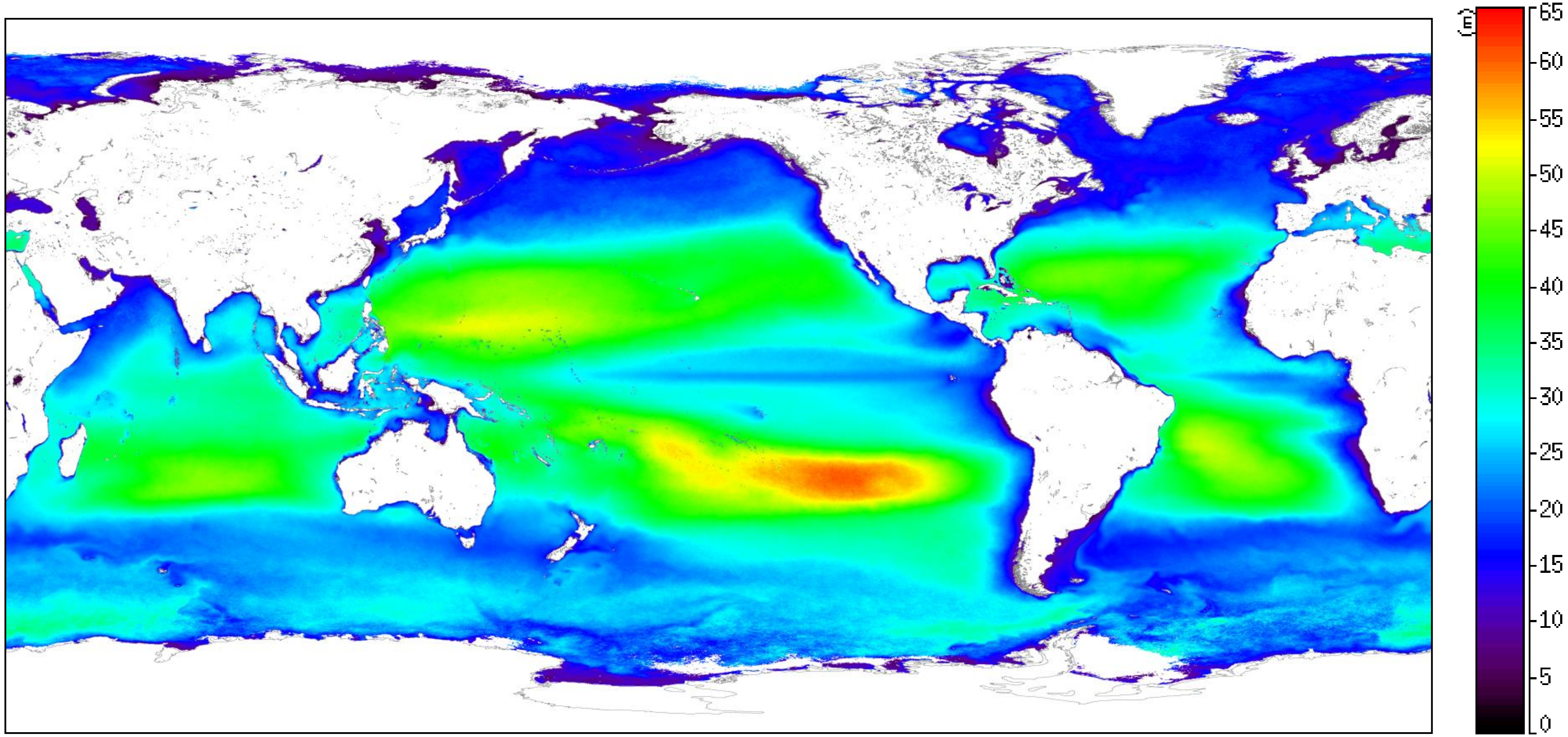

A much more straightforward product for water clarity!

Components for PP estimation:

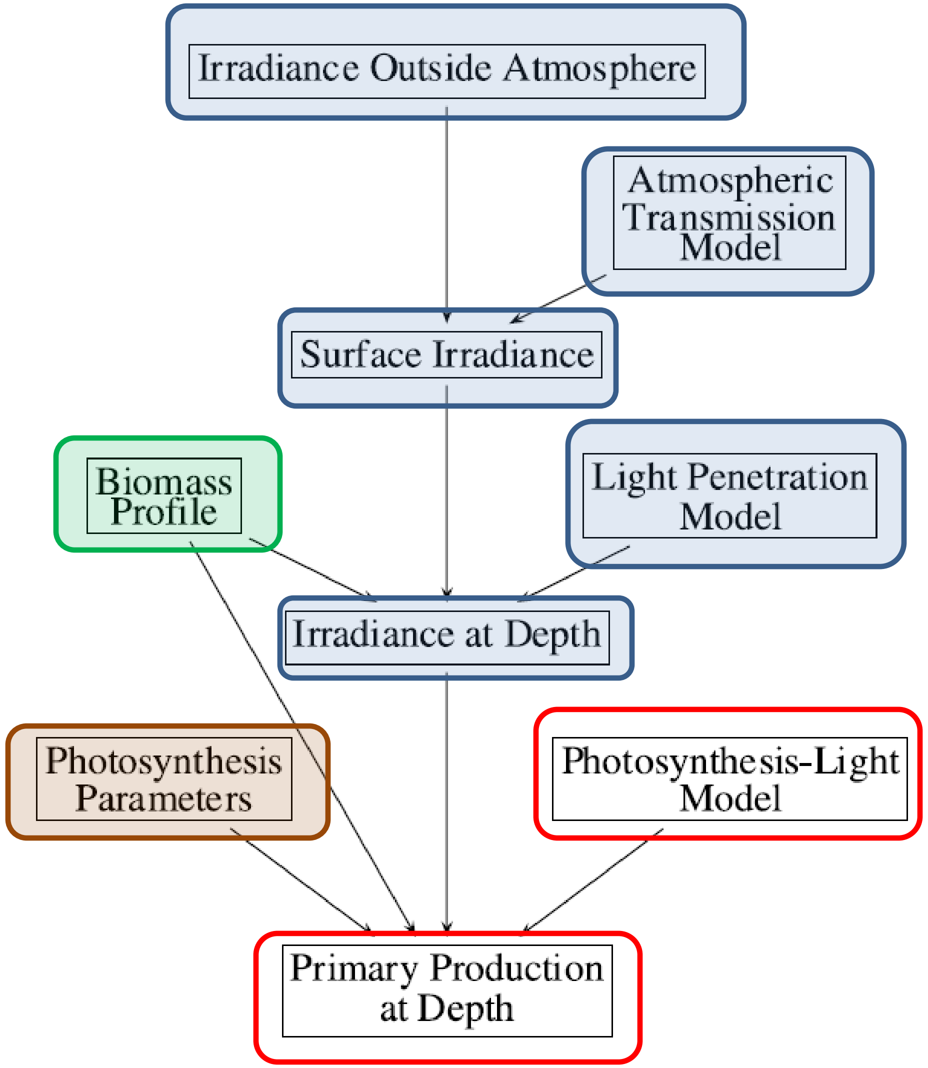

1. Phytoplankton

2. Light penetration

3. Photosynthesis parameters

(Platt and Sathyendranath, 2007)

Empirical:

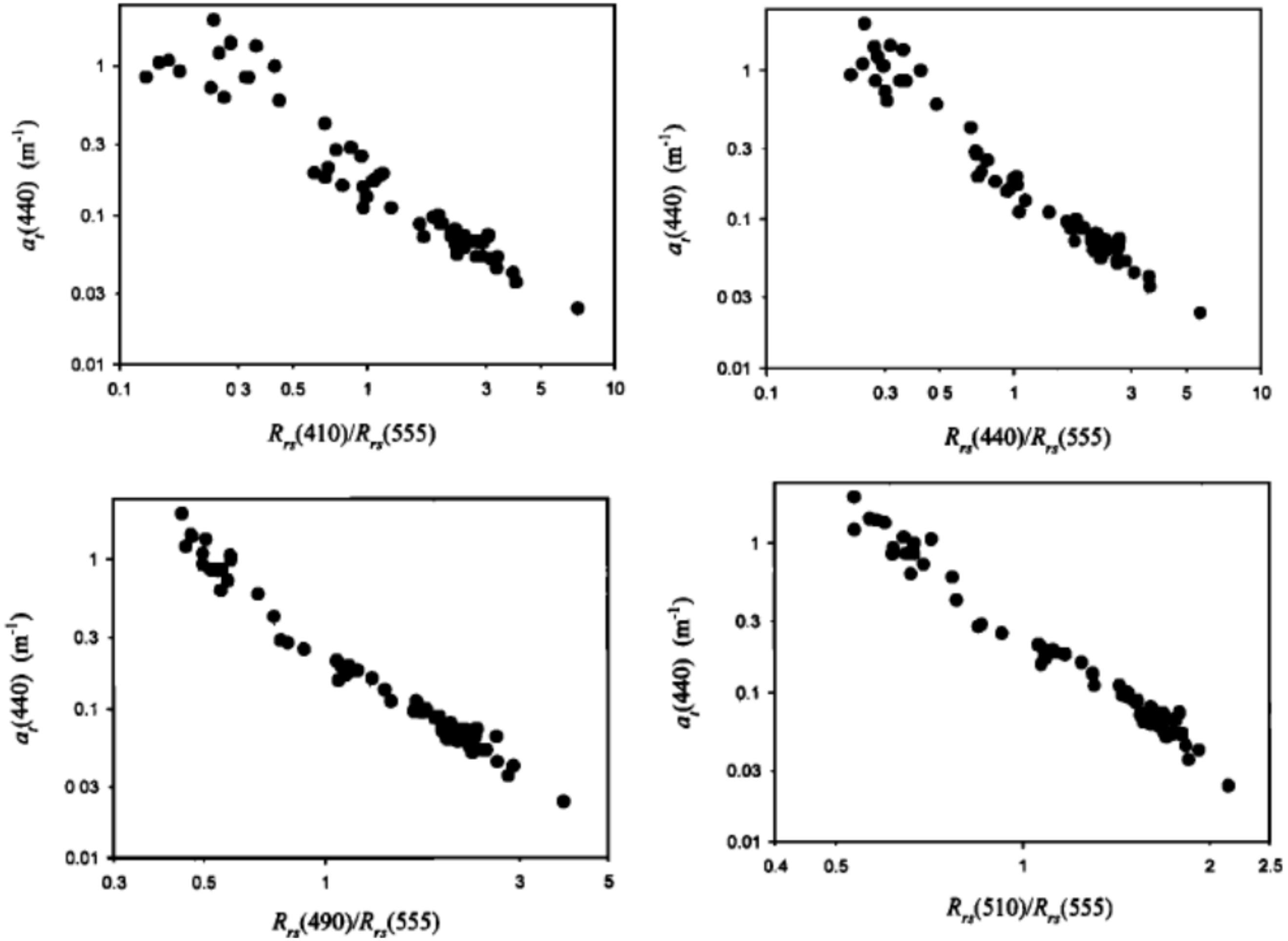

$$a_t(440) = 10^{-0.674-0.531\rho_{25}-0.745\rho_{25}^2-1.469\rho_{35}+2.375\rho_{35}^2}, \qquad (14)$$

$$a_\phi(440) = 10^{-0.919+1.037\rho_{25}-0.407\rho_{25}^2-3.531\rho_{35}+1.579\rho_{35}^2}, \qquad (20)$$

(Lee et al. 1998)

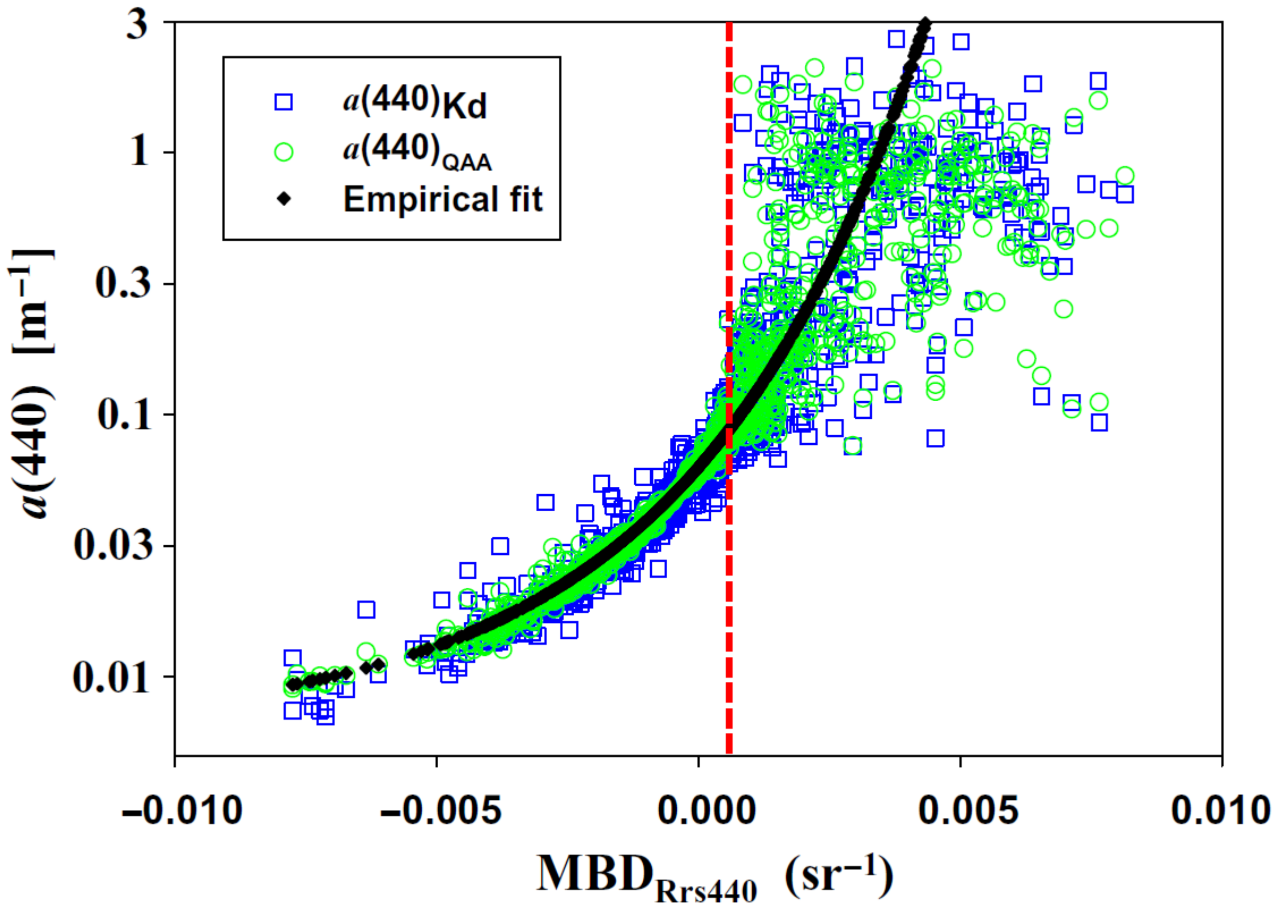

Fig. 3. Relationship between *a*(440) and MBD_{Rrs440}. The red vertical line indicates the location of $MBD_{Rrs440} = 0.0005\ sr^{-1}$.

(Lee et al., 2023)

$$MBD_{Rrs440} = R_{rs}(555) - \left[R_{rs}(443) + \frac{555-443}{670-443}\left(R_{rs}(670) - R_{rs}(443)\right)\right]$$